Technische Universität München

TUM School of Engineering and Design

# Uncoupled Shared Control Designs for Teleoperation of Highly-Automated Vehicles

Andreas Julius Schimpe, M.Sc.

Vollständiger Abdruck der von der TUM School of Engineering and Design der Technischen Universität München zur Erlangung eines

Doktors der Ingenieurwissenschaften (Dr.-Ing.)

genehmigten Dissertation.

| | |
|---|---|
| Vorsitz: | Prof. Dr.-Ing. Johannes Betz |
| Prüfende der Dissertation: | 1. Prof. Dr.-Ing. Markus Lienkamp |
| | 2. Prof. Dr.-Ing. Frank Flemisch |

Die Dissertation wurde am 20.06.2023 bei der Technischen Universität München eingereicht und durch die TUM School of Engineering and Design am 01.11.2023 angenommen.

# Acknowledgements

I would like to express my gratitude to everyone who has contributed to the successful completion of my dissertation at the Institute of Automotive Technology, Technical University of Munich, during the period from 2019 to 2023.

A special thanks goes to my supervisor, Prof. Dr.-Ing. Markus Lienkamp, for his guidance, expertise, and support throughout this journey. I am also grateful to Prof. Dr.-Ing. Frank O. Flemisch for serving as the second assessor and providing valuable advice. I would like to acknowledge Prof. Dr.-Ing. Johannes Betz for taking over the chairmanship of the examination.

Special thanks go to the research teams of the projects 5GCroCo and SAFESTREAM for the fruitful discussions and great collaborations in demonstrations.

I would like to express my appreciation to my colleagues at the Institute of Automotive Technology, especially the members of the Safe Operation research group led by Dr.-Ing. Frank Diermeyer. Their collaboration and support have been instrumental in the progress of my research. I am excited to have had the opportunity to work with a talented and dedicated ToF team including Jean-Michael, Johannes, Simon, Domagoj, Florian, Maria, Tobias, Nils, and David. In particular, I would also like to thank Lasse for the encouragement in finishing up the thesis.

I would also like to extend my gratitude to the proofreaders, David Brecht, Dr.-Ing. Johannes Feiler, Sarah Koch, and Dr.-Ing. Stefan Riedmaier, for their valuable feedback and suggestions.

My deepest appreciation for the encouragement and support goes to my family, including my parents, Regina and Robert, my sisters, Silvia and Christina, and my brother, Michael. Lastly, I am grateful to my wife, Yanqin, for her understanding, patience, and belief in me throughout the ups and downs of this Ph.D. journey.

Garching, May 2023

Andreas Julius Schimpe

# Contents

# List of Abbreviations

| | |
|---|---|
| DC | Direct Control |
| SSVC | Shared Steering and Velocity Control |
| SVC | Shared Velocity Control |

# Formula Symbols

| Formula Symbols | Unit | Description |
|---|---|---|
| $a$ | m/s$^2$ | Longitudinal acceleration |
| $a_{\mathrm{lat}}$ | m/s$^2$ | Lateral acceleration |
| $a_{\mathrm{lat,max}}$ | m/s$^2$ | Maximum lateral acceleration |
| $a_{\mathrm{max}}$ | m/s$^2$ | Maximum longitudinal acceleration |
| $a_{\mathrm{min}}$ | m/s$^2$ | Minimum longitudinal acceleration |
| $a_{\mathrm{stop}}$ | m/s$^2$ | Deceleration to stop vehicle in planning horizon |
| $f_{\mathrm{disk}}$ | - | Implicit scalar function for checking intersection of disk and ellipse |
| $f_{\mathrm{ell}}$ | - | Implicit scalar function of ellipse |
| $\boldsymbol{f}_{\mathrm{eq}}$ | - | Function vector of equality constraints |
| $\boldsymbol{f}_{\mathrm{ineq}}$ | - | Function vector of inequality constraints |
| $\boldsymbol{f}_{\mathrm{mdl}}$ | - | Differential vehicle model equations vector |
| $i$ | - | Discretization step |
| $j$ | m/s$^3$ | Jerk |
| $j_{\mathrm{max}}$ | m/s$^3$ | Maximum jerk |
| $J$ | - | Cost function |
| $J_u$ | - | Cost function term to penalize deviation from operator's control input |
| $J_\epsilon$ | - | Cost function term to penalize slack variables from soft constraints |
| $k$ | - | Number of obstacles |
| $l_{\mathrm{f}}$ | m | Distance from center of mass to vehicle front axle |
| $l_{\mathrm{maj}}$ | m | Length of major axis of ellipse |
| $l_{\mathrm{min}}$ | m | Length of minor axis of ellipse |
| $l_{\mathrm{obj}}$ | m | Length of object |
| $l_{\mathrm{r}}$ | m | Distance from center of mass to vehicle rear axle |
| $m$ | - | Index of vehicle-approximating disk |
| $n$ | - | Number of discretization steps in planning horizon |

| | | |
|---|---|---|
| $\boldsymbol{o}_{\text{ell}}$ | - | Ellipse representation of object |
| $\boldsymbol{o}_{\text{rect}}$ | - | Rectangular representation of object |
| $\boldsymbol{o}^{k}$ | - | List of objects |
| $p$ | - | Index of sampled steering angle rate |
| $P$ | - | Number of sampled steering angle rates |
| $r_{\text{disk}}$ | m | Radius of disk |
| $s$ | m | Path progress |
| $s_{\text{safe}}$ | m | Safe progress |
| $t$ | s | Time |
| $t_{\text{s}}$ | s | Trajectory sampling time |
| $t_{\text{h}}$ | s | Trajectory planning horizon |
| $\boldsymbol{u}_{\text{a}}$ | - | Control input from automation |
| $\boldsymbol{u}_{\text{o}}$ | - | Control input from operator |
| $\boldsymbol{u}, \boldsymbol{u}_{\text{v}}$ | - | Vehicle control input |
| $\boldsymbol{u}^{n-1}$ | - | Sequence of vehicle control inputs |
| $v$ | m/s | Velocity |
| $v_{\text{o}}$ | m/s | Velocity desired by operator |
| $v_{\text{safe}}^{n}$ | m/s | Sequence of safe velocities |
| $w_{a}$ | - | Cost function weight on acceleration usage |
| $w_{\text{obj}}$ | m | Width of object |
| $w_{v}$ | - | Cost function weight on deviation from desired velocity |
| $w_{\delta}$ | - | Cost function weight on deviation from desired steering angle |
| $w_{\dot{\delta}}$ | - | Cost function weight on steering rate usage |
| $x$ | m | $x$-coordinate in Cartesian coordinate system |
| $x_{\text{disk}}$ | m | Position of disk in $x$ |
| $x_{\text{obj}}$ | m | Position of object in $x$ |
| $y$ | m | $y$-coordinate in Cartesian coordinate system |
| $y_{\text{disk}}$ | m | Position of disk in $y$ |
| $y_{\text{obj}}$ | m | Position of object in $y$ |
| $\boldsymbol{z}$ | - | Vehicle state |
| $\boldsymbol{z}_{\text{curr}}$ | - | Current vehicle state |
| $\boldsymbol{z}_{\text{ref}}$ | - | Reference vehicle state |
| $\boldsymbol{z}^{n}$ | - | Sequence of vehicle states |

| | | |
|---|---|---|
| $\mathcal{Z}_{\text{free}}$ | - | Set of collision-free vehicle states |
| $\beta$ | rad | Side-slip angle |
| $\delta$ | rad | Steering angle |
| $\delta_{\text{o}}$ | rad | Steering angle desired by operator |
| $\delta_{\text{max}}$ | rad | Maximum steering angle |
| $\dot{\delta}$ | rad/s | Steering angle rate |
| $\dot{\delta}_{\text{max}}$ | rad/s | Maximum steering angle rate |
| $\epsilon_a$ | - | Slack variables for acceleration constraints |
| $\epsilon_c$ | - | Slack variables for collision avoidance constraints |
| $\epsilon_j$ | - | Slack variables for jerk constraints |
| $\kappa$ | 1/m | Curvature |
| $\kappa^n_{\text{crit}}$ | - | Sequence of critical curvatures |
| $\lambda$ | - | Weight to allocate control authority between operator and automation |
| $\theta$ | rad | Vehicle heading |
| $\theta_{\text{obj}}$ | rad | Orientation of object |

## Formula Symbols for Results from Experimental User Study

| Formula Symbols | Unit | Description |
|---|---|---|
| $F$ | - | Test statistic for Levene test and parametric ANOVA |
| $p$ | - | Significance level |
| $r$ | - | Effect size from t-test and Wilcoxon signed-rank test |
| $W$ | - | Test statistic for Shapiro-Wilk test |
| $\chi^2$ | - | Test statistic for non-parametric Friedman's ANOVA |

# 1 Introduction and Motivation

Autonomy of machines is a field of research and development that has been around since the last century. Nowadays, with the increasing performance, compactness, and energy efficiency of computation, sensing, and actuation technologies, the deployment of mobile robots in particular is on the rise. This includes the automation of the vehicle driving task, which has been pursued as a technology holding great promises. For instance, the potential to improve the productivity of current human drivers as well as increase the comfort of passengers is among the greatest motivators for automated driving. In addition, given more than one million road fatalities occur each year [1], the vision of zero road fatalities through safer automated driving has led to a long history of research and development of automated vehicles.

As early as 1979, Tsugawa et al. [2] described tests with a vehicle that perceives its surroundings and determines control actions in an automated manner. Led by Dickmanns, the project Prometheus, running from 1987 to 1994, laid the foundation in machine vision for automated guidance of road vehicles [3]. Another decade later, in the early 2000s, the popular DARPA challenges brought the technology of automated driving to a new level of maturity [4, 5]. As a result of these achievements, the Google Self-Driving Car project was launched in 2009 [6]. Today, it is known as Waymo [7]. In Germany, history was made in 2013, when the automated vehicle named Bertha drove along the 103 kilometers long Bertha Benz Memorial Route in an automated manner under the supervision of a human safety driver. In the years after, further self-driving car competitions were launched, e.g., the SAE AutoDrive Challenge in 2017 [8] and the Indy Autonomous Challenge in 2021 [9].

Over the years, public and private funding has provided automated vehicle development with a generous budget. Estimates range up to a total of 100 billion US dollars [10]. Although companies such as Waymo and Cruise [11] manage to safely deploy fully-driverless vehicles with expanding service areas on public roads [12], optimism about automated driving technology, in particular robotaxis in urban areas, seems to be on the decline [13]. Hence, many companies have a different focus that goes beyond the robotaxi use case. Believing that profitability lies in market segments where the vehicles are driving on the same route over and over again, companies such as Gatik [14], Aurora [15], or Waabi [16] are developing systems for automated trucking on highways and logistic sites. The key to their strategy is a well-defined and limited domain in which the automated vehicle is designed to operate.

Under the aforementioned conditions, the system is expected to operate functionally safe. However, as is the case for any robotic system deployed in the real world, it cannot be guaranteed that all operating conditions are within these constraints. In these situations, often referred to as edge cases, the automated vehicle is no longer capable to continue driving in an automated manner. In the case of an automated vehicle on the public road, such a constraint may be a traffic intersection that is temporarily controlled by a policeman. Although there are clear rules on how to drive based on the policeman's gestures, it is deemed complex to teach this to the software algorithms of an automated vehicle. In other situations, such as a blocked road ahead, it may be required for the vehicle to temporarily cross a solid lane marking in order to continue driving. A human driver knows that this is acceptable in certain circumstances. However, similar to the case of the policeman, it is challenging to teach this and other temporary rule violations to software algorithms.

An automated vehicle is expected to realize when it can no longer safely operate in an automated manner. If this is the case, a state with minimal risk for the vehicle and its surroundings should be achieved. Usually, this is a standstill of the vehicle, potentially on the side of the road [17, p. 15]. Resolving edge cases can be an easy task for human drivers. Hence, it is a plausible solution to temporarily bring a human back into the decision making and control loop of the automated vehicle. However, the automated vehicle is meant to be highly-automated and driverless. Hence, it is not desirable to ask passengers or send a human fallback operator to take over for a short moment in order to resolve the situation.

Vehicle teleoperation represents a viable and economical solution to deal with automated vehicle fail cases [18–20]. Thereby, a remote operator connects to the vehicle via a mobile network and is provided with information, e.g., video streams to understand the current traffic situation. Based on this, the remote operator takes actions to remotely assist or drive the automated vehicle temporarily, as shown in Figure 1.1. After this intervention, the automated vehicle can continue its journey in an automated manner.

Figure 1.1: Picture of a remote operator performing remote driving. The remote workstation consists of three monitors for the visualization of data from the vehicle. Commands for the vehicle are created using a steering wheel and pedals.

The way to teleoperate a vehicle is not limited to the concept shown in the figure. Instead, the teleoperation of an automated vehicle can be performed in different forms, e.g., through the specification of desired waypoints the vehicle should follow. Choosing the appropriate teleoperation concept based on the fail case is an active field of research [21]. The present work develops a teleoperation concept in which the remote operator and the automation are continuously collaborating on the driving task. Thereby, their abilities are complemented. In particular, the focus is on shared control designs. In these, the automation is capable to evaluate the control actions from the remote operator and correct them if deemed unsafe. Through this, the automation can improve the safety of the vehicle.

The following two sections in this chapter provide a general introduction to automated driving and vehicle teleoperation technology. Next, the scope of the proposed shared control designs for the teleoperation of highly-automated vehicles is defined in the problem statement. The chapter is concluded with the outline for the remainder of the present work.

## 1.1 Automated Driving

In this section, after the introduction of some terms and definitions, the general system architecture for automated driving is described. Finally, the levels of driving automation are introduced.

### Terms and Definitions

Specified by the Society of Automotive Engineers, in short SAE in the SAE J3016:2021 [17], the **dynamic driving task** “includes all of the real-time operational and tactical functions required to operate a vehicle in on-road traffic” [17, p. 9]. Quoting again, it includes the following subtasks:

1. Lateral vehicle motion control via steering (operational).
2. Longitudinal vehicle motion control via acceleration and deceleration (operational).
3. Monitoring the driving environment via object and event detection, recognition, classification, and response preparation (operational and tactical).
4. Object and event response execution (operational and tactical).
5. Maneuver planning (tactical).
6. Enhancing conspicuity via lighting, sounding the horn, signaling, gesturing, etc. (tactical).

If an automated vehicle is no longer able to handle the entire dynamic driving task, a **minimal risk condition** is sought. This is a stable and stopped condition of the vehicle [17, p. 15]. It should be achieved when the automation, controlling the vehicle, is no longer capable to continue driving. In this context, a minimal risk condition is the result of a dynamic driving task fallback, i.e., the performance of a minimum risk maneuver [22, p. 237].

An **operational design domain** describes the “operating conditions under which a given driving automation system or feature thereof is specifically designed to function, including, but not limited to, environmental, geographical, and time-of-day restrictions, and/or the requisite presence or absence of certain traffic or roadway characteristics” [17, pp. 17-18].

**Trajectory** is a technical term from robotics. In the context of automated vehicles, a trajectory describes the past or future motion of the vehicle over time, i.e., a function of the system states over time [23, p. 171].

The definition of a **path** is closely related to the definition of a trajectory. However, instead of describing the vehicle motion over time, a path describes it over a progress variable. This can be the distance that is traveled along the path [24].

### Automated Driving System Architecture

Besides so-called End-to-End approaches [25], which consist of a single neural network, an automated driving system is usually developed in a modular manner. Simplified, these modules are summarized in the blocks to sense, plan, and act, as shown in Figure 1.2. This architecture has evolved from the tactical and operational functions that a human performs when driving a vehicle.

The sensing block contains various sensor components of different modalities, e.g., camera, ultrasonic, RADAR, LiDAR, GNSS, and IMU. Fed by this, there is the perception module, performing the localization of the vehicle as well as the detection and classification of lane markings, traffic signs, and other traffic participants. Dynamic objects also need to be tracked and predicted over time.

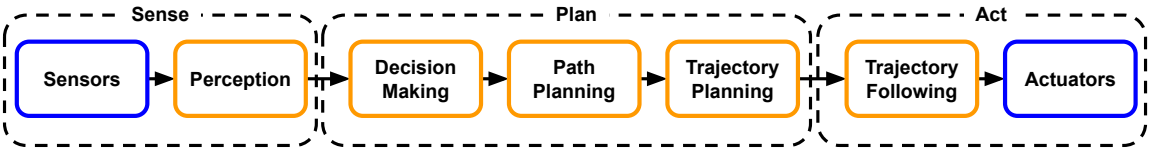


Figure 1.2: Architecture of an automated driving system. Grouped into the blocks sense, plan, and act, the system consists of several hardware components and software modules. These are depicted in blue and orange, respectively.

The outputs from the perception module are taken by the planning block. Therein, behavior planning usually contains a state machine that makes decisions, e.g., taking a turn or performing a lane change. Based on this, path planning is performed in order to spatially plan for the decision. It is then the objective of the trajectory planning module to create a motion plan over time, i.e., the trajectory that travels along the planned path while considering dynamic obstacles.

Finally, the acting module is responsible for the execution of the planned trajectory. To achieve this, a trajectory following controller continuously computes control commands, i.e., throttle and brake pressure as well as the steering wheel angle. These are then executed by the actuators of the vehicle.

## Levels of Driving Automation

Based on Gasser and Westhoff [26], the prominent levels of driving automation have been introduced in the SAE J3016:2021 [17, pp. 24-34]. For each level, the allocation of roles in the dynamic driving task, the dynamic driving task fallback, and, if applicable, operational design domain restrictions are specified. In the following, the levels are briefly introduced one by one.

- Level 0 – No Driving Automation: The human driver performs the entire dynamic driving task.
- Level 1 – Driver Assistance: Within a given operational design domain, an automated driving system is able to perform parts of the subtasks of lateral or longitudinal vehicle motion control. The human driver performs the remainder of the dynamic driving task and is always ready to perform the dynamic driving task fallback.
- Level 2 – Partial Driving Automation: Within a given operational design domain, the automated driving system is able to perform the lateral and longitudinal vehicle motion control task simultaneously. However, the human driver is required to continuously monitor the operation of the automated driving system and always be ready to perform the dynamic driving task fallback.
- Level 3 – Conditional Driving Automation: In this case, the automated driving system performs the entire dynamic driving task within a certain operational design domain. No human supervision is required. However, within sufficient time, the human driver must be receptive to dynamic driving task fallback when requested by the automated driving system. In case of no response, the automated driving system can be capable to achieve a minimal risk condition in an automated manner.
- Level 4 – High Driving Automation: For a specific operational design domain, the automated driving system performs the entire dynamic driving task as well as the dynamic driving task fallback. Hence, the automated driving system is required to achieve a minimal risk condition when needed. After this, an intervention through a human driver to recover the automated vehicle may be necessary.

- Level 5 – Full Driving Automation: With no operational design domain restrictions, the automated driving system performs the entire dynamic driving task as well as the dynamic driving task fallback.

## 1.2 Vehicle Teleoperation

Vehicle teleoperation complements an automated driving system by establishing a connection between the remote operator and the vehicle via a mobile network [18–20]. Through this, the automated vehicle can be supported remotely in situations that cannot be resolved by the automated driving system in an automated manner. The architectural overview of a teleoperation system is shown in Figure 1.3. Feedback from the vehicle, e.g., videos or vehicle state information, is transmitted and shown to the remote operator. As illustrated, a common visualization setup is a set of three monitors which are mounted side-by-side.

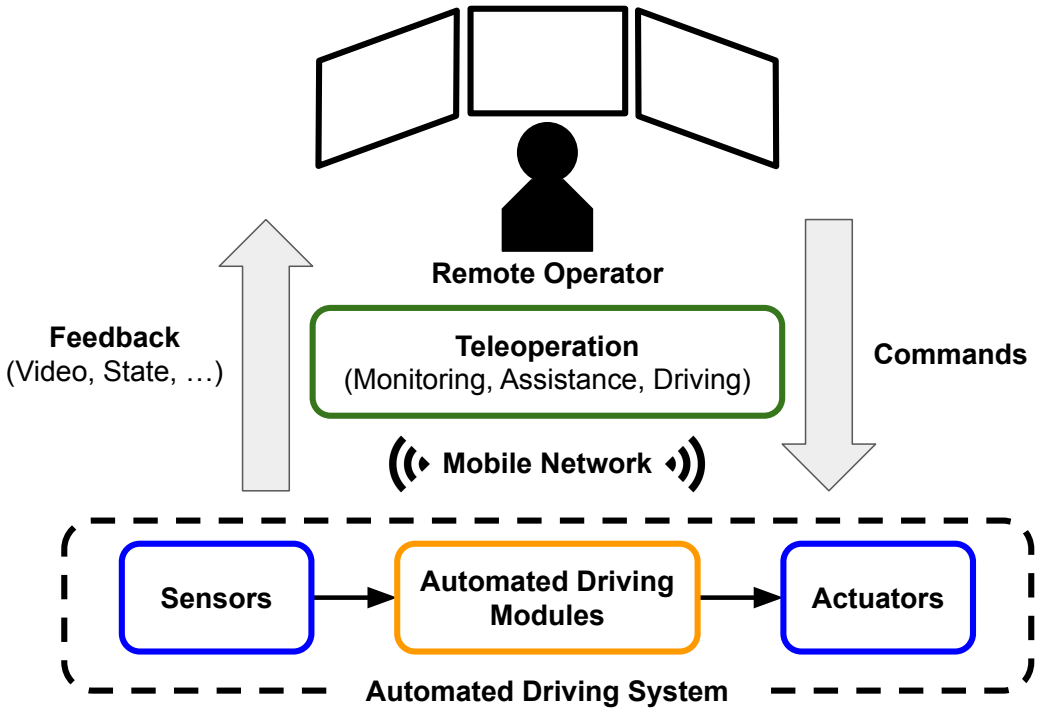


Figure 1.3: Architecture of a teleoperation system to remotely support an automated vehicle. At the bottom, the automated driving system is shown. Transmitted via a mobile network, feedback from the vehicle provides the remote operator with an understanding of the vehicle surroundings. Based on this, teleoperation is performed in various forms by transmitting commands back to the vehicle.

The concept of the remote operator driving the vehicle is the most prominent form of vehicle teleoperation. Imitating the control interface for a human driver in the vehicle, the remote operator also uses a steering wheel and pedals to create lateral and longitudinal motion control commands. These are transmitted to the vehicle for execution. The scope of this work is within the context of automated vehicles. Hence, the presence of an automated driving system in the vehicle is assumed.

In the remainder of this section, the taxonomy for vehicle teleoperation that is used in this work is introduced. This is followed by an overview of industry activities in the field. Thereafter, challenges are described.

### 1.2.1 Taxonomy

Teleoperation is a wide field, coming in various flavors for different domains and use cases. Over the years, many concepts for teleoperating vehicles were described and different terms, partially describing similar things, were introduced. An extensive overview of the terminology that is used across the automotive domain is given by Bogdoll et al. [27]. Building upon this, the SAE J3016:2021 standard [17] and the guidelines on automated vehicles [28, 29], Majstorović, Schimpe, et al. [21] established the taxonomy that is used in the present work.

In the context of automated vehicle teleoperation, the terms remote monitoring, remote assistance, and remote driving are used under the hypernym of teleoperation, as shown in Figure 1.3. Remote Monitoring enables the remote operator to remotely monitor, but not intervene in the operation of the automated vehicle. In remote assistance, the remote operator can support the automated driving system through high-level commands such as assistance in taking the decision to perform a certain maneuver. Finally, remote driving refers to the vehicle being remotely driven completely by the remote operator, as shown in Figure 1.1.

### 1.2.2 Industry Activities

Given the great number of use cases as a standalone solution or for the assistance of automated vehicles, the industry interest in the field of vehicle teleoperation is on the rise. Figure 1.4 shows the number of patents in English published globally from the years 2000 to 2022[1]. The data are obtained through the Google Patents search engine. Using the search term “Vehicle Teleoperation”, patents that are not directly related to automotive technology are filtered out.

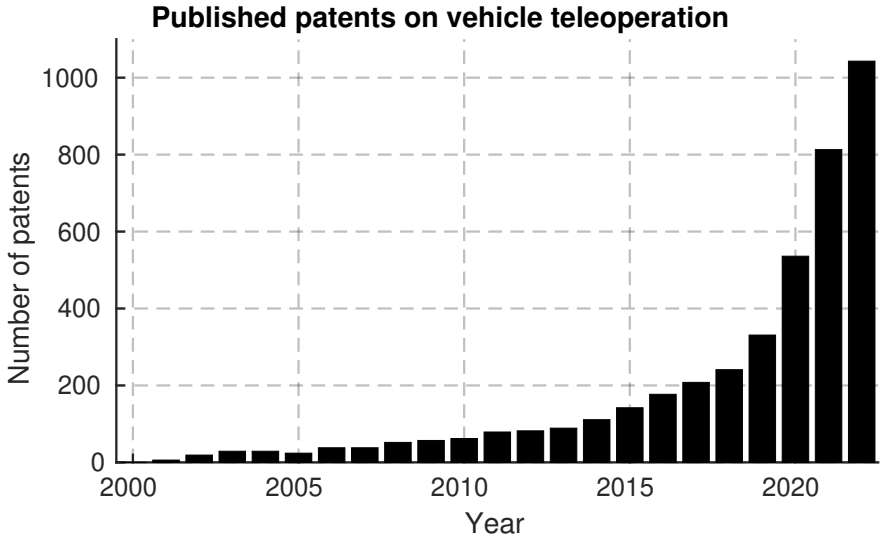


Figure 1.4: Published patents on “Vehicle Teleoperation” per year between 2000 and 2022.

From only six patents that were filed until 2001, it took until the end of 2016 for a total of 1000 filed patents to accumulate. For a long time, teleoperation technology for mobile robots was developed for specific use cases only, e.g., space exploration. In essence, it should enable the operation of vehicles at locations that are dangerous or inaccessible to humans. However, since 2017, the exponential growth of patent publications can be observed. Probable causes are the increasing relevance of teleoperation as a fallback for automated vehicles as well as mobile networks of the fourth and fifth generation. By the end of 2022, more than 4,200 patents were published.

[1] The data were accessed on April 8th, 2023 at https://patents.google.com/?q=%28vehicle+teleoperation%29&before=priority:20221231&after=priority:20000101&language=ENGLISH

Several existing companies developing automated vehicles increased the effort in the field [30]. For instance, the company Zoox became prominent and filed several patents, e.g., Gogna et al. [31, 32]. Zoox also explained and demonstrated its vision of TeleGuidance to support its automated vehicles on the streets of San Francisco [33]. A short insight into remote support for its automated vehicles has also been given by Cruise [34]. Also, Volkswagen published a number of patents related to vehicle teleoperation, e.g., Rech et al. [35].

Given the great economic opportunities, new startups emerged and collaborations have been announced. For instance, EasyMile is collaborating with the specialized teleoperation company DriveU and other partners to enable remote assistance of its automated shuttles in order to advance their operation to SAE Level 4 [36, 37]. Motional announced a partnership with Ottopia in order to integrate remote assistance support into its automated vehicles [38–40]. Volkswagen and the German teleoperation startup Fernride are collaborating to perform field tests in which trucks are remotely driven on Volkswagen premises in Wolfsburg [41]. Most recently, in early 2023, a major milestone has been achieved by the German startup Vay, which got clearance to perform remote driving without a safety driver on public roads in Germany [42].

### 1.2.3 Challenges of Remote Driving

As the previous section showed, there are a great number and variety of activities in the field of vehicle teleoperation. However, despite technological progress, several challenges persist. In the following, these challenges, along with mitigation techniques, are described.

#### Latency

Especially in teleoperation, latency is relevant. In the uplink from the vehicle, latency is caused by the capture, compression, transmission, and visualization of the video to the remote operator. In the downlink, it takes time to create, transmit and execute the remote operator's control commands in the vehicle [43].

The challenge has been recognized since the last century and early so-called predictor displays were proposed, e.g., in the field of space teleoperation [44]. These ideas have been adopted for vehicle teleoperation. First, the motion of the vehicle is predicted based on a vehicle model. Next, this information is used to enhance the visual interface by projecting the prediction into the video streams [45–49]. Similarly, detections of dynamic obstacles in the vehicle surroundings can be predicted and visualized [50, 51] or communicated through haptic feedback [52]. Furthermore, approaches to perform sliding and zooming video transformations as well as ways to reduce the video transmission delay have been worked on [53, 54]. Also, concepts have been proposed, incorporating the delay in the control approach of the vehicle [55].

Given time, the latency in state-of-the-art vehicle teleoperation systems could be reduced significantly. For instance, through the use of fifth-generation mobile networks [56–59], the total latency, i.e., the sum of the uplink and the downlink, can be well below 200 milliseconds [43]. However, as this value is known to still degrade the performance of the remote operator [60], latency will always persist as a challenge in remote driving [61–63].

#### Situation Awareness

In a basic teleoperation system, the remote operator gets an understanding of the surroundings and motion of the vehicle based on video and audio data, which are transmitted from the vehicle. Based on this, the remote operator creates a mental representation of the vehicle surroundings. Compared to a driver in the vehicle, the remote operator does not experience any accelerations from the movement of the vehicle [63]. On top of this, the displayed videos are often subject to distortion or reduced quality. In consequence, the

remote operator does not experience the same sense of embodiment as a driver in the vehicle, and mental effort is required to compensate for this and recreate missing information [64]. In addition, when deploying remote driving as a fallback for an automated driving system, the so-called out-of-the-loop syndrome poses another challenge. This describes the problem of remote operators being asked to resolve traffic situations for the automated vehicle at short notice [65]. When the situation is not fully clear to the remote operator, the safety of the teleoperated vehicle can be influenced negatively.

Over the years, various techniques have been adopted in order to improve the remote operator's situation awareness and immersion. For instance, the usage of a head-mounted display is described [18, 66–68]. Furthermore, a spherical projection [69] and blur effects of the videos [70] have been presented as means to enhance the remote operator's immersion. Even more complex concepts include motion platforms with greater haptic feedback [71]. Overall, the quantification of the remote operator's situation awareness [65, 72] and work on the interface for the remote operator [73–76] are active research fields.

## Connectivity

In order to remotely drive a vehicle, a lot of data are transmitted via mobile network connections. Besides the introduction of latency that impairs the driving performance of the remote operator, there is the risk of losing transmitted packets. This can corrupt the transmitted video streams or fragment the signal of the remote operator's control commands. There is also the issue of network jitter, i.e., a variable latency when transmitting signals. Depending on the time of day and location of the teleoperated vehicle, the available bandwidth can also vary [77]. In the worst case, the connection between the remote operator and the vehicle can even be lost completely.

The aforementioned issues show that quality of service-awareness and maintaining a reliable connection yield further complex challenges that need to be addressed. Solutions, e.g., predicting the communication quality [78, 79], exist and are also adopted for the use case of vehicle teleoperation [80–84]. However, given the various causes of reduced communication quality, making reliable predictions is challenging. Hence, effort is also put into the optimization of the data rate of the video stream [85, 86], robustification of its transmission [87], and fallback techniques in the event of connection loss [88, 89].

This overview shows that the challenge of connectivity is being tackled and various solutions are being proposed. However, if these are not available, great risks can still evolve from technical shortcomings when performing remote driving.

## Regulation

Although the technology has been developed for more than a decade, with only a few exceptions, teleoperation on public roads is still being performed with a safety driver in the vehicle. There exist several regulatory uncertainties, leaving some legal questions open.

In 2021, Linné and Andersson examined and compared the road vehicle teleoperation regulation in the United Kingdom, Sweden, and Germany [90]. In the United Kingdom, there is the code of practice for trialing automated vehicles [91]. It is mentioned that remote driving is possible. However, a full risk assessment should be carried out as it has to be assured that the teleoperation system is equally safe as having a driver in the vehicle. In the Decree 2017:309 on the experimental operation of automated vehicles from Sweden [92], remote driving is not explicitly mentioned. However, it is stated that a driver can either be inside or outside the vehicle when testing automated vehicles. As no limitation is given to the distance between the driver and the vehicle, remote driving can be deemed possible.

At the time of writing [90], a draft for the act on automated driving was being prepared in Germany. In July 2022, this act, the Automatisiertes-Fahren-Genehmigungs-und-Betriebs-Verordnung, in short AFGBV [93] went into effect and its concepts were also adopted into the Straßenverkehrsgesetz, in short StVG [94]. Therein, the remote operator is referred to as the Technische Aufsicht, who is allowed to clear a maneuver that is proposed by the automated driving system. In case this maneuver is not intended, the remote operator can propose an alternative maneuver. In both cases, i.e., maneuver clearance and proposal, the automated driving system is responsible to validate that the execution of the maneuver is safe. In August 2022, around the same time of passing the acts in the AFGBV and the StVG, the regulation 2022/1426 of the European Union [95] was put into force. Therein, a so-called remote intervention operator is permitted similar interactions with the automated vehicle as the Technische Aufsicht in the AFGBV and StVG. By the two acts passed in Germany [93, 94] and the European Union [95], remote driving does not seem to be compliant on public roads.

## 1.3 Problem Statement and Thesis Outline

Remote driving can be leveraged as a fallback for an automated driving system. For example, in situations in which the system is not capable to make the next decision or plan the next path to follow, the remote operator can provide support. Similar to the control interface in the vehicle, the remote driving interface consists of a steering wheel and pedals, as shown in Figure 1.1. However, besides the obvious benefits, remote driving presents challenges that raise concerns about safety. In particular, latency, reduced situation awareness, or unstable connectivity pose the risk that the remote operator's control actions are unsafe. The goal of the present work is to contribute to the use of remote driving and introduce shared control in order to safeguard the vehicle and assist the remote operator in the task of obstacle avoidance. For this, it is relied on a functional perception of the automated driving system.

Shared control is introduced as a remote driving concept. In consequence, this term needs to be differentiated. In the remainder of the present work, remote driving without any assistance and involvement of an automated driving system will be referred to as direct control. In contrast to this, in shared control, the remote operator and the automation are performing the dynamic driving task collaboratively. This is shown in Figure 1.5, which was inspired by Flemisch et al. [96]. It is noted that shared control designs can also be differentiated in terms of how the control commands are coupled. As the title of the present work suggests, the focus of the designs in the present work lies on the uncoupled shared control mechanism in which the automation has the capability to uncouple and correct the remote operator's control commands from the actuators when their execution would pose a risk. This will be described in more detail in the state of the art on shared control in the next chapter.

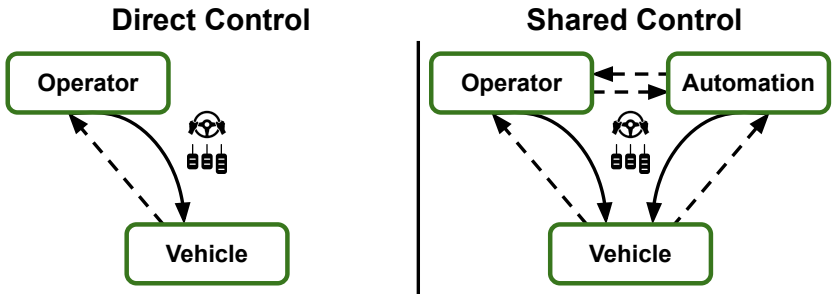


Figure 1.5: Comparison of direct control and shared control as remote driving concepts. Signals for the control commands are depicted by solid arrows. For communication and feedback, dashed arrows are used. In direct control, the operator directly controls the actuators of the vehicle. In shared control, the vehicle control task is shared between the operator and the automation.

The outline of this thesis is provided in Figure 1.6. In Chapter 1, the present work has been introduced and motivated. In Chapter 2, the state of the art is presented. First, an overview of different vehicle teleoperation concepts is given. This is primarily based on the survey that was published by Majstorović, Schimpe et al. [21]. After this, the field of shared control is introduced. Finally, the two research questions of the present work are derived. In Chapter 3, the methodology to answer the research questions is described. Two different shared control designs are introduced. Foundations for these approaches have been published by Schimpe et al. [97, 98]. Both approaches are integrated into a teleoperation system, which was described and published by Schimpe et al. [99, 100]. As will be described in Chapter 4, the designs have first been validated in simulation. Chapter 5 then presents an experimental user study that has been carried out. First, an overview of the study design is given. After this, the results, providing the input to answer the research questions, are described. Finally, the present work is concluded with the discussion in Chapter 6 and the conclusion with an outlook on future work in Chapter 7.

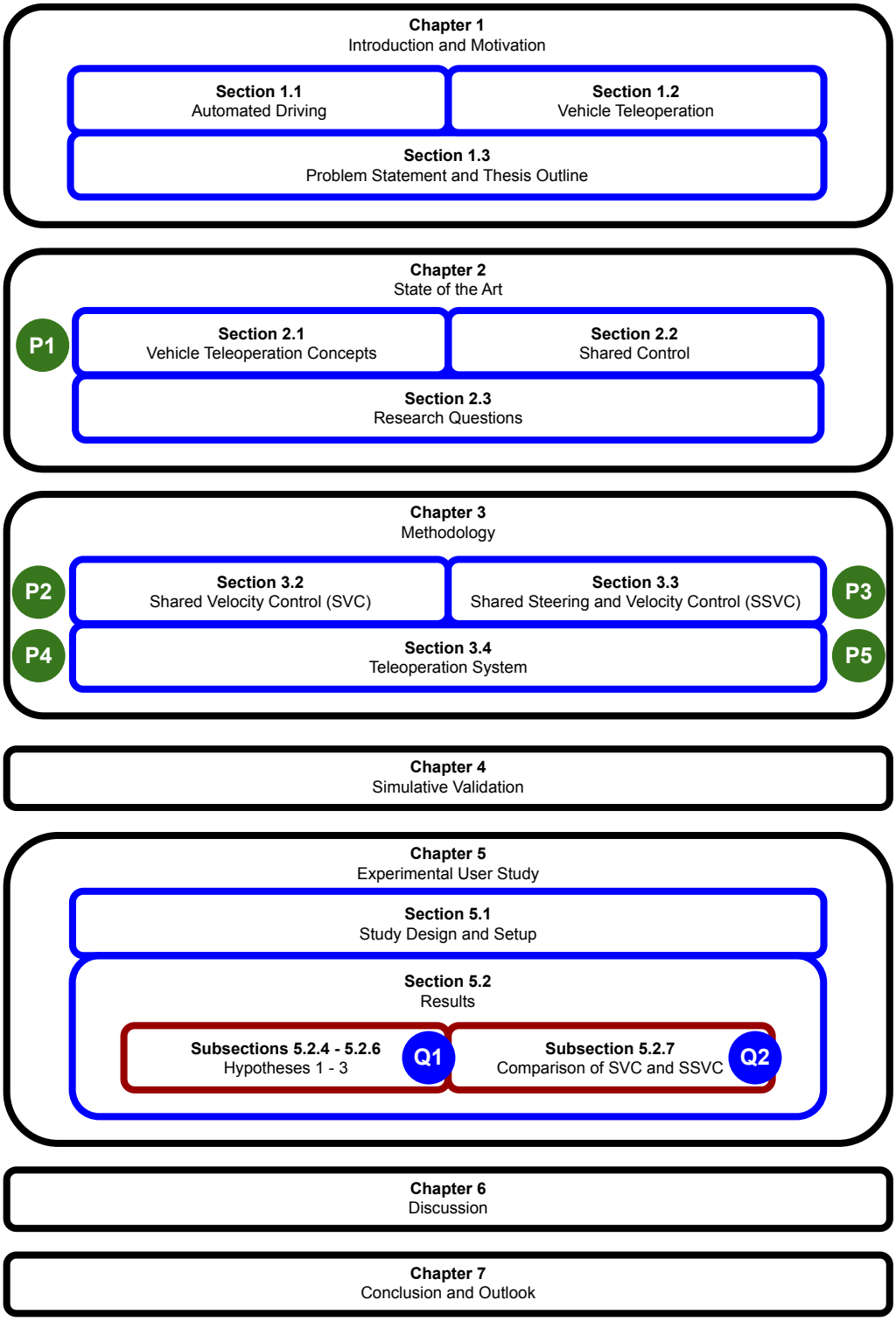


Figure 1.6: Thesis outline. Chapters, sections, and subsections are depicted as black, blue, and dark red boxes, respectively. In addition, the five publications [21, 97–100], which were published (P) in first or shared first authorship on a certain topic of a section are marked by green circles. Similarly, blue circles mark subsections that yield the results answering a research question (Q) of the present work.

# 2 State of the Art

In Chapter 1, an introduction to automated driving and the teleoperation of vehicles was given. It was derived that the application of direct control, as one concept of remote driving, raises safety concerns. Based on this, the introduction of shared control, as a remote driving concept that improves safety, was formulated as the goal of the present work. In this chapter, the state of the art is presented. First, different vehicle teleoperation concepts from the literature are introduced. Second, the research field of shared control is described and different shared control designs are classified. Finally, the two research questions of the present work are derived.

## 2.1 Vehicle Teleoperation Concepts

As introduced in the previous chapter, vehicle teleoperation technology is developed with various objectives and techniques to enable remote support for automated vehicles [101, 102]. To cope with the multitude of automated driving system fail cases, different teleoperation concepts have been proposed in literature throughout the years. These concepts make various assumptions about the functionality of modules in the automated driving system. It is noted that creating a consistent method to illustrate and differentiate them in any possible detail is challenging. The figures and descriptions in the present work are only one way of presenting the concepts in an abstract and clear way.

In shared first authorship, the presented survey has initially been described and published by Majstorović, Schimpe et al. [21]. Shortly after this publication, another survey on the remote operation of road vehicles has been published by Amador et al. [103]. While the primary focus of [21] lies on the technical functionality of the teleoperation concepts, the scope of the review in [103] is broader. Nevertheless, when it comes to the categorization of comparable concepts into remote assistance and remote driving at a high level, the understanding is in line.

Taken and adapted from [21], a graphical overview of the teleoperation concepts is shown in Figure 2.1. In the bottom part, the simplified functionality of an automated driving system, as introduced in Section 1.1, is depicted. Above, the reviewed teleoperation concepts, as they relate to the automated driving system pipeline, are illustrated by denominated bars. The position and width of each bar correspond to the functionality at a high level. This means that a teleoperation concept, which spans over one or more modules of the automated driving system, either enables a remote interaction with these modules or replaces them. In case modules are replaced, the respective tasks from the automated driving system are either performed in collaboration by the remote operator and automation from the teleoperation concept or by the remote operator alone. To keep the illustration clear, these details have not been incorporated in Figure 2.1.

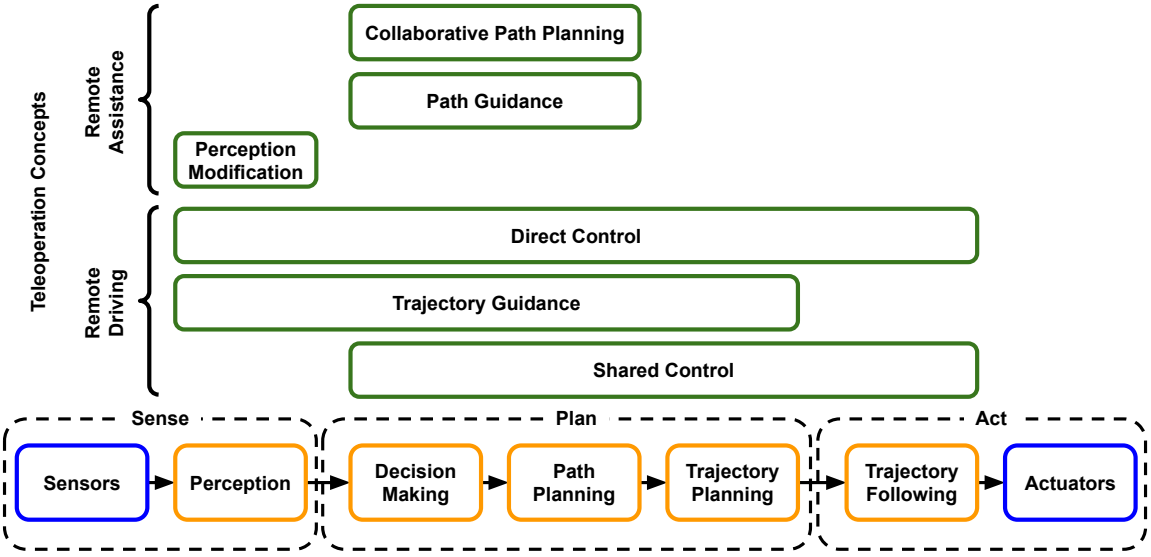


Figure 2.1: Overview of vehicle teleoperation concepts, taken and adapted from Majstorović, Schimpe et al. [21]. At the bottom, the simplified architecture of an automated driving system with the contained modules is shown. Above, the concepts are displayed. The position and width of each denominated bar, spanning over one or more modules of the automated driving system, indicate which modules are replaced or can be interacted with through the respective concept.

Grouped into remote assistance and remote driving, the concepts are reviewed and described in more technical detail in the following. To display the aforementioned details on the allocation of driving tasks across the remote operator and the automation, a new illustration, inspired by Flemisch et al. [104], is introduced for each concept. Therein, the automated driving system modules decision making and path planning are located at the tactical level of the dynamic driving task. Trajectory planning and following make up the operational level. For brevity, the strategical level as well as the perception, which is assumed to be performed by the remote operator and the automation, are not displayed.

### 2.1.1 Remote Assistance

In this section, three concepts for remote assistance are introduced. Through these, the remote operator can assist the automated driving system in an event-driven manner at the tactical level of the dynamic driving task. For example, the remote operator can support in making a decision or give a hint on how to classify an object. As the interaction of the remote operator is not continuous, remote assistance concepts have less strict requirements on the quality of the network service as the remote operator is not involved at the operational level of the dynamic driving task.

#### Collaborative Path Planning

In the collaborative path planning concept, the remote operator takes over decision making, while the automated driving system retains the responsibility for path planning at the tactical level as well as the complete operational level, as shown in Figure 2.2. In Figure 2.3, an example illustrates the idea. Adapted to this concept, the automation proposes several paths, which it can execute. These are shown to the remote operator, who selects one of them.

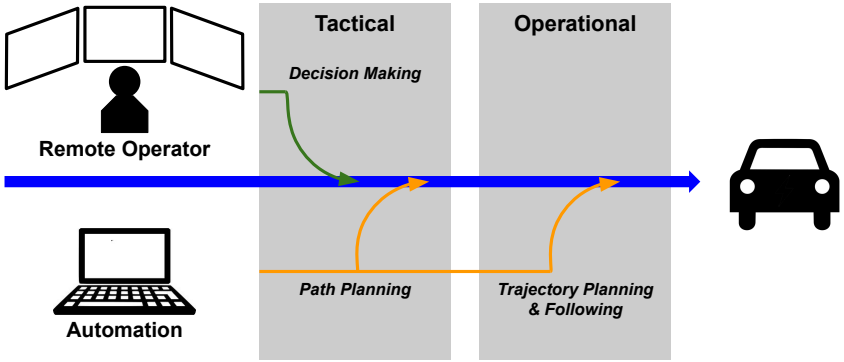


Figure 2.2: Allocation of dynamic driving subtasks for the collaborative path planning concept. The remote operator takes decisions at the tactical level. The automation retains the responsibility for path planning at the tactical level as well as trajectory planning and following at the operational level.

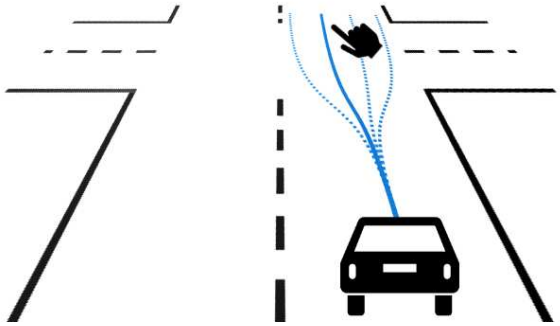

Figure 2.3: Illustration of the collaborative path planning concept, taken and adapted from Majstorović, Schimpe et al. [21]. The automation is computing and suggesting multiple paths to the remote operator, who chooses one of them.

In the context of vehicle teleoperation, collaborative path planning was initially proposed as interactive path planning by Hosseini et al. [105] and later extended by Schitz et al. [106]. Majstorović et al. [107] described another variant of collaborative path planning. Instead of computing path proposals in the drivable area, the automated driving system suggests decisions based on relaxations of operational design domain restrictions.

## Path Guidance

Path guidance is a remote assistance concept in which the remote operator takes over both tasks at the tactical level of the dynamic driving task, as shown in Figure 2.4. As illustrated in Figure 2.5, the remote operator typically specifies waypoints through mouse clicks or a touchpad on a perspective view of camera images or a top-down view, e.g., showing a map. Before transmission to the vehicle, these waypoints are used to create a path, e.g., through interpolation. It is then the responsibility of the automated driving system to perform the operational level of the dynamic driving task, i.e., plan and follow local trajectories in order to execute this plan.

Different variants of path guidance have been showcased and proposed in the literature. Referred to as indirect control, a basic implementation has been shown in the project 5GCroCo [108]. In the work by Schitz et al. [109], the specified waypoints are not used to create a path, but a corridor in which the automated driving system performs trajectory planning in an automated manner. By driving a simulated vehicle in a virtual environment, waypoints are created in the concept by Björnberg [110]. Imitating these actions, the automated vehicle follows the recorded path. Finally, in video demonstrations, path guidance variants have also been shown by the companies Zoox [33], Cruise [34] and Motional [40]. This shows that this remote assistance concept is also well-established in the automated vehicle industry.

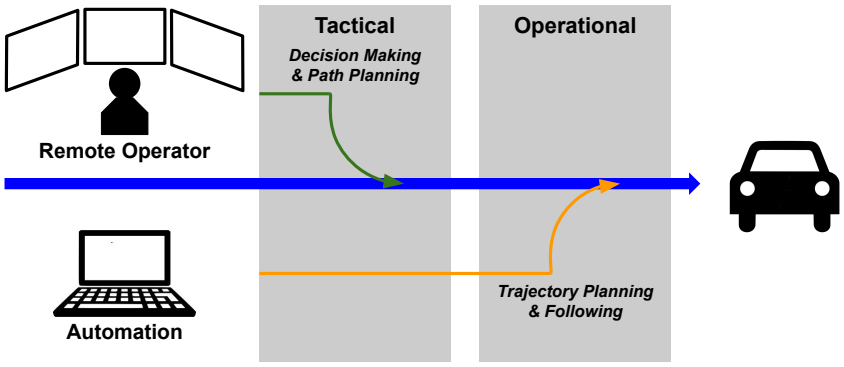


Figure 2.4: Allocation of dynamic driving subtasks for the path guidance concept. The remote operator makes decisions and plans desired paths at the tactical level. The automation remains in charge of trajectory planning and following at the operational level.

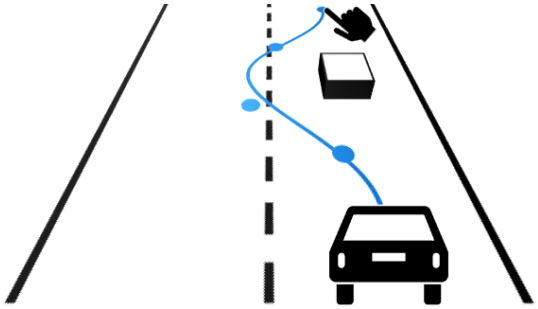

Figure 2.5: Illustration of the path guidance concept, taken from Majstorović, Schimpe et al. [21]. The remote operator is guiding the vehicle by specifying waypoints. These are connected to a path, which is then followed by the automation.

## Perception Modification

With the objective to assist the perception module of the automated driving system, the concept of perception modification has been described in the literature by Feiler and Diermeyer [111, 112]. The concept is illustrated in Figure 2.6, taken from Majstorović, Schimpe, et al. [21]. As perception modification does not involve the remote operator in the dynamic driving task, the method to allocate the dynamic driving subtasks across the remote operator and the automation is not applicable.

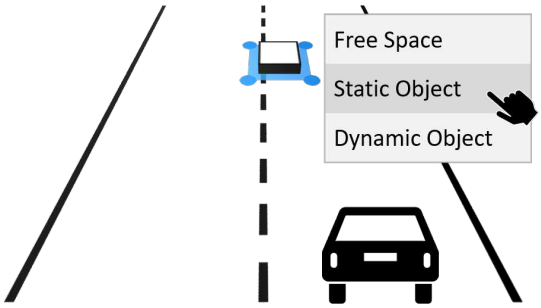


Figure 2.6: Illustration of the perception modification concept, taken from Majstorović, Schimpe et al. [21]. Perception data, e.g., object lists and grid maps, are visualized to the remote operator. Based on this, the remote operator assesses the situation and assists the automated driving system, e.g., by labeling an area as free space or an object as static.

Potential use cases of perception modification include false positive detections, or indeterminate and neglectable objects that hinder the automated vehicle to continue driving. In order to resolve such situations, perception data, e.g., object lists and grid maps are transmitted from the vehicle and visualized to the remote operator in addition to video streams. Provided with these data, the remote operator can assess the situation and provide assistance, e.g., by labeling an area as free space. This information is then transmitted back to the vehicle, where the automated driving system incorporates this information accordingly. The company Zoox showcased a variant in their TeleGuidance demonstration [33], classifying an object as static.

### 2.1.2 Remote Driving

In remote driving, the remote operator is also getting involved at the operational level of the dynamic driving task. Given different degrees of collaboration with the automation, three different remote driving concepts are differentiated in the present work. These are introduced in the following.

#### Direct Control

The most fundamental and prominent remote driving concept is direct control. The allocation of dynamic driving subtasks is illustrated in Figure 2.7. As described in Section 1.2, the remote operator uses a steering wheel and pedals, or a joystick to continuously create lateral and longitudinal motion control commands. The remote operator is taking over the complete dynamic driving task. The automation is not involved.

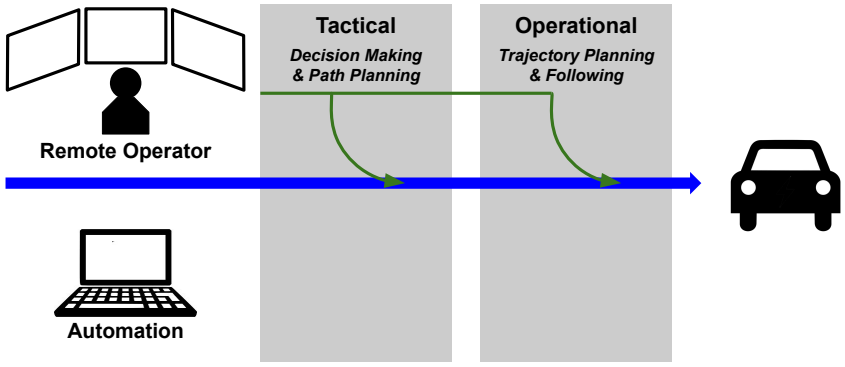


Figure 2.7: Allocation of dynamic driving subtasks for the direct control concept. The remote operator is taking over all subtasks at the tactical as well as the operational level. The automation is not involved.

Given a long history, the direct control concept is the subject of numerous publications and has reached a high level of maturity. Dating back to 1997, a description of a direct control setup for small, urban carsharing vehicles with a focus on the hardware is given by Benoussan and Parent [113]. Since then various systems for direct control were described, e.g., to remotely drive a truck [114], an off-road combat vehicle [115], a physical miniature vehicle [116], the driving simulator CARLA [117, 118], or a full-size passenger vehicle [119].

#### Trajectory Guidance

As shown in Figure 2.8, in the trajectory guidance concept, the remote operator is taking over all tasks at the tactical level as well as trajectory planning at the operational level of the dynamic driving task. The automated driving system is responsible for performing trajectory following. This relieves the remote operator from the latency-critical low-level control task of stabilizing the motion of the vehicle. As can be seen in Figure 2.1, another advantage of the trajectory guidance concept is that it does not rely on a functional perception of the automated driving system. All the planning, including the velocity profile, as illustrated in Figure 2.9, is performed by the remote operator.

Several trajectory guidance variants have been proposed in the literature. As early as 1995, a trajectory guidance concept has been described by Kay and Thorpe [120], associating a discrete waypoint sequence with a desired velocity, which is strictly followed by the vehicle. Gnatzig et al. [121] propose a concept in which the remote operator provides one trajectory segment at a time. The vehicle follows this trajectory and stops at the end if no further segment has been received. Another concept has been described by Hoffmann et al. [122]. In this, the remote operator's control commands, provided through a steering wheel and pedals, are continuously converted into desired trajectories that end at a standstill. This allows for dynamic adaptation of the desired vehicle motion. However, the level at which the remote operator is decoupled from the vehicle stabilization task is reduced. Another trajectory guidance concept is mentioned by Jatzkowsi et al. [123]. However, no further details on how these trajectories are specified are given. Finally, a more advanced design has been presented by Zhang et al. [124]. Also incorporating delay compensation, a long short-term memory is used to predict the remote operator's intended trajectory, based on LiDAR point clouds and control commands from the remote operator. This trajectory is then followed by the automated driving system.

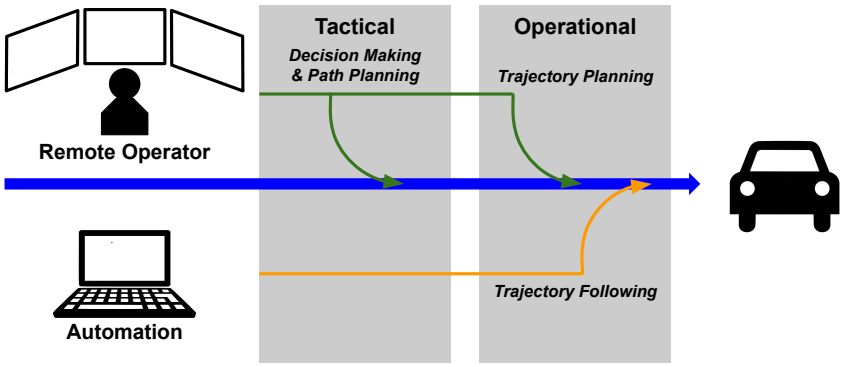


Figure 2.8: Allocation of dynamic driving subtasks for the trajectory guidance concept. The remote operator is performing all tasks at the tactical level as well as the trajectory planning at the operational level. The automation is responsible for trajectory following at the operational level.

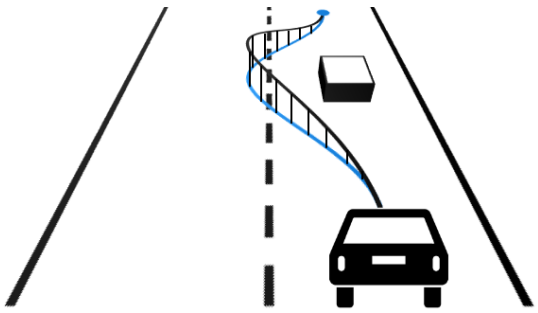

Figure 2.9: Illustration of the trajectory guidance concept, taken from Majstorović, Schimpe et al. [21]. The remote operator is guiding the vehicle by specifying a trajectory, which is followed by the automation.

## Shared Control

To conclude the review on remote driving concepts, shared control for vehicle teleoperation is introduced. In recent years, this emerged as a concept that copes with the inherent safety concerns related to the direct control concept. Li et al. [125] describe that shared control for teleoperation in general promises "great benefits [when] combining the human intelligence with the higher power/precision abilities of robots". Vreeswijk et al. [126] also sees the potentials of shared control in remote support.

Shared control approaches work with an environment model. The assumption is that the perception module of the automated driving system is functional, as shown in Figure 2.1. The control interface for the remote

operator is a steering wheel and pedals for generating lateral and longitudinal motion control commands, respectively. These are transmitted to the vehicle, where the shared control approach is capable of uncoupling them from the actuators of the vehicle. The dynamic driving task involvement of the remote operator and the automation in the case of shared control is shown in Figure 2.10. The remote operator is responsible for the complete tactical level. For the tasks at the operational level, it is collaborated with the automation. As illustrated in Figure 2.11, the primary purpose of shared control in the present work is to support the task of collision avoidance. In the next section, shared control and this focus are introduced in more detail.

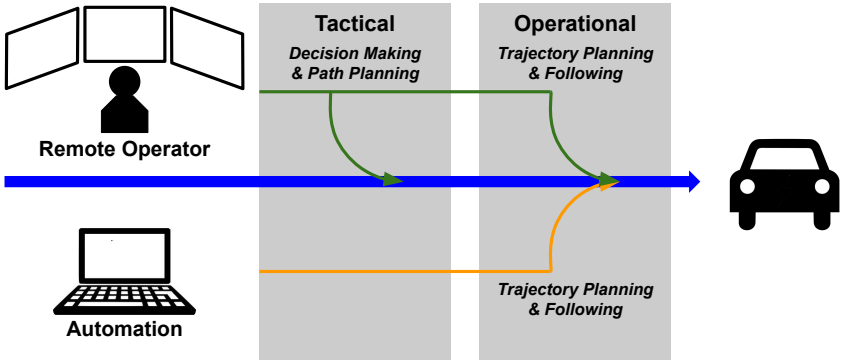


Figure 2.10: Allocation of dynamic driving subtasks for the shared control concept. The remote operator is performing the tasks at the tactical level. At the operational level, the tasks are shared between the remote operator and the automation.

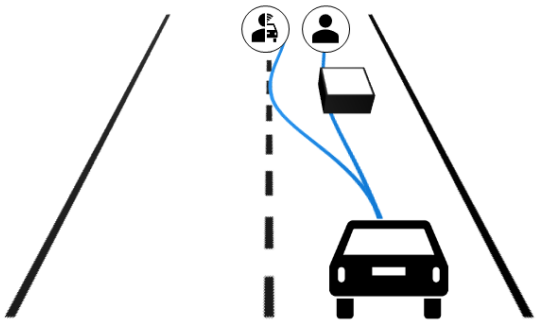

Figure 2.11: Illustration of the shared control concept, taken from Majstorović, Schimpe et al. [21]. The remote operator is driving the vehicle while being assisted in collision avoidance by the automation.

## 2.2 Shared Control

Defined by Sheridan and Verplank [127] in 1978, shared control is “the case where both automation and human work on the same task and at the same time”. It is present in various robotics domains. For instance, it has been applied to the case of an operator remotely controlling a robotic arm in space in collaboration with a co-automation system [128, 129]. Further prominent shared control applications are the control of aircraft and highly-automated vehicles [130]. The latter is the primary focus of the present work. In this context, Li et al. [131] motivate shared control by stating that it “incorporates the capabilities of human drivers into vehicle control. This largely expands the scope of situations that the automation can handle”.

Research on shared control for automated vehicles has a long history. In 2003, not long after the description of the first automated driving systems by Dickmanns [3], Flemisch et al. [132] introduced the popular Horse-Metaphor, in short H-Metaphor, to provide an intuition for sharing control with an automated vehicle. In comparison to riding a horse, several similarities are described. For instance, a horse has eyes, while an

automated vehicle is equipped with sensors in order to perceive its surroundings. This enables a horse and an automated vehicle to navigate safely, i.e., avoid obstacles with a certain level of autonomy. The commands of a driver, i.e., steering or acceleration can be compared to the commands of a rider who guides the horse, e.g., using the reins. After all, as shown in Figure 2.12, Flemisch et al. [133] considered shared control as the sharp end of the cooperation between human and machine at the operational level of the dynamic driving task. Besides shared control, as several previously introduced teleoperation concepts showed, cooperation is also possible at the strategic and the tactical level in the form of cooperative guidance or supervisory control.

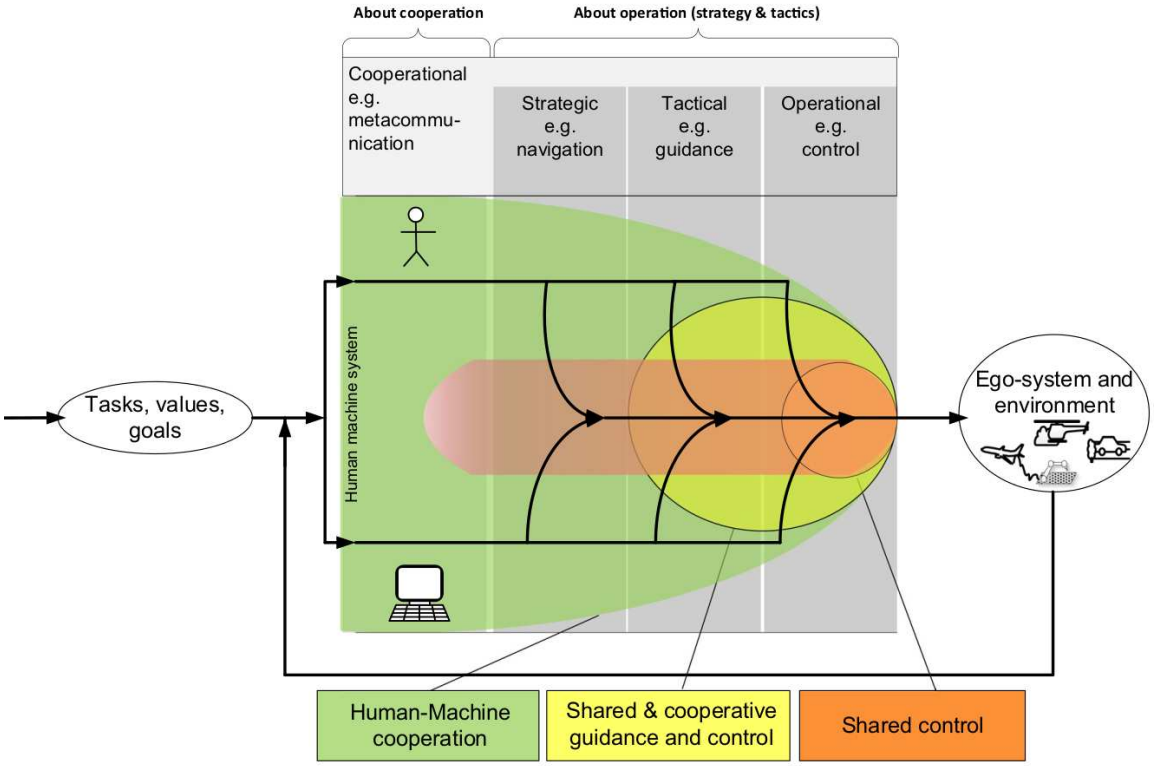


Figure 2.12: Illustration of human-machine cooperation at different levels of the driving task, taken from Flemisch et al. [133]. While humans and machines can also cooperate at the strategic or tactical levels, e.g., in the navigation or the guidance of the vehicle, shared control takes place at the operational level of the dynamic driving task.

Interest in research on shared control for automated vehicles is on the rise. For instance, as part of the SAE Demo Days held in the United States in 2019 that showcased automated vehicle technology to the public, a survey was carried out. Therein, it was found that “92% [of the people asked] want to have control shared between human and self-driving [cars]” [134]. Furthermore, Marcano et al. [135] presented a survey on shared control of automated vehicles, which shows this trend of increasing interest in the published literature. This review has been of great inspiration to classify the present work and put it into context.

When designing a shared control framework for automated vehicles, certain design principles should be followed. In [135], a proposal is given. First, a bidirectional communication channel should be established between the operator and the automation. Second, if it is deemed safe, the intentions of the operator should be followed by the automation. Third, only if the automation recognizes the presence of a risk should it assist the operator in proportion to this. Fourth and last, the assistance for the operator can be either active or passive. These design principles describe a conservative layout for the development of shared control frameworks. However, with increasingly mature autonomy, the automation can also have individual intentions. If these are communicated properly and accepted by the operator, the automation can also be the leader in certain control tasks. In the present work, shared control is applied to avoid obstacles and improve the safety of the teleoperated vehicle. Besides this, the automation does not have a superior objective, which could

evolve into individual intentions. Hence, the design principles in [135] are considered applicable. However, different points of view are possible, in particular around the use case for shared control as well as the maturity of the automation.

In the following, a methodology for classifying literature on shared control for automated vehicles is described. Based on this, a more detailed review of works on shared control approaches that can uncouple the operator's control commands for obstacle avoidance is presented. In this section, the reviewed literature is not limited to the field of teleoperation. For this purpose, the term operator is used as an umbrella term for the human driver in the vehicle as well as the remote operator, controlling the vehicle remotely.

### 2.2.1 Classification

In this section, a high-level overview is given of the research field of shared control for automated vehicles. In Figure 2.13, the approach for classifying shared control designs, as proposed in [135], is shown. In the first layer, there are the use cases for shared control. In the second layer, it is distinguished between different shared control coupling mechanisms. In the third and last layer, it is differentiated between methods that do or do not make use of a model for the operator. In the following, each layer, with the focus of the present work marked in green in Figure 2.13, is introduced. The relevant literature for this focus is then reviewed in more technical detail in the next section.

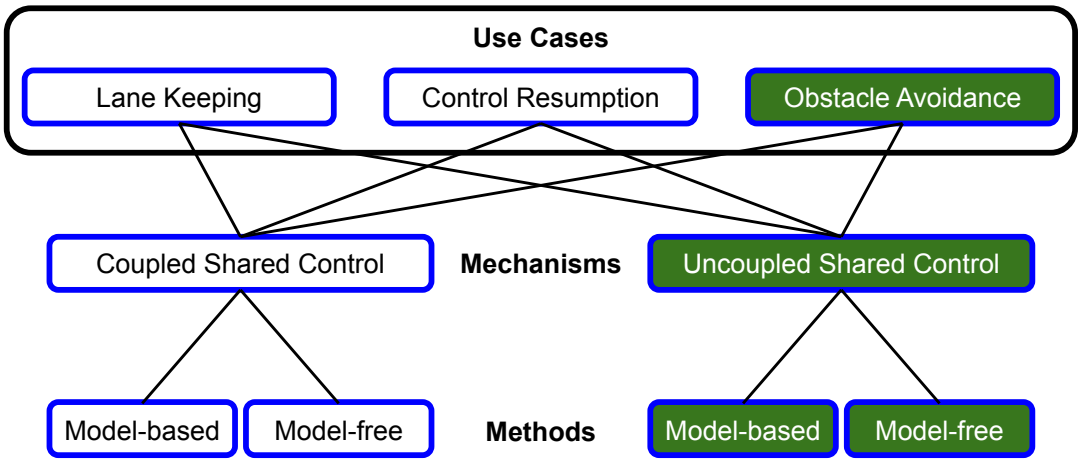


Figure 2.13: Layers to classify shared control approaches. The classification is divided into three layers. At each layer, the focus of the present work is marked in green.

#### Use Cases

There are three main use cases for shared control. The first and most prominent is the lane keeping use case, e.g., tackled in [136–139]. In this case, the support from the automation has different objectives, e.g., the enhancement of lane tracking performance or the prevention of lane departure. The second use case for shared control of automated vehicles is the resumption of the vehicle control task by the operator after it has been performed by the automated driving system. With the primary focus of enabling smoothness and safety of the handover, examples of works on this include [140–144]. Although it is not the focus of the present work, it is noted that the control resumption use case is of great interest for vehicle teleoperation. Enabling a transition between automated driving and remote driving without the automated vehicle coming to a stop, can significantly increase the efficiency of an intervention through teleoperation. The third use case for shared control is obstacle avoidance. This is the use case that is the most relevant to the present work. In consequence, this literature is the focus of the review in the following section.

## Interaction Mechanisms

There are various mechanisms to describe the interaction between the remote operator, the automation, and the vehicle [145]. Following [135], the coupling schemes in the present work are differentiated at a high level between coupled shared control and uncoupled shared control. These schemes are depicted on the left and the right in Figure 2.14, respectively. This differentiation is common. For instance, Li et al. [125] describe the same mechanisms as state-guidance shared control and state-fusion shared control.

In coupled shared control, the operator and the automation are acting on the same mechanically coupled interface to control the vehicle. Usually, the automation is providing support and haptic feedback for the operator. The aforementioned works [136–139] are categorized as coupled shared control designs. To be specific, these works are only sharing the control task of the lateral motion through steering. Only a few works consider coupled shared control of the longitudinal motion, i.e., the operator and the automation are acting on mechanically coupled pedals. To name a few, there are works assisting the operator in the tasks of car-following [146], eco-driving [147], and vehicle stabilization [148].

In uncoupled shared control, also referred to as indirect shared control [131, 149, 150], the commands from the operator are input to the automation. While uncoupling of the automation is also technically possible, uncoupled shared control only refers to the uncoupling of the operator in the present work. Such designs are only feasible in drive-by-wire systems. In a remote driving system, this condition is fulfilled. To introduce shared control for active safety, uncoupled shared control designs for obstacle avoidance become the focus of the present work.

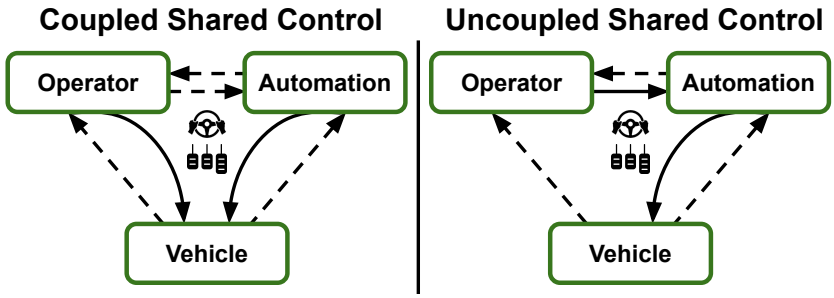


Figure 2.14: Shared control coupling mechanisms. In coupled shared control, the operator and the automation are acting on mechanically coupled actuators of the vehicle. Uncoupled shared control is possible in a drive-by-wire system when the operator's commands are uncoupled from the vehicle through the automation.

## Methods

The minimization of conflict between the operator and the automation is of great importance in shared control. Affecting the operator's acceptance when using the assistance, this motivates model-based methods, which incorporate a model of the operator. Using this, future actions can be anticipated and accounted for in the actions of the automation [135]. For lateral motion, a popular choice is the two-point preview driver model [151]. This is based on the assumption that operators use a near and a far vision of the roadway for steering. Flad et al. [139] uses an alternative model, which is based on the concept that the operator's behavior for steering consists of a finite set of motion primitives. In the shared control design, it is then anticipated which motion primitive is currently executed. One longitudinal motion model that has been widely used is the intelligent driver model [152]. With this, the longitudinal motion control actions of an operator are anticipated based on the following distance to a preceding vehicle.

Model-free approaches, such as the aforementioned works on control resumption [140, 141], are not incorporating the operator's future actions. Instead, the automation acts independently and the control commands are fused later in the shared control framework [135].

### 2.2.2 Uncoupled Shared Control for Obstacle Avoidance

As the related use case for the present work, literature on uncoupled shared control approaches for obstacle avoidance is reviewed. Several works and their approaches are presented as well as how they are validated and potentially evaluated in user studies. Since the focus is exclusively on uncoupled shared control, the distinction from coupled shared control will be neglected and the term “uncoupled” will be omitted in many cases throughout the remainder of this thesis for brevity. This means that shared control refers to uncoupled shared control unless otherwise stated.

In literature, two techniques for uncoupling the operator’s commands are well-established. To refer to them in the following review, these are introduced briefly. In the first technique, the authority can be allocated adaptively, i.e., arbitrated using a weight metric $\lambda \in [0,1]$. For instance, its computation can be based on the present risk of the vehicle. With the general control inputs of the operator $\boldsymbol{u}_\mathrm{o}$ and the automation $\boldsymbol{u}_\mathrm{a}$, the control input for the vehicle $\boldsymbol{u}_\mathrm{v}$ is computed by

$$\boldsymbol{u}_\mathrm{v} = (1-\lambda)\,\boldsymbol{u}_\mathrm{o} + \lambda\,\boldsymbol{u}_\mathrm{a}. \tag{2.1}$$

With this, $\boldsymbol{u}_\mathrm{v}$ can deviate from $\boldsymbol{u}_\mathrm{o}$ depending on $\lambda$. This concept is also referred to as arbitration-based shared control [135, 153], weighted combination [125], the coupling valve [154] or blended shared control [155, 156]. If $\lambda$ switches between its two extreme values 0 and 1, i.e., control is fully owned by either the operator or the automation, the control paradigm is referred to as traded control [133] or phase-switching [125].

In the second uncoupling technique, the automation control commands are directly taken as the commands for the vehicle, i.e., $\boldsymbol{u}_\mathrm{v} = \boldsymbol{u}_\mathrm{a}$. It is then one of the automation objectives to track the operator’s commands when possible. In this case, a cost function term $J_u$ can be given by

$$J_u = (\boldsymbol{u}_\mathrm{a} - \boldsymbol{u}_\mathrm{o})^2. \tag{2.2}$$

Its minimization becomes part of the shared control problem, which is solved through an optimization procedure with $\boldsymbol{u}_\mathrm{a}$ as a decision variable. Its result can yield commands which deviate from the operator’s commands. This uncoupling technique has also been referred to as input correction [125].

In the present work, it is differentiated between three uncoupled shared control design variants. Depending on what control types, i.e., steering and velocity, are shared between the operator and the automation, the variants are named shared steering control, shared velocity control, and shared steering and velocity control. This is shown in the overview in Figure 2.15. In the following, the variants are reviewed one by one.

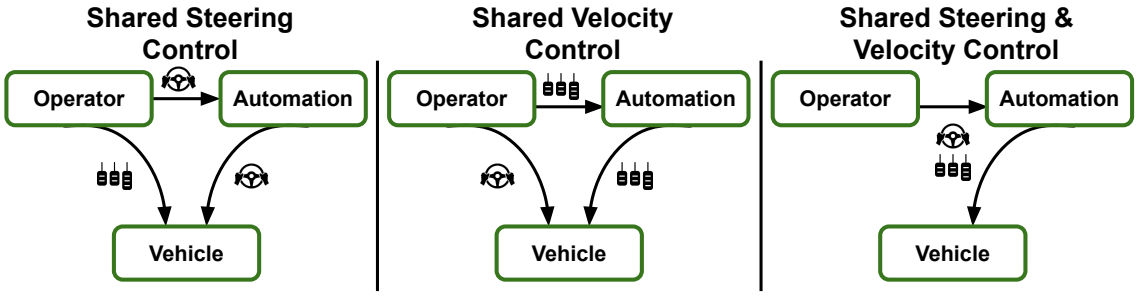


Figure 2.15: Uncoupled shared control design variants. The arrows with a steering wheel or pedals as labels indicate whether the operator’s steering or velocity commands are uncoupled from the vehicle by the automation. For clarity, the feedback signals from the vehicle as well as the communication from the automation to the operator are not shown. The term “uncoupled” is left out for brevity.

## Shared Steering Control

The majority of works address sharing the control of the lateral motion, i.e., the case of shared steering control. An overview of related works for obstacle avoidance is given in Table 2.1. This table presents a total of 16 references that were published in 13 different streams of work. In the following, a summary of these is given concerning different aspects. To start with, the functionality of the automation and how obstacle avoidance is incorporated are described. Then details are given on how the operator is modeled and which uncoupling technique is used. This is followed by descriptions of how the approaches are validated and evaluated, i.e., the performance of simulations, experiments, and user studies. Finally, in this context, it is described if and which modalities of feedback for the operator were provided.

Many of shared steering control approaches apply the method of model predictive control for the automation [157–169]. On the one hand, model predictive control can formulate control objectives such as following a previously planned trajectory. On the other hand, as will be described in more detail in Subsection 3.1.1, it is also applicable for planning collision-free trajectories through the formulation of obstacle avoidance constraints.

There are a number of methods to incorporate obstacle avoidance. The most prominent choice among the reviewed works is the pre-computation of an obstacle-free driving corridor in which the automation computes safe trajectories [157, 158, 165–167, 169]. Also common is the usage of potential field methods that model obstacles and road boundaries as repulsive forces [159, 163, 168, 170]. Other options include the approximation of obstacles using circles and ellipses [161, 162] or grid maps [171].

Several of the reviewed works are making use of a dedicated model for the operator. For instance, fuzzy logic is used to recognize the operator's intentions [159]. In the domain of game theory, Nash and Stackelberg equilibria are computed [160, 164]. Some methods use historic data to pre-train operator models, e.g., using a long short-term memory [171], Gaussian mixture models [172] or the Koopman operator [168]. Several works are categorized as model-free [157, 158, 161–163, 170].

Given the automation and potentially an operator model, the question of how control is shared between the automation and the operator arises. For this, two variants, namely arbitration-based shared control and cost function-based correction of the operator's control actions, were introduced. In the reviewed works, the majority applies a continuous and adaptive, threat-based arbitration technique [157–160, 163, 171, 172]. Some works only consider the extremes to allocate the control authority, i.e., traded control [161, 162, 170]. One work studied different constant arbitration values [164]. As the second-most prominent uncoupling technique, several works incorporate a cost function term that formulates the control objective of minimal automation intervention [165–169]. For completeness, it is noted that this cost function term qualifies an approach as model-based.

There is also a great variety in how the proposed approaches are validated and evaluated. Some works do this in a pure simulative manner [159, 163, 167, 169]. A bigger part of works conducts operator-in-the-loop experiments in either a virtual environment or a driving simulator [160–162, 164, 168, 171]. Few works also conduct real-world experiments with small-scale, ground robots [170, 172] or full-scale vehicles [157, 158, 165, 166].

When an actual operator is in the loop, the design principle of bidirectional communication, i.e., feedback for the operator becomes relevant. The most prominent modality is haptic feedback [161, 162, 165, 166]. One stream of work incorporated haptic and visual feedback [157, 158].

The most extensive way to experimentally validate shared control approaches is a user study. In the works that report this, many compare the performance of the operators when directly controlling the vehicle or with assistance through shared control [157, 158, 160–162, 168]. Some works also studied the effects when using operator models [164, 168] or when incorporating operator feedback [157, 158, 161, 162, 165, 166].

Table 2.1: Literature on uncoupled shared steering control for obstacle avoidance.

| Reference(s) | Description | Validation and Evaluation |
|---|---|---|
| Anderson et al. [157, 158] | **Automation:** Model predictive control-based planning & control in safe corridor<br>**Uncoupling Technique:** Threat-based arbitration | **Setup:** Teleoperation of full-scale vehicle with visual & haptic feedback<br>**Experimental User Study:** Direct control & shared control with & without feedback in scenarios with static obstacles, 20 participants |
| Li et al. [159] | **Automation:** Potential field-based planning & model predictive control-based following<br>**Operator Model:** Fuzzy logic-based intention recognition<br>**Uncoupling Technique:** Threat-based arbitration | **Setup:** Driving in a virtual environment<br>**Simulations:** Scenarios with static & dynamic obstacles |
| Li et al. [160] | **Automation:** Separate planning & model predictive control-based following<br>**Operator Model:** Nash game-based<br>**Uncoupling Technique:** Threat-based arbitration | **Setup:** Driving simulator<br>**Experimental User Study:** Performance indices in overtaking scenarios, 6 participants |
| Bhardwaj et al. [161, 162] | **Automation:** Model predictive control-based planning & control<br>**Uncoupling Technique:** Trading of control to automation in the presence of obstacles | **Setup**: Driving simulator with haptic feedback<br>**Experimental User Study:** Direct, coupled & traded control, 64 participants |
| Yue et al. [163] | **Automation:** Potential field-based planning & model predictive control-based following<br>**Uncoupling Technique:** Threat-based arbitration | **Setup:** Driving in a virtual environment<br>**Simulations:** Scenarios with & without need for automation intervention |
| Liu et al. [164] | **Automation:** Separate planning & model predictive control-based following<br>**Operator Model:** Stackelberg game-based<br>**Uncoupling Technique:** Constant arbitration | **Setup:** Driving simulator<br>**Experimental User Study:** Operator models with & without consideration of neuromuscular delay, 3 participants |
| Erlien, Balachandran et al. [165, 166] | **Automation:** Model predictive control-based planning & control in two safe driving envelopes<br>**Operator Model & Uncoupling Technique:** Cost function term formulating minimal intervention objective | **Setup**: Control of full-scale, steer-by-wire vehicle with haptic feedback<br>**Experimental User Study:** Shared control with & without feedback, 11 participants |
| Gray et al. [167] | **Automation:** Model predictive control-based planning & control in safe corridor<br>**Operator Model:** Preview-based & stochastic<br>**Uncoupling Technique:** Cost function term | **Setup:** Driving in a virtual environment<br>**Simulations:** Scenario with static obstacle |
| Guo et al. [168] | **Automation:** Potential field & model predictive control-based obstacle avoidance<br>**Operator Model:** Data-driven, Koopman operator-based<br>**Uncoupling Technique:** Cost function term | **Setup:** Driving simulator<br>**Experimental User Study:** Direct control, model-free & model-based shared control in overtaking scenarios, 6 participants |
| Chen et al. [169] | **Automation:** Model predictive control-based planning & control in safe corridor<br>**Operator Model & Uncoupling Technique:** Cost function term formulating minimal intervention objective | **Setup:** Driving in a virtual environment<br>**Simulations:** Avoidance of dynamic obstacles in two overtaking scenarios |
| Seppänen et al. [170] | **Automation:** Potential field-based obstacle avoidance<br>**Uncoupling Technique:** Delay- & control-dependent trading of control to automation | **Setup:** Control of small-scale ground robot<br>**Experiments:** Direct control, automated control & traded control |
| Yan et al. [171] | **Automation:** Grid map-based obstacle avoidance<br>**Operator Model:** Long short-term memory-based prediction of operator's steering actions<br>**Uncoupling Technique:** Threat-based arbitration | **Setup:** Driving in a virtual environment<br>**Experiments:** Direct control & shared control |
| Huang et al. [172] | **Automation:** Separate planning of safe control actions<br>**Operator Model:** Gaussian mixture model-based prediction of operator's driving risk<br>**Uncoupling Technique:** Threat-based arbitration | **Setup:** Control of small-scale ground robot<br>**Experiments:** Two scenarios with static obstacles |

## Shared Velocity Control

In the case of shared velocity control, control of the longitudinal motion of the vehicle is shared between the operator and the automation. Summarizing two works, an overview of uncoupled shared velocity control approaches is given in Table 2.2. Adaptive cruise control approaches, e.g., [173–177] are also a case of shared velocity control. However, since the operator can regain control authority immediately when operating the pedals, these works do not qualify as uncoupled shared control and are therefore excluded from this review.

Schweidel et al. [178] propose a contingency model predictive control formulation. With the primary objective of tracking the operator's acceleration commands, modeled using the intelligent driver model [152], the formulation is capable to deviate from these in order to adhere to safety. The design is validated in simulations of two scenarios. These include following a braking vehicle and yielding to cross-traffic at an intersection.

The approach by Schitz et al. [179] follows a similar idea. A model predictive control is presented that tracks the desired velocity from the operator. In order to satisfy constrained longitudinal distances to other vehicles, the approach is capable to deviate from the operator's control actions. Validation is carried out with a full-scale vehicle in urban scenarios during vehicle following as well as yielding to cross-traffic.

Table 2.2: Literature on uncoupled shared velocity control for obstacle avoidance.

| Reference(s) | Description | Validation and Evaluation |
|---|---|---|
| Schweidel et al. [178] | **Automation:** Contingency model predictive control-based planning of safe velocity profiles<br>**Operator Model:** Intelligent driver model<br>**Uncoupling Technique:** Cost function term formulating minimal intervention objective | **Setup:** Driving in a virtual environment<br>**Simulations:** Vehicle following and cross-traffic scenarios |
| Schitz et al. [179] | **Automation:** Model predictive control-based planning of safe velocity profiles<br>**Operator Model & Uncoupling Technique:** Cost function term formulating minimal intervention objective | **Setup:** Control of full-scale vehicle<br>**Experiments:** Vehicle following and cross-traffic scenarios |

## Shared Steering and Velocity Control

To conclude the review on uncoupled shared control for obstacle avoidance, a number of shared steering and velocity control approaches are presented. In these, the automation uncouples the operator's steering and velocity control commands from the vehicle actuators. The overview of the reviewed literature is given in Table 2.3.

Model predictive control is a popular choice for designing the approach and incorporating cost function terms that formulate a minimal intervention objective [180–183]. Tran et al. [184] use another planning variant to minimize the collision probability. In this work, further separate modules monitor the operator and recognize intentions through Hidden Markov Models. The control commands are arbitrated between the operator and the automation based on drowsiness and threat. Cho et al. [185] uncouple the operator's control commands through a long short-term memory. With the primary objective to denoise control commands from unskilled operators, the network is trained with data from an expert operator.

Carrying out simulations and experiments, the reviewed approaches have been validated and evaluated in virtual environments [181–183] and driving simulators [180, 184, 185]. Experiments with operators in the loop have been reported without [184, 185] and with visual feedback [180–182]. Finally, user studies have compared direct control and shared control [180, 185].

Table 2.3: Literature on uncoupled shared steering and velocity control for obstacle avoidance.

| Reference(s) | Description | Validation and Evaluation |
|---|---|---|
| Storms et al. [180] | **Automation:** Model predictive control-based planning & control, following operator's commands<br>**Operator Model & Uncoupling Technique:** Cost function term formulating minimal intervention objective | **Setup:** Teleoperation of small-scale ground robot in driving simulator with visual feedback<br>**Experimental User Study:** Direct control & shared control, 20 participants |
| Schwarting et al. [181, 182] | **Automation:** Model predictive control-based planning & control, following operator's commands & road centerline<br>**Operator Model & Uncoupling Technique:** Cost function term formulating minimal intervention objective | **Setup:** Driving in a virtual environment with visual feedback<br>**Experiments:** Left-turn and overtaking scenarios with dynamic obstacles |
| Weiskircher et al. [183] | **Automation:** Model predictive control-based planning & control, following operator's commands & road centerline<br>**Operator Model & Uncoupling Technique:** Cost function term formulating minimal intervention objective | **Setup:** Driving in a virtual environment<br>**Simulations:** Vehicle following and overtaking scenarios |
| Tran et al. [184] | **Automation:** Optimization-based planning, minimizing collision probability<br>**Operator Model:** Operator monitoring & Hidden Markov Model-based intention recognition<br>**Uncoupling Technique:** Threat- & drowsiness-based arbitration | **Setup**: Driving simulator<br>**Experiments:** Lane departure & obstacle avoidance scenario with drowsy operator |
| Cho et al. [185] | **Automation:** Long short-term memory, trained on expert data<br>**Operator Model & Uncoupling Technique:** Denoising of unskilled operator's control actions | **Setup:** Driving simulator<br>**Experimental User Study:** Direct control & shared control, twelve participants |

## 2.3 Research Questions

In this chapter, different vehicle teleoperation concepts have been introduced. Besides remote assistance concepts that make advanced assumptions about the functionality of the automated driving system, trajectory guidance and shared control were presented alongside direct control as concepts for remote driving. While trajectory guidance yields the advantage of relieving the remote operator from the trajectory following task, i.e., stabilization of the vehicle, the remote operator retains the responsibility of keeping the vehicle safe. The same applies to direct control. In particular, uncoupled shared control designs have the potential to evaluate and possibly correct unsafe control actions from the remote operator. In addition to the benefits for safety, the question arises of how this affects the workload and performance of remote operators in the remote driving task. In consequence, the first research question of the present work is formulated as follows.

*In comparison to direct control, how does uncoupled shared control affect*
*the workload and the performance of remote operators as well as the safety in remote driving?*

Given the existence of three uncoupled shared control design variants, with shared steering control being the most commonly studied, and with few studies for shared steering and velocity control and even fewer for shared velocity control, a need for evaluation of uncoupled shared control design variants for remote driving arises. While some user studies have evaluated shared steering control and shared steering and velocity control against direct control for vehicle teleoperation, no evaluation exists for shared velocity control. Furthermore, no comparison between different uncoupled shared control design variants for obstacle avoidance exists. Therefore, to address these gaps in the literature, the second research question of the present work is formulated as follows.

*Among the possibilities to share control of the steering or the velocity,*
*what is the most suited uncoupled shared control design variant for remote driving?*

With these two research questions being derived, the chapter on the state of the art of vehicle teleoperation concepts and shared control is concluded. In the next chapter, the methodology is presented in order to tackle and answer the research questions.

# 3 Methodology

In the previous chapter, shared control has been introduced as a way to combine the strengths of a remote operator and an automation for the vehicle control task. Also, it has been proposed as a remote driving concept to overcome the safety concerns of direct control. In this chapter, the methodology of the present work to leverage the potentials of shared control in the application of vehicle teleoperation and answer the derived research questions is presented.

Since the inherent challenges of direct control yield the risk that the control actions from the remote operator are not safe at all times, the objective is to improve remote driving from a safety perspective. For this purpose, an automation component is introduced in the system that assists the remote operator in the task of collision avoidance. In particular, uncoupled shared control is capable of ensuring safety as it can always uncouple and correct the remote operator's control actions. As shown in Figure 2.15, there are three different uncoupled shared control design variants. Depending on the design, either the steering, the velocity, or both control commands from the remote operator can be overridden. In the following, the three variants are considered for the collision avoidance task from a theoretical point of view.

In the case of shared steering control, the remote operator is in full control of the longitudinal vehicle motion. Control of the lateral motion through the steering angle is shared between the remote operator and the automation. With this capability, the automation can avoid close collisions with obstacles through little steering angle corrections. Frontal collisions are also preventable. However, these evasions require greater intervention from the automation. Finally, representing a clear limitation of shared steering control are scenarios, such as dead ends, in which collisions can only be avoided through braking. For this reason, this first uncoupled shared control design variant is not considered in the present work.

The second uncoupled shared control design variant is shared velocity control. While the remote operator holds the full control authority to steer the vehicle, control of the velocity is shared between the remote operator and the automation. In contrast to shared steering control, it is evident that the limitation in dead-end scenarios is not present as the automation can always stop the vehicle in front of the obstacle. However, one concern with the sole capability of braking is a scenario in which the remote operator performs unforeseen lateral maneuvers. In particular, these are critical when an obstacle is next to the vehicle and the distance to completely stop the vehicle is insufficient. This implies that the velocity in proximity to obstacles needs to be limited such that there is always enough distance to safely stop the vehicle. This will be accounted for and incorporated in the shared velocity control design that is proposed and analyzed in the present work.

The last and third uncoupled shared control design variant is shared steering and velocity control. Capable of controlling both, obstacles can be avoided through steering angle corrections as well as through braking to a standstill. By its design, aforementioned limitations do not apply. Thus, it is included as the second uncoupled shared control design variant that is analyzed in the present work.

The remainder of this chapter is structured as follows. First, the background to develop the considered uncoupled shared control design variants is introduced. This includes concepts for motion planning and control from automated driving functions as well as the modalities for the remote operator interface, used to communicate the intentions of the automation. After this, the technical implementations of the two considered

uncoupled shared control design variants are presented. The chapter is concluded with a description of how the uncoupled shared control designs are integrated into a teleoperation system. In the following chapters, the two approaches are then validated in simulation and compared against direct control in an experimental user study.

## 3.1 Background

In this section, the background for the two uncoupled shared control designs is presented. First, an introduction to concepts for motion planning and control in an automated driving function is given. After this, the modalities adopted for the feedback to communicate the intentions from the automation to the remote operator are described.

### 3.1.1 Motion Planning and Control

The uncoupled shared control designs in the present work have the primary objective of improving the safety of the teleoperated vehicle, i.e., avoiding collisions with obstacles. For this purpose, the algorithms perform motion planning in order to evaluate if the future vehicle motion is collision-free. To achieve this, several concepts from automated driving functions are adopted.

In general, as was introduced in Section 1.1, the motion of a vehicle is planned as a trajectory, which is a function of vehicle states over time [23, p. 171]. In the following, it is described how the vehicle motion is characterized through a set of model equations and how these are used to perform model-based trajectory planning. Exploiting this, the principle of model predictive control is introduced. Finally, the basics of how to model obstacles for the purpose of performing collision checking for trajectories are described.

#### Vehicle Modeling

Many motion planning algorithms in automated driving functions make use of a vehicle model. This is a set of differential equations that describes the motion as a function of system states and control inputs. For vehicles with four wheels, the simplification to a bicycle, for which two wheels are centered at the front and rear axles, is common practice [186, p. 20].

Vehicles can be modeled with respect to their kinematics or dynamics. Assuming that the vehicle tires do not slip, a kinematic model only has geometrical considerations. This is accurate for low velocities up to 5 m/s [187]. For higher velocities, a dynamic vehicle model that takes slip into account becomes necessary. This describes the motion of the vehicle through the forces that act on the tires [186, p. 88]. However, this requires an accurate model for the tires themselves. Options include a linear tire model, the Brush tire model [186, p. 361] or the Pacejka tire model [188], which require the identification of several parameters, e.g., the cornering stiffness.

Overall, the choice and fidelity of the vehicle model depend on the use case. As only low velocities are considered for vehicle teleoperation in the present work, it is deemed appropriate to make use of the kinematic vehicle model. Its system parameters, which are described in the following, can easily be measured and identified.

The kinematic bicycle model with a steerable front wheel is shown in Figure 3.1. Therein, the center of mass is located at its position in $x$ and $y$. The distance from the center of mass to the front and rear axles are given by $l_\mathrm{f}$ and $l_\mathrm{r}$. The heading of the vehicle and the steering angle at the front wheel are denoted by $\theta$ and $\delta$. Lastly, the side-slip angle and the velocity of the center of mass are given by $\beta$ and $v$.

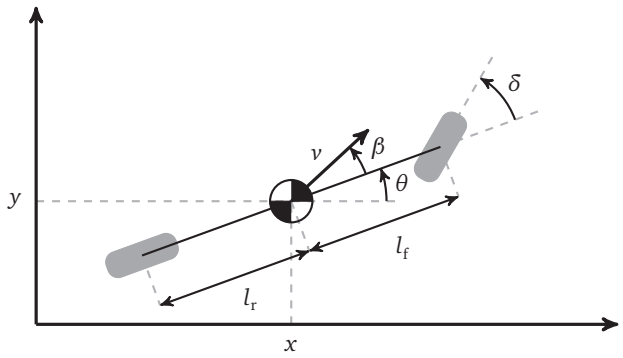


Figure 3.1: Notation of the kinematic bicycle model with a steerable front wheel. With the distances $l_f$ and $l_r$, the center of mass lies at the position $x$ and $y$ between the front and rear wheel. The velocity, heading angle, steering angle, and side-slip angle are denoted by $v$, $\theta$, $\delta$, and $\beta$, respectively.

Through geometric considerations, the differential equations of the kinematic bicycle model can be derived. Given a constant steering angle, the center of mass is traveling on a circular trajectory with a constant radius. Thereby, the position of the center of mass in $x$ and $y$ is changing by

$$\dot{x} = v\,\cos(\theta + \beta) \tag{3.1}$$

and

$$\dot{y} = v\,\sin(\theta + \beta). \tag{3.2}$$

The rate of change of the heading angle $\theta$ is computed by

$$\dot{\theta} = \frac{v}{l_r}\,\sin(\beta). \tag{3.3}$$

With dependence on the steering angle $\delta$, the side-slip angle $\beta$ is given by

$$\beta = \arctan\left(\frac{l_r}{l_f + l_r}\,\tan(\delta)\right). \tag{3.4}$$

For the kinematic bicycle model, the system states are summarized in the state vector $\boldsymbol{z}$, given by

$$\boldsymbol{z} = [x,\ y\ ,\theta\ ,\delta\ ,v]^T. \tag{3.5}$$

The control inputs $\boldsymbol{u}$ are summarized by

$$\boldsymbol{u} = [\dot{\delta},\ a]^T, \tag{3.6}$$

where $a$ denotes the longitudinal acceleration, i.e., the derivative of $v$. As mentioned before, the center of mass is traveling on a circular trajectory for a constant steering angle. Its curvature is denoted by $\kappa$ and computed by

$$\kappa = \frac{\sin(\beta)}{l_r}. \tag{3.7}$$

In a steady state, this can be used to calculate the lateral acceleration of the vehicle $a_{\text{lat}}$, which is given by

$$a_{\text{lat}} = \kappa\, v^2. \tag{3.8}$$

In addition to the kinematic bicycle model, the one-dimensional point mass model with the jerk as input is used in the present work. For brevity, given its simple equations, its description is left out here and will be given later.

## Model-based Trajectory Planning

A trajectory is a function of the system states $\boldsymbol{z}$ over time $t$, starting at some initial state $\boldsymbol{z}_0$ [23, p. 171]. In order to perform model-based trajectory planning, the system states are integrated over time.

Strictly speaking, a trajectory is time-continuous. However, in algorithms and their implementation, the functions are discretized in time as a finite set of trajectory points. The transition between trajectory points is calculated through implicit or explicit numerical integration schemes. Different explicit variants include the Runge-Kutta methods of orders 1 or 4 [189]. In the present work, the order 1 method, which is also referred to as Euler's method, is used for numerical integration. Given the differential system of model equations $\dot{\boldsymbol{z}} = \boldsymbol{f}_{\mathrm{mdl}}(\boldsymbol{z}, \boldsymbol{u})$, its formula is given by

$$\boldsymbol{z}_{i+1} = \boldsymbol{z}_i + t_\mathrm{s}\, \dot{\boldsymbol{z}}_i = \boldsymbol{z}_i + t_\mathrm{s}\, \boldsymbol{f}_{\mathrm{mdl}}(\boldsymbol{z}_i, \boldsymbol{u}_i), \tag{3.9}$$

with the discretization step $i$ and the sampling, i.e., discretization time of the trajectory $t_\mathrm{s}$.

With Euler's method, a trajectory can be planned through forward integration. For this, Equation (3.9) is recursively evaluated by incrementing $i$ over an arbitrary number of discretization steps $n$. Hence, applying a sequence of control inputs $\boldsymbol{u}^{n-1}$, given by

$$\boldsymbol{u}^{n-1} = \{\boldsymbol{u}_0, \boldsymbol{u}_1, \dots \boldsymbol{u}_{n-1}\}, \tag{3.10}$$

yields a sequence of states $\boldsymbol{z}^n$, given by

$$\boldsymbol{z}^n = \{\boldsymbol{z}_0, \boldsymbol{z}_1, \dots \boldsymbol{z}_n\}. \tag{3.11}$$

Finally, this represents a discretized trajectory, obtained through model-based planning over the time horizon $t_\mathrm{h} = n\, t_\mathrm{s}$.

## Model Predictive Control

Model predictive control is a well-known, model-based planning and control strategy that has been used for various purposes, including shared control formulations. Given its flexibility, coping with control objectives and constraints at the same time, it is also used for the uncoupled shared control approaches in the present work. In this section, concepts of model predictive control are described. However, these are kept brief as there exist many sources on model predictive control theory already, e.g., the textbooks from Camacho and Bordons [190] or Rawlings et al. [191].

In model predictive control, from the current state of the system, future states are predicted over a certain time horizon, yielding a trajectory prediction. With the sequence of states and control inputs as decision variables, an optimization problem is solved at each sampling instant. In this optimization problem, control objectives subject to a system model and other constraints are formulated. The capability to combine objectives and constraints into one control law represents one of the core strengths of model predictive control. Finally, solving the optimization problem yields optimal state and input sequences. Usually, the first input of this sequence is applied to the actual system. At the next sampling instant, the described procedure is repeated.

Omitting the time index for the current sampling instant, the optimization problem of a model predictive controller is formulated analytically as

$$\min_{\boldsymbol{z}^n, \boldsymbol{u}^{n-1}} \; J(\boldsymbol{z}^n, \boldsymbol{u}^{n-1}) \tag{3.12a}$$

subject to

$$\begin{aligned}
\boldsymbol{z}_{i+1} &= \boldsymbol{z}_i + t_\mathrm{s} \boldsymbol{f}_\mathrm{mdl}(\boldsymbol{z}_i, \boldsymbol{u}_i), && (3.12b)\\
\boldsymbol{z}_0 - \boldsymbol{z}_\mathrm{curr} &= 0, && (3.12c)\\
\boldsymbol{f}_\mathrm{eq}(\boldsymbol{z}^n, \boldsymbol{u}^{n-1}) &= 0, && (3.12d)\\
\boldsymbol{f}_\mathrm{ineq}(\boldsymbol{z}^n, \boldsymbol{u}^{n-1}) &\leq 0, && (3.12e)\\
\text{for } i &= 0,\ 1,\ \ldots\ n-1.
\end{aligned}$$

The cost function $J$ in Equation (3.12a) formulates the control objectives, e.g., the minimization of the control effort or deviation from a certain reference. Based on the state sequence, the discretized trajectory of the system is predicted with the vector of system model equations in Equation (3.12b). In addition, formulated in Equation (3.12c), the trajectory is constrained to begin at the measurement of the current state $\boldsymbol{z}_\mathrm{curr}$. Finally, further equality and inequality constraints, e.g., for obstacle avoidance or to limit the control inputs are imposed with the function vectors $\boldsymbol{f}_\mathrm{eq}(\boldsymbol{z}^n, \boldsymbol{u}^{n-1})$ and $\boldsymbol{f}_\mathrm{ineq}(\boldsymbol{z}^n, \boldsymbol{u}^{n-1})$ in Equation (3.12d) and Equation (3.12e), respectively.

## Modeling of Objects and Collision Checking

Motion planning algorithms require a model of the vehicle and surrounding obstacles. In the automated driving system, it is the task of the perception module to localize and estimate the state of the vehicle. Furthermore, obstacles need to be detected, tracked, and predicted. An object list represents an input to the presented uncoupled shared control approaches and is assumed to be available. In the following, options are described how the vehicle and obstacles, collectively referred to as objects, can be modeled.

An object can often be approximated as a rectangle. This is described through its location at $x_\mathrm{obj}$ and $y_\mathrm{obj}$, orientation $\theta_\mathrm{obj}$, width $w_\mathrm{obj}$, and length $l_\mathrm{obj}$. These parameters are summarized in the vector $\boldsymbol{o}_\mathrm{rect}$, given by

$$\boldsymbol{o}_\mathrm{rect} = [x_\mathrm{obj},\ y_\mathrm{obj},\ \theta_\mathrm{obj},\ w_\mathrm{obj},\ l_\mathrm{obj}]^T. \tag{3.13}$$

Besides this, an ellipse represents a popular choice that yields an analytic expression to approximate an obstacle [182, 192, 193]. The implicit function of an ellipse, located at the origin, is given by

$$\left(\frac{x}{l_\mathrm{maj}}\right)^2 + \left(\frac{y}{l_\mathrm{min}}\right)^2 - 1 = 0, \tag{3.14}$$

with the semi-major axis $l_\mathrm{maj}$ and semi-minor axis $l_\mathrm{min}$, as shown in Figure 3.2. An ellipse can also be translated to the location of the object. The implicit function of a translated ellipse is given by

$$\left(\frac{x - x_\mathrm{obj}}{l_\mathrm{obj}}\right)^2 + \left(\frac{y - y_\mathrm{obj}}{l_\mathrm{min}}\right)^2 - 1 = 0. \tag{3.15}$$

Furthermore, an ellipse can be rotated about the angle of orientation of the object $\theta_{\text{obj}}$. The implicit function of a rotated ellipse is given by

$$\left(\frac{x\,\cos(\theta_{\text{obj}}) - y\,\sin(\theta_{\text{obj}})}{l_{\text{maj}}}\right)^2 + \left(\frac{x\,\sin(\theta_{\text{obj}}) + y\,\cos(\theta_{\text{obj}})}{l_{\text{min}}}\right)^2 - 1 = 0. \tag{3.16}$$

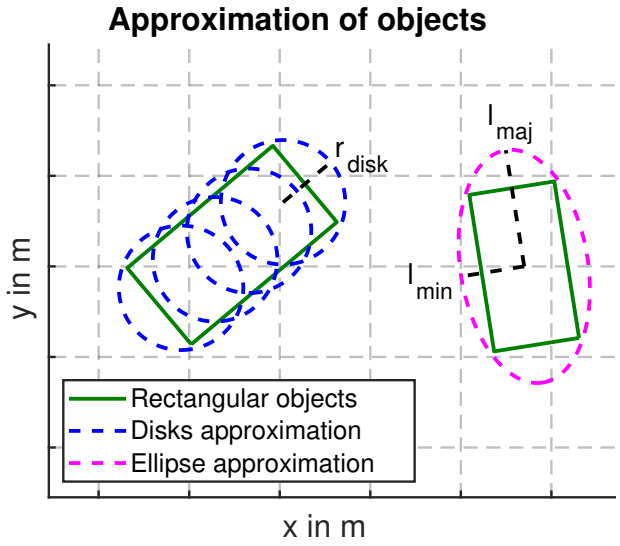


Figure 3.2: Approximation of rectangular objects based on four shifted disks and an ellipse. The object on the left is approximated through four shifted disks with the radius $r_{\text{disk}}$. On the right, the object is approximated by an ellipse with the lengths of the major axis $l_{\text{maj}}$ and the minor axis $l_{\text{min}}$.

Substituting $x$ and $y$ in Equation (3.16) by $x - x_{\text{obj}}$ and $y - y_{\text{obj}}$ yields the combination of both transformations, i.e., the implicit function of a rotated and translated ellipse $f_{\text{ell}}(x, y)$. This representation is shown on the right in Figure 3.2. The parameters of an ellipse are summarized in the vector $\boldsymbol{o}_{\text{ell}}$, given by

$$\boldsymbol{o}_{\text{ell}} = [x_{\text{obj}},\ y_{\text{obj}},\ \theta_{\text{obj}},\ l_{\text{maj}},\ l_{\text{min}}]^T. \tag{3.17}$$

As described by Schwarting et al. [182], four disks have also proven their usability to accurately approximate a rectangular vehicle. As shown in Figure 3.2, the disks are shifted along the center axle of the vehicle such that the front and rear bumpers as well as the sides of the vehicle are enclosed by the union of the disks. With the disk index $m \in \{1, 2, 3, 4\}$, the four disks are given by their radius $r_{\text{disk}}$ and their location at $x_{\text{disk},m}(\boldsymbol{z})$ and $y_{\text{disk},m}(\boldsymbol{z})$, in dependence of the vehicle state $\boldsymbol{z}$.

The presented approximations are used to perform collision checking. From the rectangular representation $\boldsymbol{o}_{\text{rect}}$, the four corner points of the object can easily be calculated. Based on this, the separating axis theorem forms the option for the most precise collision checking in sampling-based motion planning algorithms [194, p. 46]. In a model predictive control formulation, an analytical function that can be evaluated in the optimization problem is required. In the present work, the vehicle is approximated with the described methodology of four shifted disks, as shown in Figure 3.2. The obstacle is approximated through an ellipse. In order to check for collisions, it is evaluated if one or more disks of the vehicle are intersecting with the ellipse of an obstacle. For this, the locations of the disks at $x_{\text{disk},m}(\boldsymbol{z})$ and $y_{\text{disk},m}(\boldsymbol{z})$ are inserted into $f_{\text{ell}}(x, y)$. Furthermore, $l_{\text{maj}}$ and $l_{\text{min}}$ are substituted by $l_{\text{maj}} + r_{\text{disk}}$ and $l_{\text{min}} + r_{\text{disk}}$, respectively. This yields the implicit function $f_{\text{disk},m}(\boldsymbol{z})$ for each disk. When evaluating this for all four disks, it can be checked if the given vehicle state $\boldsymbol{z}$ collides with the ellipse of the obstacle. On the one hand, given that all four evaluations yield a result greater or equal to zero, the state is deemed collision-free. On the other hand, if at least one result is smaller than zero, the state is colliding.

### 3.1.2 Feedback Modalities

With an operator in the loop, it is of great importance to communicate the intentions of the automation. In particular, in situations in which an uncoupled shared control approach intervenes in the operator's control commands, distinct communication is required. For this purpose, haptic, visual, and auditory cues, the so-called haptic multi-modal interfaces, can be exploited [154]. In the present work, the more prominent haptic and visual feedback modalities are considered. Their applications are introduced in the following.

#### Haptic Feedback

Haptic feedback, i.e., torque on the steering wheel or force on the pedals, is a valuable modality and most prominent in shared control frameworks. In particular, in coupled shared control, it is inevitable as the operator and the automation are acting on mechanically coupled control interfaces. Through the provision of feedback, the operator can better interpret and respond to the actions of the automation.

In the context of uncoupled shared control, the direction and strength of the haptic feedback can be dependent on the actual or the predicted intervention of the system. For example, when the system detects a potential safety risk, it may apply a small amount of torque to the steering wheel to alert the operator. If the situation becomes more critical, the torque may be increased to indicate the severity of the situation and to prompt the operator to take immediate action. This can help the operator to understand the level of intervention of the automation and the urgency of the situation. In the literature review in Subsection 2.2.2, several works considered the provision of haptic feedback for the operator [157, 158, 161, 162, 165, 166]. Having shown its usefulness in existing works, the communication of steering interventions through haptic feedback is also included in the shared steering and velocity control design in the present work.

#### Visual Feedback

The second feedback modality, which is considered in the present work, is visual feedback. Similar to the idea of head-up displays [195, 196], visual elements can be overlaid with the videos in a teleoperation system and provide additional information to the remote operator. This is beneficial to improve the transparency, i.e., the predictability and observability, of the system behavior in an uncoupled shared control framework. For instance, the visualized information can be the trajectory that is currently planned by the uncoupled shared control approach. This provides the remote operator with intuition and insights into the objectives and potential causes for the intervention of the automation.

In Figure 3.3, three examples from literature for such visual overlays are shown. Taken from Anderson [158], the visual feedback on the left illustrates the drivable space. In the middle, taken from Storms et al. [180], a trajectory plan is visualized. Lastly, taken from Sharma et al. [197], the visual feedback on the right shows a risk profile in variable color intensities from yellow to red. In the present work, visual feedback is incorporated in both uncoupled shared control designs.

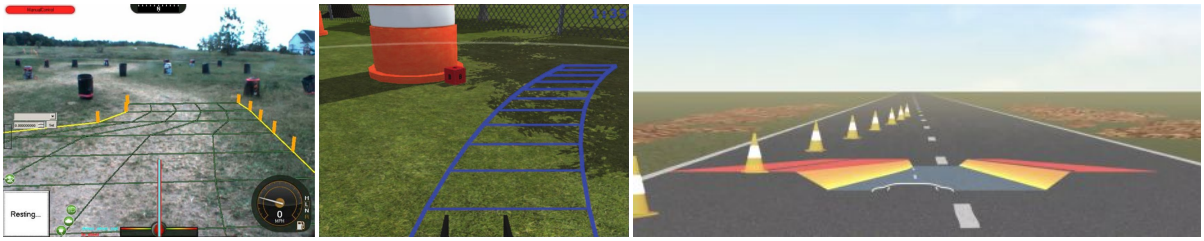

Figure 3.3: Examples of visual feedback in shared control designs. Taken from Anderson [158], drivable space is shown on the left. Taken from Storms et al. [180], a trajectory plan is visualized in the middle. Taken from Sharma et al. [197], the visual feedback on the right shows a risk profile in variable color.

## 3.2 Shared Velocity Control (SVC)

The first uncoupled shared control design that is presented is an approach for Shared Velocity Control (SVC). It was first described and published by Schimpe et al. [97]. As illustrated in Figure 2.15, the capability of SVC is uncoupling the remote operator's velocity commands from the vehicle. At first thought, the ability of this design to keep the vehicle safe using only braking maneuvers is limited as the future steering actions from the remote operator are unknown. To mitigate this, the approach is made aware of the remote operator's current and potential future steering actions. Hence, the given name of the approach in [97] was steering action-aware adaptive cruise control. However, in order to improve the clarity of the capabilities of the approach in the present work, the given name is SVC. Ultimately, the purpose of the proposed SVC design is to keep the vehicle in a state in which it can always be stopped safely. Through the steering action-awareness, this safe stop is possible no matter which steering actions are taken by the remote operator.

It is noted that this concept is different from regular adaptive cruise control systems, e.g., [173–177], which make the assumption that the operation of the vehicle is based on maneuvers in an environment that is structured through lane markings. For the case of vehicle teleoperation, high speeds are not a priority, but safety in the presence of steering actions from the remote operator that would otherwise lead to a collision.

The proposed SVC approach consists of two stages, as shown in Figure 3.4. There are three inputs to the approach. These are the control commands from the remote operator, the list of detected obstacles in the surroundings of the vehicle, and the current vehicle state. Based on these, trajectory sampling and velocity optimization are performed, yielding the safe velocity control command for the vehicle.

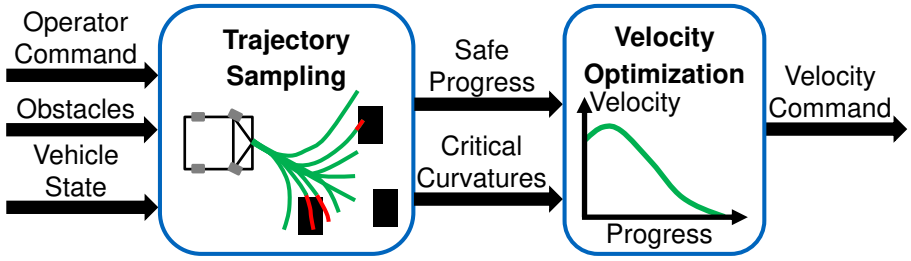


Figure 3.4: Stages of the shared velocity control approach, taken from Schimpe et al. [97]. In the first stage, trajectory sampling is performed based on the control command from the (remote) operator, a list of detected obstacles, and the current vehicle state. This yields a value for the global safe progress and a critical curvature profile. Based on these, a safe velocity profile is optimized for, yielding the velocity command for the vehicle.

The procedure of the approach is given in Algorithm 1. In line 2, the `TrajectorySampler` samples various future steering actions, planning trajectories that start at the current vehicle state $\boldsymbol{z}_{\mathrm{curr}}$. In line 3, these trajectories are checked for collisions with the list of $k$ detected obstacles $\boldsymbol{o}^k$. With this, a value of the collision-free, i.e., the safe, progress in meters along each trajectory is computed. Taking the minimal safe progress from all trajectories in line 4 yields the global safe progress $s_{\mathrm{safe}}$. In addition, in line 5, a profile of critical curvatures $\kappa^n_{\mathrm{crit}}$, which reaches the maximum steering angle the earliest, is taken from the `TrajectorySampler`. Based on this and the desired velocity from the remote operator $v_{\mathrm{o}}$, the `VelocityOptimizer` computes a safe velocity profile by solving an optimization problem in line 6. Together with the steering angle command from the remote operator $\delta_{\mathrm{o}}$, the first future entry of this velocity profile is set as the control command from the SVC approach $\boldsymbol{u}_{\mathrm{v}}$ in line 7. Finally, this is returned to be executed by the vehicle in line 8. In the remainder of this section, the steps of the algorithm will be described in more technical detail. Lines 2 to 5 of the algorithm are summarized as the trajectory sampling stage. Line 6 is the velocity optimization. Finally, a description is provided on how visual feedback is incorporated in the SVC design.

**Algorithm 1** Computation of the shared velocity control command, adapted from Schimpe et al. [97].

**procedure** ComputeSharedVelocityControlCommand($\boldsymbol{u}_\mathrm{o}$, $\boldsymbol{o}^k$, $\boldsymbol{z}_\mathrm{curr}$)
  `TrajectorySampler.PlanTrajectoriesFrom`($\boldsymbol{z}_\mathrm{curr}$)
  `TrajectorySampler.CheckForCollisionsWith`($\boldsymbol{o}^k$)
  $s_\mathrm{safe} \leftarrow$ `TrajectorySampler.GetGlobalSafeProgress`()
  $\kappa^n_\mathrm{crit} \leftarrow$ `TrajectorySampler.GetCriticalCurvatures`()
  $v^n_\mathrm{safe} \leftarrow$ `VelocityOptimizer.solve`($\boldsymbol{z}_\mathrm{curr}$, $v_\mathrm{o}$, $s_\mathrm{safe}$, $\kappa^n_\mathrm{crit}$)
  $\boldsymbol{u}_\mathrm{v} \leftarrow [\delta_\mathrm{o},\ v_\mathrm{safe,1}]^T$
  `return` $\boldsymbol{u}_\mathrm{v}$
**end procedure**

### 3.2.1 Trajectory Sampling

At each sampling instant of the SVC approach, a trajectory tree is planned in order to obtain the current global safe progress $s_\mathrm{safe}$ and the critical curvature profile $\kappa^n_\mathrm{crit}$. The trajectory tree is a set of trajectories. In the following, it is explained how this is planned. Then, it is introduced how collision checks are performed in order to assess the global safe progress. Finally, the procedure to compute the critical curvature profile is described.

#### Trajectory Tree Planning

The planning of the trajectories is carried out with the model-based method, described in Subsection 3.1.1. Given that only low velocities are considered, the kinematic bicycle model is used. Its state and the control input are denoted by $\boldsymbol{z}$ and $\boldsymbol{u}$, respectively. Using Euler's method, the vehicle state is integrated forward in time with Equation (3.9).

The trajectories of the tree are planned in order to evaluate various potential future steering actions from the remote operator. For this, the steering inputs are varied by applying $P$ different constant steering angle rates over the planning time horizon $t_\mathrm{h}$, discretized in $n$ steps by the sampling time $t_\mathrm{s}$. The applied steering angle rates are in the range $[-\dot{\delta}_\mathrm{max},\ \dot{\delta}_\mathrm{max}]$. Thereby, $\dot{\delta}_\mathrm{max}$ denotes the maximum steering angle rate that is assumed to be applied by the remote operator. In order to enable safe stopping of the vehicle, all trajectories of the tree are planned to brake the vehicle into a standstill. Over the time $t_\mathrm{h}$, the standstill is reached by applying the constant deceleration $a_\mathrm{stop}$, computed by

$$a_\mathrm{stop} = -\frac{v_\mathrm{curr}}{t_\mathrm{h}}, \tag{3.18}$$

with the velocity of the currently measured vehicle state $v_\mathrm{curr}$. In summary, the $P$ trajectories of the tree are planned by applying the $P$ constant control inputs $\boldsymbol{u}_p = [\dot{\delta}_p,\ a_\mathrm{stop}]^T$, for $p = 1,\ 2,\ \ldots\ P$. Thereby, the $p$th steering angle rate $\dot{\delta}_p$ is computed by

$$\dot{\delta}_p = -\dot{\delta}_\mathrm{max} + 2\,\dot{\delta}_\mathrm{max}\frac{p-1}{P-1}. \tag{3.19}$$

As an example of the parameters from a passenger vehicle, which are also used in the simulative validation in the following chapter, a snapshot of a planned trajectory tree in the $xy$ plane is shown in Figure 3.5. Starting at the origin with $v_\mathrm{curr}$ = 4.34 m s$^{-1}$ and $\delta_\mathrm{curr}$ = –0.11 rad, the corresponding velocities and steering angles along each trajectory are plotted in Figure 3.6.

At this point, the question arises whether the steering action-awareness is sufficient when planning the trajectories with constant steering rates, only. Constant steering rates do not evaluate all possible steering maneuvers. Instead, it would be expected that the `TrajectorySampler` varies the steering rate along

the trajectories, effectively increasing the density of the planned trajectory tree. However, it has been found that the results from the described trajectory sampling stage, i.e., the global safe progress and the critical curvature profile, would not be affected by the increased density of the tree. In consequence, it is deemed sufficient to plan with constant steering rates, only.

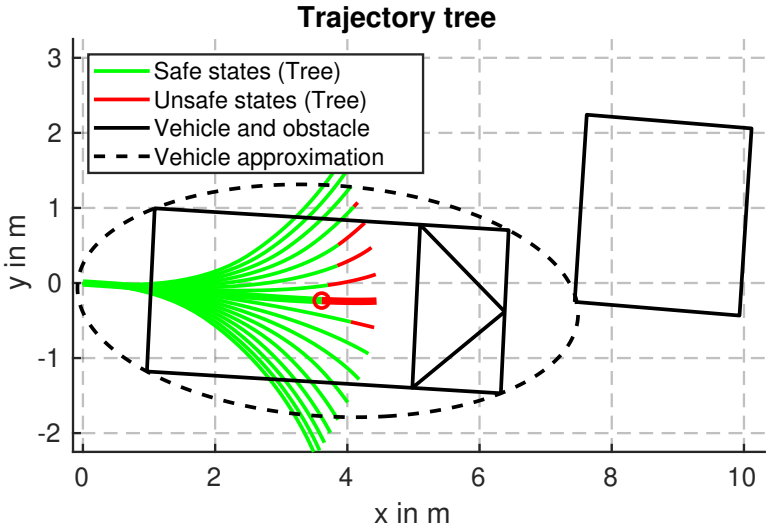


Figure 3.5: Trajectory tree planned by the shared velocity control approach, taken and adapted from Schimpe et al. [97]. Starting in the origin, the trajectories are plotted in the $xy$ plane. The safe and unsafe states are depicted in green and red, respectively. One obstacle is shown in black. In addition, as implemented in [97], the vehicle and its elliptical approximation are drawn in black for the marked state of the thicker trajectory that is about to collide with the obstacle.

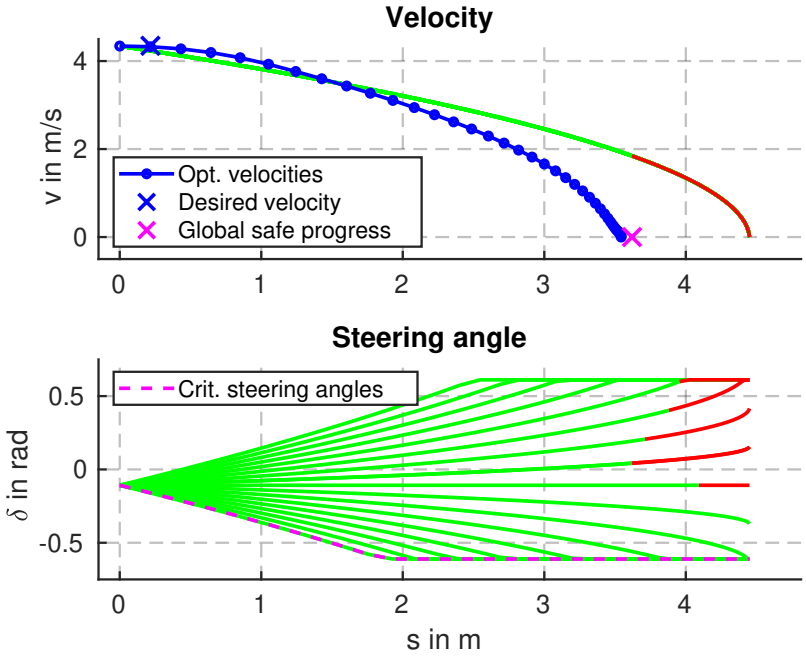


Figure 3.6: Velocities and steering angles planned over the progress by the shared velocity control approach, taken and adapted from Schimpe et al. [97]. In the top plot, the velocity profiles from the trajectories in the tree are shown in green for safe states and in red for unsafe states beyond the marked global safe progress. In addition, the result from the velocity optimization procedure is drawn in blue, planning into the standstill before exceeding the global safe progress. In the bottom plot, the steering angle profiles from the trajectories in the tree are shown, again in green and red for safe and unsafe states. Finally, the critical steering angle profile, which reaches either the left or the right maximum steering angle the earliest, is depicted.

### Collision Checking and Assessment of Global Safe Progress

After the trajectory tree planning, collision checks are performed in order to assess the global safe progress from the current vehicle state. For this, all states from the planned trajectory tree are checked for collisions with the list of detected obstacles $\boldsymbol{o}^k$. Through this, the safe progress in meters along each trajectory is computed.

In Figure 3.5 and 3.6, the safe and unsafe states are plotted, respectively. In addition to the trajectory tree states in Figure 3.5, one obstacle as well as the vehicle, at the location of the first state for which a collision with the obstacle is detected, are shown. As visualized, in this implementation, the rectangular vehicle is approximated as an ellipse. Collision checks are performed by checking if at least one of the four corner points or an edge point of the obstacle lies within the ellipse. This is done by evaluating $f_{\text{ell}}(x, y)$, parametrized by $\boldsymbol{o}_{\text{ell}}$ for the vehicle, at the locations of each obstacle point.

Finally, after the computation of the safe progress along each trajectory, the values are compared. The minimum then yields the global safe progress $s_{\text{safe}}$, which is passed to the velocity optimization stage.

### Computation of Critical Curvature Profile

In the form of lateral acceleration constraints, the proposed SVC approach also accounts for comfort in the velocity optimization stage. For this, a critical curvature profile is computed by the `TrajectorySampler`. This profile stems from the steering angle profile that reaches the maximum steering angle the earliest. In short, it is created by constantly applying the assumed maximum steering angle rate $\dot{\delta}_{\max}$ until either the maximum left or right steering angle is reached. Hence, the steering angle profile is created by applying

$$\dot{\delta}_i = \text{sign}(\delta_{\text{curr}})\, \dot{\delta}_{\max}, \tag{3.20}$$

for $i = 0,\ 1,\ \ldots\ n-1$. For the presented snapshot from the previous sections, the resulting critical steering angle profile is shown in Figure 3.6. From this, the corresponding critical curvature profile $\kappa^n_{\text{crit}}$, given by

$$\kappa^n_{\text{crit}} = \{\kappa_{\text{crit},1},\ \kappa_{\text{crit},2},\ \ldots\ \kappa_{\text{crit},n}\}, \tag{3.21}$$

is computed using Equation (3.7).

## 3.2.2 Velocity Optimization

In the second stage, after obtaining the results from the trajectory sampling, the velocity profile is computed through optimization. The objectives are twofold. On the one hand, the vehicle velocity should reach the velocity desired by the remote operator. On the other hand, the velocity profile should brake the vehicle into a standstill. Reaching these objectives is subject to the satisfaction of additional constraints for safety and comfort. Through these, the approach will brake the vehicle into a standstill comfortably even in the case that the remote operator steers the vehicle on a collision course without stopping.

In a model predictive control fashion, the optimization problem is also discretized in $n$ time steps of length $t_{\text{s}}$. It is given by

$$\min_{s^n, v^n, a^n, j^{n-1}} w_v\,(v_1 - v_{\text{o}})^2 + w_{v,n}\, v_n^2 + J_\epsilon \tag{3.22a}$$

subject to

$$s_0 = 0\,\mathrm{m},\ v_0 = v_{\mathrm{curr}},\ a_0 = a_{\mathrm{curr}}, \tag{3.22b}$$

$$s_{i+1} = s_i + t_s\, v_i,\ v_{i+1} = v_i + t_s\, a_i,\ a_{i+1} = a_i + t_s\, j_i, \tag{3.22c}$$

$$s_{i+1} \leq s_{\mathrm{safe}}, \tag{3.22d}$$

$$-a_{\mathrm{lat,max}} \leq \kappa_{\mathrm{crit},i+1}\, v_{i+1}^2 \leq a_{\mathrm{lat,max}}, \tag{3.22e}$$

$$-\epsilon_{a,i+1} + a_{\mathrm{min}} \leq a_{i+1} \leq a_{\mathrm{max}} + \epsilon_{a,i+1}, \tag{3.22f}$$

$$-\epsilon_{j,i} - j_{\mathrm{max}} \leq j_i \leq j_{\mathrm{max}} + \epsilon_{j,i}, \tag{3.22g}$$

$$\text{for } i = 0,\ 1,\ \ldots\ n.$$

The cost function is given in Equation (3.22a). Therein, the primary objective is to reach the desired velocity from the remote operator $v_{\mathrm{o}}$. This is incorporated through penalizing the squared deviation of $v_1$ from $v_{\mathrm{o}}$ by $w_v$. Second, to formulate the objective of planning a velocity profile reaching a standstill, the squared terminal velocity $v_n$ is heavily weighted by choosing a greater weight $w_{v,n}$. In this model predictive control formulation, the system is modeled as a simple one-dimensional point mass. The system states are the progress $s$, the velocity $v$, and the acceleration $a$. The input to the system is the jerk $j$. For this system, the corresponding initial state conditions and model equations are given in Equation (3.22b) and (3.22c), respectively. In order to plan a velocity profile that keeps the motion of the vehicle collision-free, the planned progress is constrained with Equation (3.22d) to not exceed the global safe progress $s_{\mathrm{safe}}$. To account for comfort, the velocity optimization also incorporates the constraint of the lateral acceleration in Equation (3.22e). Therein, using Equation (3.8), the lateral acceleration is computed depending on the critical curvature profile and the planned velocity. Resulting of the preceding trajectory sampling stage, $s_{\mathrm{safe}}$ and $\kappa_{\mathrm{crit}}^n$ are parameters that are updated at each sampling instant. Finally, the acceleration and the jerk are constrained through Equation (3.22f) and (3.22g), respectively. In order to cope with noise in the state measurement and imperfect control command tracking of the vehicle, and yet achieve feasibility when solving the optimization problem, these two constraints are made soft. This is achieved through the introduction of the slack variables $\epsilon_a$ and $\epsilon_j$. These are heavily penalized linearly and quadratically in the cost function term $J_\epsilon$ [198].

For the sampling instant, visualized in the previous section, the result from the velocity profile optimization is also shown in Figure 3.6. The corresponding acceleration profile is shown in the acceleration diagram in Figure 3.7.

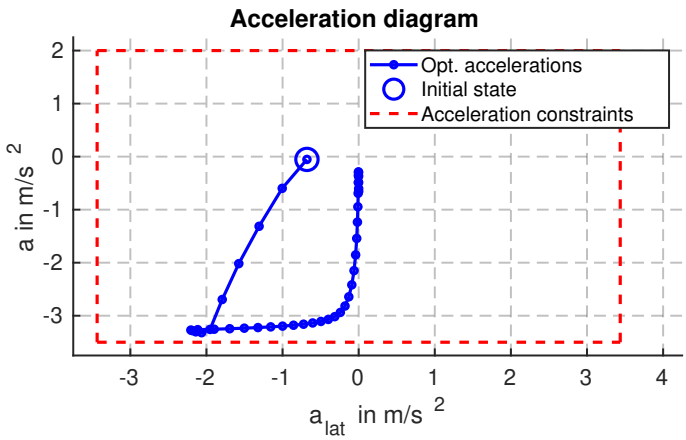


Figure 3.7: Snapshot of the acceleration profile planned by the shared velocity control concept, taken and adapted from Schimpe et al. [97]. In blue, the planned acceleration profile is shown. The initial state is marked by a circle. The longitudinal and lateral acceleration constraints are depicted in dashed red.

In the trajectory sampling stage, it was found that not all trajectories of the tree are collision-free. This results in a reduced global safe progress, requiring stronger braking than the constant deceleration $a_{\text{stop}}$ to a standstill over $t_{\text{h}}$. The velocity optimization accounts for this by planning the velocity profile to reach a standstill sooner, i.e., before exceeding a progress of $s_{\text{safe}}$. Visible in Figure 3.6, the velocity desired by the remote operator can still be tracked at the first prediction instant. This means that the vehicle will not yet start to brake. In the acceleration diagram in Figure 3.7, the related acceleration profile is shown together with the acceleration constraints. At the current sampling instant, neither the planned longitudinal nor lateral accelerations exceed the imposed constraints. However, from the fifth prediction instant onwards, the longitudinal accelerations come close to the constraint of $a_{\text{min}}$. Given the current course of the vehicle heading towards the obstacle, this means that an actual braking maneuver will be initiated soon, unless future steering actions circumvent the obstacle, keeping a sufficient distance.

### 3.2.3 Visual Feedback

To improve the remote operator's understanding of the actions from the SVC approach, visual feedback is introduced. For this, several data are transmitted from the vehicle, in addition to the video.

The concept of visual feedback is shown in Figure 3.8. At the bottom, the desired and actual gear position as well as the velocity are shown as letters and numbers. Depicted through the white lines, the motion of the vehicle is predicted forward based on the current steering angle. Finally, the transparent cone-shaped polygon illustrates the area from the sampled trajectories. At this sampling instant, a possible collision is detected with the obstacle on the left. In consequence, the polygon is colored in red for the colliding future states. As the states on the right are safe and colored in green, the rendering mechanism automatically draws a smooth transition from red to green. In the actual system, the yellow boxes, depicting obstacles in this snapshot, are not shown as they are visible in the actual video from the vehicle camera. The visual feedback should inform the remote operator ahead of time when the SVC approach will uncouple control of the velocity, i.e., is about to intervene and initiate a braking maneuver, which possibly goes into a standstill. The helpfulness of this concept is evaluated in the experimental user study that is described in Chapter 5.

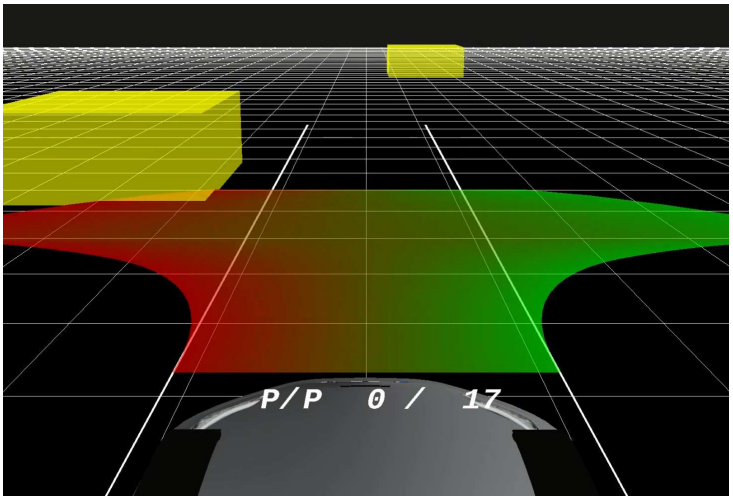


Figure 3.8: Visual feedback in the shared velocity control design. Except for the yellow boxes, depicting obstacles in this snapshot, the following elements are overlaid in perspective with the video. The tachometer at the bottom informs about the desired and actual gear position and velocity. Depicted through the white lines, the motion of the vehicle is predicted forward based on the current steering angle. The transparent cone-shaped polygon illustrates the area of the safe and unsafe states in the trajectory tree.

## 3.3 Shared Steering and Velocity Control (SSVC)

The second uncoupled shared control design that is analyzed in this work is an Shared Steering and Velocity Control (SSVC) design. Preliminary work in the form of a shared steering control design was described and published by Schimpe and Diermeyer [98]. This was extended to an SSVC design by Saparia, Schimpe, and Ferranti [199]. These works form the foundation of the design and the implementation in its final form which is described in the following.

As shown in Figure 2.15, SSVC uncouples the steering as well as the velocity commands from the remote operator. With this capability, it is up to the controller to decide which overriding action to take in order to keep the vehicle safe. SVC and SSVC can be compared by a theoretical point of view. First, in an equivalent situation with the risk of a frontal collision, both designs are expected to bring the vehicle to a standstill in front of the obstacle. Second, in a situation in which the vehicle is closely cutting the corner of an obstacle, the SVC would stop the vehicle as well. In contrast to this, the SSVC should prefer a correction in the steering angle as an overriding action. Third, when closely but safely passing an obstacle, the SVC will still reduce the velocity of the vehicle. The SSVC, aware of its capability to override the remote operator's steering angle, can maintain the velocity. Overall, with the SSVC, it is expected that the vehicle will be slowed down and stopped less frequently as intended by the remote operator. While this forms a clear advantage of the SSVC over the SVC, a potentially critical factor is introduced with an uncoupled shared control design being capable to override the steering actions. To some extent, the vehicle can deviate from the remote operator's intentions and travel a different course, which may not be desirable. Effectively, the criticality will depend on the magnitude of the intervention.

Throughout this section, a technical description of the SSVC design is provided. First, the underlying formulation of the approach, based on model predictive control, is given. Second, snapshots of trajectory plans during obstacle avoidance maneuvers are shown as examples. Finally, the feedback concept is described.

### 3.3.1 Model Predictive Control Formulation

In this section, the model predictive control formulation of the SSVC approach is described. It is given by

$$\min_{\boldsymbol{z}^n, \boldsymbol{u}^{n-1}} \sum_{i=0}^{n-1} w_{\dot{\delta}}\, \dot{\delta}_i^2 + \sum_{i=0}^{n-1} w_a\, a_i^2 + \sum_{i=1}^{n} w_\delta\, (\delta_i - \delta_\mathrm{o})^2 + \sum_{i=1}^{n-1} w_v\, (v_i - v_\mathrm{o})^2 + w_{v,n}\, v_n^2 + J_\epsilon \tag{3.23a}$$

subject to

$$\boldsymbol{z}_{i+1} = \boldsymbol{z}_i + t_\mathrm{s}\, \boldsymbol{f}_\mathrm{mdl}(\boldsymbol{z}_i, \boldsymbol{u}_i), \tag{3.23b}$$

$$\boldsymbol{z}_0 - \boldsymbol{z}_\mathrm{curr} = 0, \tag{3.23c}$$

$$-\delta_\mathrm{max} \leq \delta_i \leq \delta_\mathrm{max}, \tag{3.23d}$$

$$-\dot{\delta}_\mathrm{max} \leq \dot{\delta}_i \leq \dot{\delta}_\mathrm{max}, \tag{3.23e}$$

$$a_\mathrm{min} \leq a_i \leq a_\mathrm{max}, \tag{3.23f}$$

$$\boldsymbol{z}_{i+1} \in \mathcal{Z}_\mathrm{free}, \tag{3.23g}$$

$$\text{for } i = 0,\ 1,\ \ldots\ n-1.$$

This formulation can be separated into the cost function, model equations, constraints on the control actions, and collision avoidance constraints. In the following, each part is described in more detail.

## Cost Function

Multiple objectives are incorporated in the cost function in Equation (3.23a). In order to regularize the optimization problem and avoid unnecessary control actions, the first two terms of the cost function penalize the usage of the control inputs $\dot{\delta}$ by $w_{\dot{\delta}}$ and $a$ by $w_a$. Weighted by $w_\delta$, the third term penalizes the deviation of the planned steering angle $\delta$ from steering angle $\delta_\mathrm{o}$, currently desired by the remote operator. Similarly, weighted by $w_v$, the objective of the fourth term is to minimize the squared deviation of the planned velocity $v$ from the desired velocity $v_\mathrm{o}$. However, this is only done for the discretization steps up to $n-1$. In order to improve the robustness of the controller and prefer braking over excessively large steering interventions, the velocity profile planned by the SSVC approach should also reach a standstill. For this, the fifth cost function term penalizes the deviation of the terminal velocity $v_n$ from zero velocity through the rather heavy weight $w_{v,n}$. The last, sixth term of the cost function penalizes the usage of slack variables $\epsilon$ in the soft collision avoidance constraints, introduced later.

## Model Equations

The kinematic bicycle model is also used as a prediction model in the model predictive control formulation of the SSVC. This and the theory for model-based trajectory planning were introduced in the background for vehicle motion planning and control in Subsection 3.1.1. Hence, the model equations in Equation (3.23b) are Equation (3.9) with the equations from the kinematic bicycle model $\boldsymbol{f}_\mathrm{mdl}(\boldsymbol{z}, \boldsymbol{u})$. As in every model predictive control formulation, the equality constraint for the initial state is to start at the currently measured state $\boldsymbol{z}_\mathrm{curr}$, incorporated in Equation (3.23c).

## Constraints on Control Actions

Given the actuation limitations of the vehicle, the model predictive control formulation incorporates constraints on the applicable control actions. In Equation (3.23d), the maximum steering angle in both directions is constrained to be less than $\delta_\mathrm{max}$. Similarly, the steering angle rate is bound symmetrically to less than $\dot{\delta}_\mathrm{max}$. Finally, with different upper and lower limits, the acceleration of the vehicle is bound to values between $a_\mathrm{min}$ and $a_\mathrm{max}$ in Equation (3.23f).

## Constraints Incorporating Collision Avoidance

Finally, there are constraints that incorporate collision avoidance. Summarized in Equation (3.23g), these ensure that each of the planned vehicle states $\boldsymbol{z}$ is in the set of collision-free vehicle states $\mathcal{Z}_\mathrm{free}$, i.e., the drivable space.

Applying the methodology, introduced in the background in Subsection 3.1.1, the vehicle is approximated by four shifted disks. A rectangular obstacle is approximated through an ellipse. Based on this, the constraints to avoid collisions with one obstacle are formulated by

$$-\epsilon_{\mathrm{c},i} \leq f_{\mathrm{disk},m}(\boldsymbol{z}_i)\,, \text{ for } m = 1,\ 2,\ 3,\ 4. \tag{3.24}$$

To avoid collisions with multiple obstacles, these constraints need to be duplicated with variable ellipse parametrizations. Also, to cope with noisy dimensions in the obstacle detections from the perception module, the collision avoidance constraints are made soft. Similar to the model predictive control formulation of the SVC approach, this is achieved through the introduction of slack variables $\epsilon_\mathrm{c}$, whose usage is penalized in the cost function term $J_\epsilon$.

### 3.3.2 Snapshots of Trajectory Plans during Obstacle Avoidance Maneuvers

In this section, snapshots during obstacle avoidance maneuvers of the SSVC approach are shown as examples. The focus here lies on briefly illustrating the planned trajectories of the model predictive control formulation and not on the quantification of the intervention. The latter is validated in the simulations, which are presented in the following chapter.

In Figure 3.9, the trajectory plans during two obstacle avoidance maneuvers are shown. On the left, the trajectory plans during an evasion are illustrated. First, as the traveled trajectory shows, the vehicle is on the course of a close collision with the obstacle. As this is realized by the SSVC approach, evasion to the left is planned and executed. On the right, an obstacle avoidance maneuver through stopping is shown. The vehicle is on a collision course with a centered, wider obstacle. In this case, instead of avoiding it by greater a steering maneuver, the SSVC approach plans to slow down and stops the vehicle.

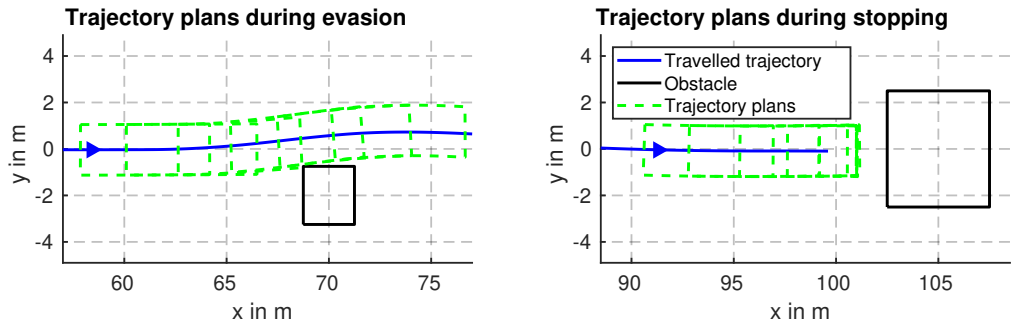


Figure 3.9: Trajectory plans of the shared steering and velocity control approach during two obstacle avoidance maneuvers. With the direction of travel depicted by triangles, the traveled trajectories are shown in blue. Obstacles are illustrated in black. The trajectory plans are drawn in green every 500 milliseconds. On the left, avoidance of an obstacle through evasion to the left is shown. On the right, an obstacle is avoided by stopping.

### 3.3.3 Visual and Haptic Feedback

For the visual feedback, data from the SSVC approach are also transmitted to the remote operator and overlaid with the visualized video. In Figure 3.10, the concept is shown. Several elements are similar to the SVC design, described in Subsection 3.2.3. These include the desired and actual gear position as well as the velocity. Also, there are the white lines, depicting the predicted vehicle motion, and the obstacles, shown as yellow boxes. Although, the latter is not visualized to the remote operator in the actual system with videos.

In the case of SSVC, the transparent polygon illustrates the trajectory that is currently planned by the approach. In this situation, the vehicle is on course to collide with an obstacle. The SSVC foresees this and plans an evasion to the left. For this maneuver, the controller plans to deviate from the steering angle, commanded by the remote operator. In order to communicate this ahead of time and give the remote operator time to correct the commanded control action, the polygon is colored in red at the end of the trajectory. In the beginning, where no steering intervention is predicted, the polygon is colored green. In case an intervention takes the form of a braking maneuver, i.e., overriding the remote operator's velocity command, the planned trajectory becomes shorter. It is noted that the coloring scheme of the SSVC approach, which uses red to represent an intervention, is different from the SVC approach, which uses red to represent unsafe states.

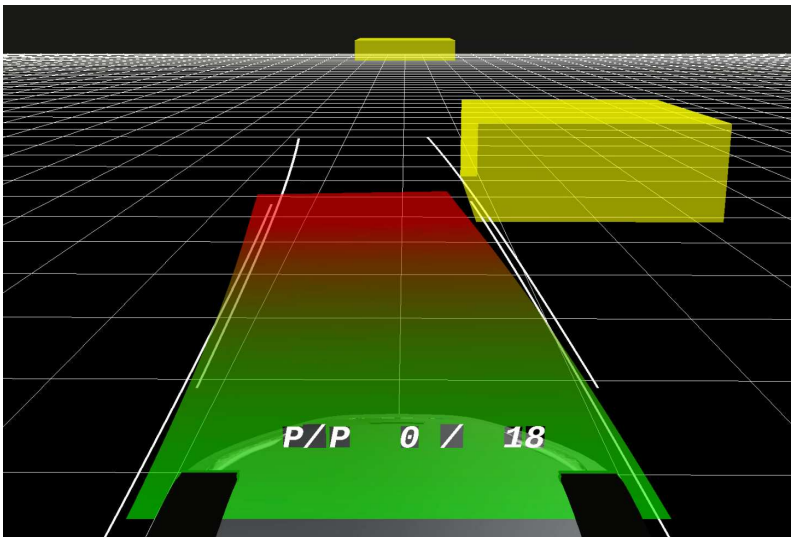


Figure 3.10: Visual feedback in the shared steering and velocity control design. Except for the yellow boxes, depicting obstacles in this snapshot, the following elements are overlaid in perspective with the video. The tachometer at the bottom informs about the desired and actual gear position and velocity. Depicted through the white lines, the motion of the vehicle is predicted forward based on the current steering angle. With the coloring depending on the predicted intervention, the transparent polygon illustrates the trajectory that is currently planned by the approach.

In order to communicate an actual steering angle intervention of the SSVC approach, haptic feedback on the remote operator's steering wheel is introduced. The magnitude of this force feedback is based on the steering angle tracking error in the model predictive control formulation of the controller. Assuming that the visual feedback prepares the remote operator for an upcoming intervention, this haptic feedback is designed to be purely reactive, i.e., it is felt by the remote operator at the moment when an actual intervention occurs. With two feedback modalities, the SSVC is more comprehensive than the SVC design. Also, the analysis in the user study in Chapter 5 will include how helpfulness is rated.

## 3.4 Teleoperation System

In order to validate and evaluate the presented uncoupled shared control approaches, they are integrated into the teleoperation system from the Institute of Automotive Technology at the Technical University of Munich. The foundations for this system have been laid with the system design, described by Gnatzig et al. [119]. In the following sections, the current state of the teleoperation system, and how it is used in the present work, is presented. First, the software architecture is described. Second, an overview of the available hardware is given. Finally, the integration of the methodology, with which the uncoupled shared control designs are integrated, is introduced.

### 3.4.1 Software Architecture

With multiple past and ongoing projects on vehicle teleoperation, contributions were made by several research associates and students. Recently, in a joint effort, the software has been made open source on GitHub [200]. Given the increasing attention, the aim is to support research in the field of vehicle teleoperation. Schimpe et al. [100] describe the software architecture and provide vehicle teleoperation demonstrations. The complete software stack is implemented in C++. With the objective to leverage modularity, it is based on ROS, the Robot Operation System [201]. Currently, the software is being ported to ROS2.

The software architecture of the system is shown in Figure 3.11. At a high level, the software is separated into the vehicle and the operator side. As depicted, several hardware components are being interfaced. Connections in between are established through the interplay of multiple ROS packages, shown as colored rectangles. These are categorized as follows.

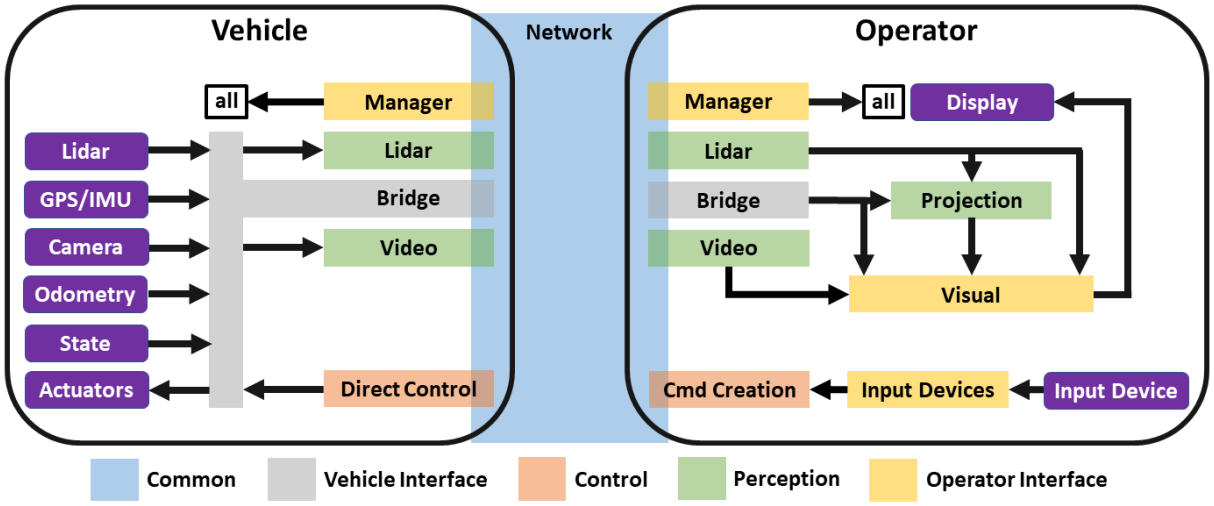


Figure 3.11: Software architecture of the teleoperation system, taken from Schimpe et al. [100]. The software is separated into the vehicle and the operator side. The interfaces to the hardware components on the sides of the vehicle and the operator are depicted with purple boxes. In between, there are several ROS packages, shown as colored rectangles and clustered into five categories.

To start with, there are the `Common` packages, which are shown in blue. On the one hand, there is the `Network` package. This connects the vehicle and the operator side. On the other hand, not being illustrated, there are packages, responsible for launching the software and providing resources, such as libraries with helper functions, for use in other packages.

The `Vehicle Interface`, shown in grey, mainly consists of the `Bridge` package, which receives data from the sensors, such as cameras and LiDAR. Also, it is responsible for sending commands, e.g., the steering angle or velocity, to the actuators of the vehicle. This package also handles the transmission of certain signals, e.g., the current vehicle state or odometry, to the operator side.

The `Perception` packages, shown in green, are processing, compressing, and transmitting data from cameras and LiDAR sensors in the `Video` and `Lidar` packages, respectively. The `Video` package implements an adaptive video streaming framework. This was published and made open source separately by Schimpe et al. [99, 202]. Upon receiving the data on the operator side, the `Projection` package prepares it for visualization to the remote operator.

The `Control` packages, shown in orange, include the `Command Creation` package, which creates control commands from the input devices. As an example where direct control is used, the `Direct Control` package passes the control commands to the `Bridge` for the actuation of the vehicle.

Finally, the `Operator Interface`, shown in yellow, includes the `Visual` package, which represents the human-machine interface for the remote operator. This renders the prepared data from the vehicle to the displays at the operator desk. A snapshot of this interface is provided in Figure 3.12, showing how videos from six cameras of the passenger vehicle, described in the following section, are stitched together in a three-dimensional environment. Moreover, the `Input Devices` also interface with additional hardware components of the operator desk, e.g., steering wheel, pedals, mouse, and keyboard. Finally, the `Manager` package manages the teleoperation session, providing a graphical user interface with various buttons. Using this, the remote operator can connect to the vehicle, select an input device or choose the control mode.

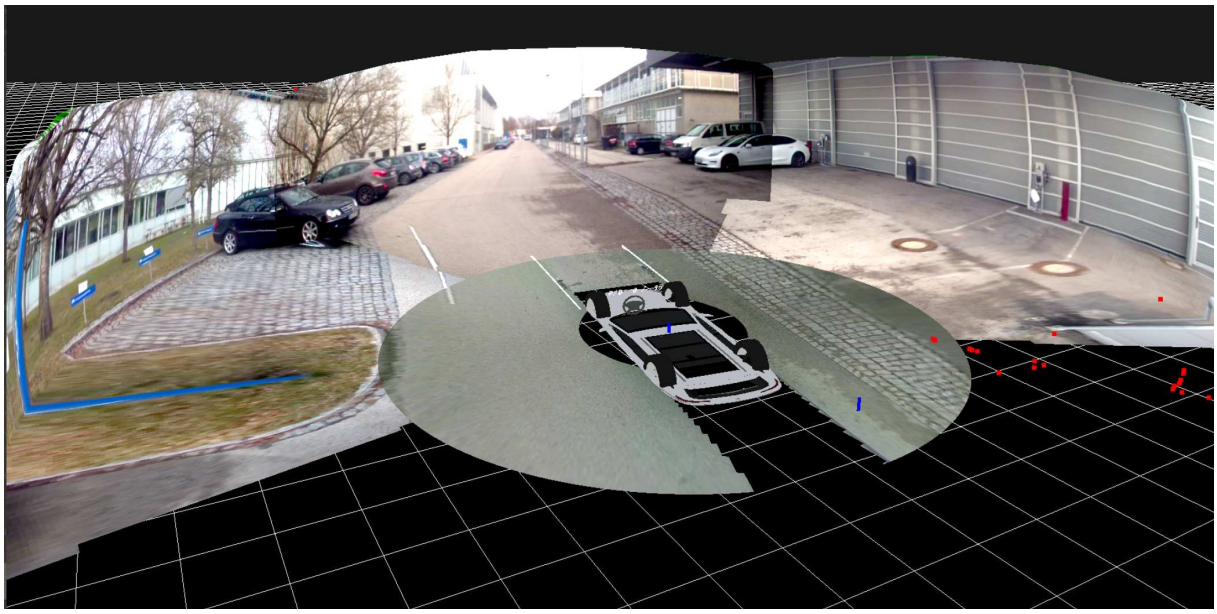

Figure 3.12: Visual human-machine interface of the teleoperation system, taken from Schimpe et al. [100]. In this snapshot, the videos from six cameras of a passenger vehicle are rendered in a three-dimensional environment, together with a geometrically true model of the vehicle.

### 3.4.2 Hardware

One of the goals during the development of the described teleoperation software has been to improve its usability. In this section, this will be described on the basis of the use of the software with different vehicles and remote operator desks.

#### Vehicles

Through an intuitive set of configuration files, the software can be deployed on various vehicles with minor overheads. In the following, the two main vehicles used for vehicle teleoperation research at the Institute of Automotive Technology are introduced. These are a full-size passenger vehicle as well as a 1:10-scale vehicle testbed. Similar to the development of automated driving software, it is described how the software is also usable with a driving simulator. Demonstrations of deploying the software on these vehicle systems are available [203].

The main vehicle for teleoperation experiments is a passenger vehicle, namely an Audi Q7, shown in Figure 3.13. This vehicle has a long history. Being described in the initial system design [119], it is still in use today. Currently, it is equipped with seven cameras, two 2D LiDAR sensors, and one 3D LiDAR sensor. The PC in the vehicle contains an Intel Xeon Gold 6130 2.10 GigaHertz 16-core processor. This vehicle has been used to validate many parts of the presented software, e.g., the visual operator interface shown in Figure 3.12.


Figure 3.13: Passenger vehicle for vehicle teleoperation experiments.

The Institute of Automotive Technology also operates a 1:10-scale vehicle testbed, based on the F1TENTH platform [204]. This vehicle is equipped with one stereo camera and one 2D LiDAR sensor. On board, computation is carried out by an NVIDIA Jetson Xavier NX with six cores, capable of WiFi for the connection to the operator side. As will be described in Chapter 5, the 1:10-scale vehicle testbed is used to experimentally validate the uncoupled shared control designs in the present work. A picture of it is shown in Figure 5.2.

Similar to the development of automated driving technology, the development of vehicle teleoperation systems can be accelerated through the use of driving simulators, simulating the dynamics and surroundings of the vehicle. At the time of writing this thesis, a vehicle bridge for the SVL (formerly LGSVL) driving simulator [205] was provided. A snapshot of the operator interface while performing teleoperation in this driving simulator is shown in Figure 3.14. Future plans include the creation of a vehicle bridge for the CARLA simulator [117].

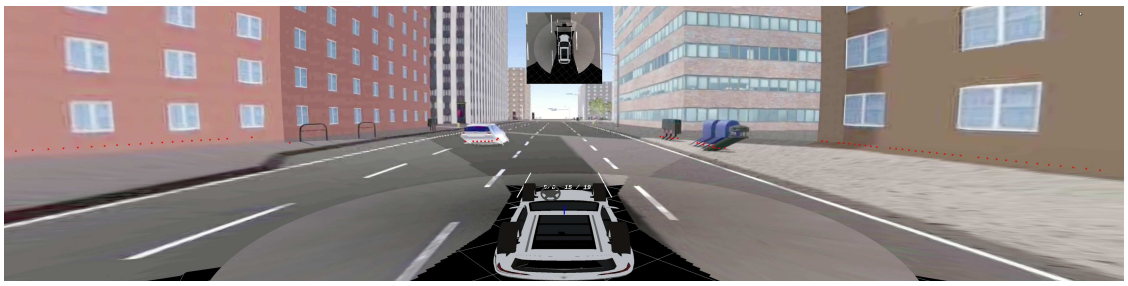

Figure 3.14: Visual operator interface while performing teleoperation in the SVL Driving Simulator, taken from Schimpe et al. [100].

In addition, for a simulation setup with minimal requirements, the `Vehicle Sim` package is included in the software. Implementing the equations of motion of the kinematic vehicle model [186], this enables the usage of the software without any additional hardware. This means that neither an actual vehicle nor a graphics processing unit for a comprehensive driving simulator is needed. As will be described in Chapter 4, this package has been used for the simulative validation of the uncoupled shared control designs.

Besides the aforementioned vehicle platforms, the software has been used in multiple different projects related to vehicle teleoperation. In the 5GCroCo project, the operator side of the software has been used to teleoperate two different passenger vehicles [108]. In the projects SToRM and UNICARagil, the software was deployed on a road marking machine as well as multiple custom-built vehicles [206, 207].

### Remote Operator Desks

The hardware of remote operator desks consists of displays and input devices. For the visualization, a set of three monitors is most commonly used, as shown in Figure 1.1. However, the system also supports the use of a head-mounted display.

For remote driving, a steering wheel and pedals are most commonly used as input devices. At the Institute of Automotive Technology, a Sensodrive SensoWheel SD-LC and different gaming wheel models from Fanatec are currently available. However, support of devices is not limited to this. Other controllers or joysticks, connected through USB, are easily integrated. This is made possible through the `Input Devices` package, which uses a common joystick interface. This makes easy switching between input devices possible. In this package, a virtual input device has also been implemented, allowing to test teleoperation functionality without any additional hardware. For the implementation of remote assistance concepts, different input modalities such as a mouse, keyboard, or touch panels replace the joystick setup.

## 3.4.3 Integration of Shared Control

The presented uncoupled shared control designs are integrated into the presented teleoperation system, conceptually shown in Figure 3.15. Implementing the approaches, the additional `Shared Control` package, also available open source on GitHub [208], replaces the `Direct Control` package. The vehicle state feedback is received from the `Bridge`. The list of objects, detected from LiDAR point clouds, are coming from the `Lidar` package. Finally, received through the `Network`, the remote operator's desired control commands are provided by the `Command Creation` package. The outputs of the `Shared Control` package are the safe control commands to actuate the vehicle through the `Bridge`, as well as visual and haptic feedback signals for the remote operator. These are transmitted via the `Network` to the operator side, where they are handled in the `Visual` and `Input Devices` packages, respectively.

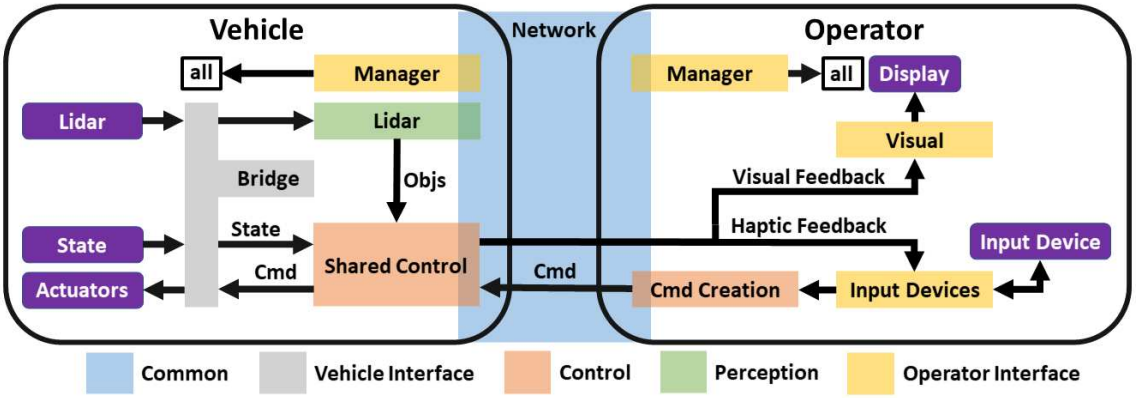


Figure 3.15: Integration of shared control as a ROS package in the teleoperation software. The package receives the vehicle state, object lists, as well as desired control commands from the operator side. Based on these, safe control commands for the actuation of the vehicle, as well as visual and haptic feedback signals for the remote operator are computed.

# 4 Simulative Validation

After presenting the methodology of the uncoupled shared control designs in the previous chapter, they are validated in simulation. The presented results are not extensive but are intended to show what reactions can be expected from the approaches in case of dynamic or unsafe control actions from the remote operator. The simulation setup and implementation details were first described by Schimpe et al. [97].

As described in the previous chapter, the uncoupled shared control designs are implemented as ROS nodes in C++ and integrated into the previously described teleoperation system. The vehicle parameters, e.g., dimensions or steering limits are from the passenger vehicle that was described in Subsection 3.4.2. The values are available in Section A.1 in the appendix. The simulations are run on an Intel Core i7-8850H 2.60 GHz CPU with six cores. Both uncoupled shared control approaches are running at 20 Hz. The prediction horizons are set to $t_\mathrm{h} = 2.0\,\mathrm{s}$. This horizon gives remote operators time to realize potential future interventions through visual feedback and possibly react predictively in order to avoid it. Aligned with the controller frequency, the horizon is discretized in $n = 40$ steps, yielding the sampling time $t_\mathrm{s} = 0.05\,\mathrm{s}$. The optimization problems of the model predictive control formulations are solved through `acados` [198]. This is a software package that enables the flexible creation of fast embedded solvers for nonlinear optimal control formulations. Allowing easy adaptation, the optimization problems are formulated through the `MATLAB` [209] interface of `acados`. For each controller, C code is generated and wrapped by a ROS node. Internally, `acados` implements a sequential quadratic programming, in short SQP, algorithm [210] to solve the optimization problem. In this work, the QP solver of choice is `HPIPM` [211]. The solver settings are also available in Section A.1 in the appendix.

In the following, to begin with, the effects on the constraints of the coupled accelerations in the SVC design are analyzed in a dynamic scenario without obstacles. In a second scenario with obstacles, the characteristics, i.e., behavior and computation times, of the two uncoupled shared control designs are compared. The chapter is concluded with a discussion.

## 4.1 Acceleration Constraints of SVC

In the first example, a dynamic simulation scenario without obstacles is set up to validate the feature of SVC to constrain the coupling of the longitudinal and lateral accelerations. Only for demonstrative purposes, a maneuver with high lateral dynamics is simulated. The longitudinal acceleration constraints are set to $a_{\min} = -3.5\,\mathrm{m/s^2}$ and $a_{\max} = 2.0\,\mathrm{m/s^2}$, respectively. The lateral acceleration is constrained by $a_{\mathrm{lat,max}} = 3.4\,\mathrm{m/s^2}$. This value is chosen such that the combined acceleration during braking with $a_{\min}$ does not exceed half of the gravitational acceleration. The jerk is constrained by $j_{\max} = 15.0\,\mathrm{m/s^3}$. In the first stage of the SVC algorithm, a total of 17 trajectories are sampled. Thereby, the maximum steering angle rate used was $\dot{\delta}_{\max} = 1.1\,\mathrm{rad/s}$.

The simulated control commands from the remote operator are shown in Figure 4.1. The desired velocity first increases to 6 m/s, where it is kept constant. Finally, the commands demand to brake back to a standstill. All three phases last over a time period of 10 s. The steering profile consists of three sine waves, each over a time period of 10 s, ranging from the left and right steering angle maximum of the vehicle. Thereby, maximum steering angle rates of approximately 0.39 rad/s are reached. A video of the presented simulation is available[1]. The velocity and steering angle over time are also shown in Figure 4.1. In the velocity plot, the SVC approach first follows the commands from the remote operator during the acceleration phase. However, at approximately 4 m/s, the controller does not further increase the velocity, given the lateral acceleration constraints and the assumption of the most critical steering angle profile. Approaching 10 s, when the steering angle decreases again, the controller accelerates the vehicle up to 5 m/s. As the steering angle rises to its positive maximum, the velocity is decreased again. While this is repeated periodically twice, the actual target velocity of 6 m/s is not reached. This shows that the acceleration constraints implicitly impose a steering angle-dependent velocity constraint. Starting at 20 s, the target velocity is decreasing back to zero, and upon reaching 4 m/s, the controller is able to track it again. The related acceleration values are plotted in Figure 4.2. Validating the acceleration constraints feature of the SVC approach, the imposed constraints are reached in some instances, but not exceeded.

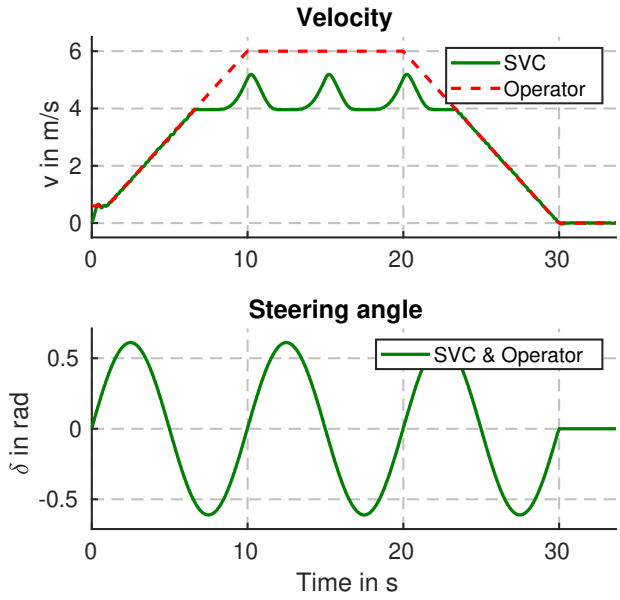


Figure 4.1: Velocity and steering angle over time of the shared velocity control (SVC) approach in the first simulation. At the top, the actual velocity from the approach and the desired velocity from the (remote) operator are shown. At the bottom, the corresponding steering angle is plotted.

[1] Video of SVC simulation with steering and no obstacles: https://youtu.be/Or6LHBkloew

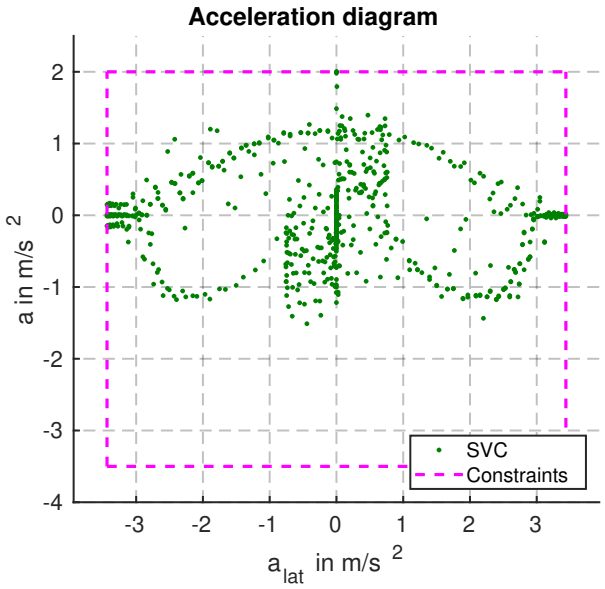


Figure 4.2: Acceleration diagram of the shared velocity control (SVC) approach in the first simulation. In addition to the acceleration samples, the constraints are shown.

## 4.2 Characteristics and Computation Times of SVC and SSVC

In the second simulation, the characteristics of SVC and SSVC are compared in a scenario with obstacles and unsafe control actions from the remote operator. This simulation has first been presented by Schimpe et al. [97]. The constraints and parametrization of the SVC approach are similar to the previous section. The same parameters of the longitudinal acceleration and the maximum steering angle rate are set for the SSVC approach. In this simulation, the steering behavior of the remote operator is simulated through a feedback linearization-based path tracking controller, taken from Burnett et al. [8]. The remote operator's goal is to follow a straight reference path with a constant desired velocity of 5 m/s. As this is not collision-free, uncoupled shared control interventions are expected.

The scenario is shown in the $xy$ plane in Figure 4.3. It consists of five obstacles. Obstacles ① to ④ are placed alternatingly left and right of the remote operator's reference path with decreasing $y$ position. The wider obstacle ⑤ is centered on the reference. In addition, the figure shows the trajectories that are traveled with the SVC and SSVC approaches. The corresponding courses of the velocity and steering angle as well as the remote operator references are shown over time in Figure 4.4. In both runs of the simulation, the vehicle starts driving from a standstill, accelerating to the constant target velocity of 5 m/s. This value is tracked consistently by the SSVC approach when passing obstacles ① to ④. In contrast to this, the SVC approach reduces the velocity to approximately 3.8 m/s and 2.3 m/s as it computes smaller values for the global safe progress $s_{\text{safe}}$ in proximity to the obstacles ② and ③. Until this point, as no obstacle had to be actively avoided, no steering actions are observed. Eventually, at approximately 15 s, it is foreseen that obstacle ④ cannot be passed without steering. As it is not capable of intervening in the steering angle, the SVC approach slows down the vehicle and brings it to a standstill at approximately $x = 65$ m and 17 s. In contrast to this, the SSVC approach takes a steering action and deviates from the reference of the remote operator in order to avoid obstacle ④. To avoid obstacle ⑤, the steering intervention would need to be much greater. Given the weighting of the cost function terms, a deviation from the velocity reference is preferred in this case. In consequence, the SSVC approach slows down the vehicle and brings it to a standstill as well at $x = 100$ m and 22 s. Videos of both described simulation runs are available[2,3].

[2]Video of simulation run showing characteristics of SVC: https://youtu.be/yFzSiwtUtq4
[3]Video of simulation run showing characteristics of SSVC: https://youtu.be/vz8slCFW140

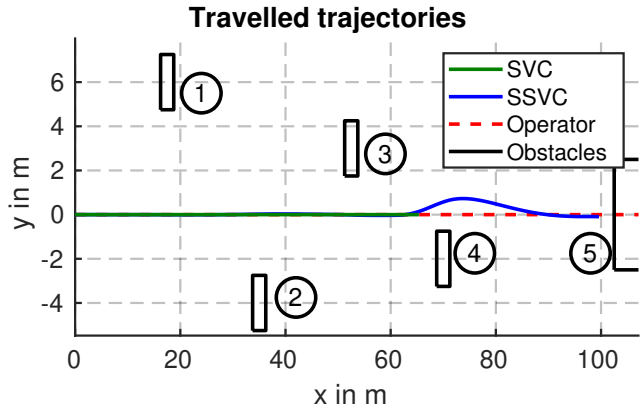


Figure 4.3: Travelled trajectories in the $xy$ plane with the shared velocity control (SVC) as well as the shared steering and velocity control (SSVC) approaches in the second simulation, taken and adapted from Schimpe et al. [97]. In addition, to the trajectories from the approaches, the reference from the (remote) operator as well as obstacles are shown.

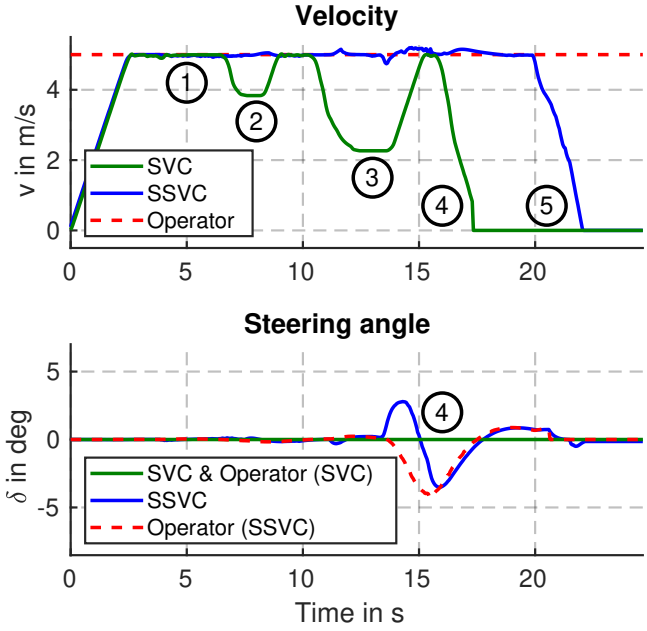


Figure 4.4: Velocities and steering angles over time of the shared velocity control (SVC) as well as the shared steering and velocity control (SSVC) approaches in the second simulation, taken and adapted from Schimpe et al. [97]. At the top, the actual velocities from the approaches and the desired velocity from the (remote) operator are shown. At the bottom, the corresponding steering angles are plotted.

Finally, the computation times of the controllers are analyzed in the two simulation runs of the second scenario. In milliseconds, these are shown in the histogram in Figure 4.5. Compared to the SVC approach with a median of 8.4 ms, the computation times of the SSVC approach with a median of 3.0 ms are noticeably lower. As the `tod_vehicle_sim` package implements the same kinematic vehicle model equations used in the model predictive control formulation of the SSVC approach, it can be assumed that there is a low mismatch between the model predictive control prediction and the actual motion of the controlled system. In consequence, given the recursive optimization of the controller, the solver can be initialized close to its solution at each sampling instant. This results in the SQP algorithm iterating only once in most cases.

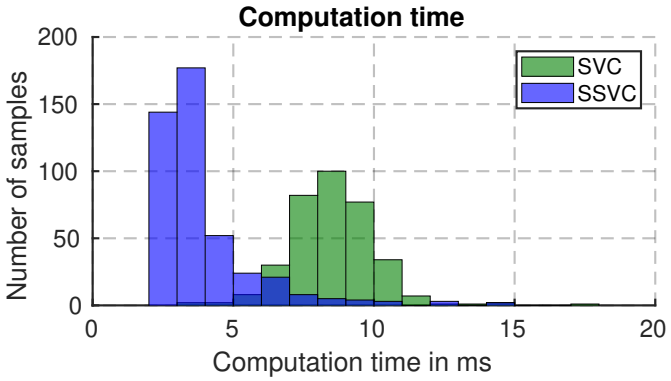


Figure 4.5: Computation times of the shared velocity control (SVC) and the shared steering and velocity control (SSVC) approaches in the second simulation. The maximum computation times are 17 ms with SVC and 15 ms with SSVC.

## 4.3 Discussion

In this chapter, a simulative validation of the proposed uncoupled shared control approaches was presented. In the first scenario, it was shown that the SVC approach is capable of increasing comfort with the constraints on the coupling of the longitudinal and lateral accelerations. Also, through the assumption of the most critical steering angle profile, a steering angle-dependent velocity constraint is imposed implicitly.

In two simulation runs in the second scenario, the characteristics of the SVC and the SSVC approaches were compared. Both designs have proven to only engage in the case of unsafe control actions from the remote operator, successfully avoiding obstacles by uncoupling, i.e., correcting, the control commands. The capability of the SSVC approach to deviate from the remote operator's steering angle reference has been demonstrated. If a greater deviation is required, the SSVC approach is also capable of stopping the vehicle. In contrast to this, the SVC approach drives much more conservatively, slowing down in proximity to obstacles and being more likely to stop the vehicle as it cannot override the steering angle commands from the remote operator. Finally, the computation times were analyzed. It was concluded that both controllers achieve the target controller frequency of 20 Hz.

In the next chapter, as part of the experimental validation in the user study, it will be evaluated how these findings translate to, for example, the rated controllability or user experience with the respective uncoupled shared control designs.

# 5 Experimental User Study

After the simulative validation in the previous chapter, the experimental user study is presented. First, the study design and setup are described. Second, the results of the user study are provided. These will provide the basis for the discussion that follows in the next chapter.

## 5.1 Study Design and Setup

The objective of the study is the evaluation and comparison of the proposed uncoupled shared control designs. Held in German, the study follows a within-subject design in which the participants teleoperate the 1:10-scale vehicle testbed, which was described in Subsection 3.4.2. In three different modes, namely Direct Control (DC), SVC, and SSVC, the vehicle is remotely driven on a circular course with static obstacles. The objective of the study is to represent extreme conditions for the uncoupled shared control approaches. Hence, the remote driving task should be demanding in order to require actual uncoupled shared control corrections. For this purpose, the study participants were asked to cover as much distance as possible in a given time while avoiding obstacles and staying on the course.

It is noted that the hypotheses are primarily concerned with the first research question, which asked about how uncoupled shared control compares to DC in terms of the workload and the performance of remote operators as well as the safety in remote driving. In order to address the second research question, which asked about the most suited uncoupled shared control design for remote driving, a separate comparison of SVC and SSVC is carried out.

In this section, first, the hypotheses and the operationalization of the study are introduced. Second, approved by the ethics commission from the Technical University of Munich, the study design is presented. Then, the teleoperation system setup is described, followed by the course setup. Finally, the testing methodology for significant differences is introduced.

### 5.1.1 Hypotheses and Operationalization

To address the first research question, three hypotheses are formulated. The first hypothesis is concerned with the cognitive workload of the remote operators. By design, the uncoupled shared control approaches only engage when the remote operators make errors. On the one hand, it is expected that this reduces the remote operators' cognitive workload. On the other hand, the system may not always behave as intended by the remote operators, which possibly increases the cognitive workload. Based on these considerations, the first hypothesis is that

*through uncoupled shared control, the cognitive workload of remote operators in remote driving is affected.*

To compare the cognitive workload across the modes DC, SVC and SSVC, the raw NASA-Task Load Index questionnaire [212], in short NASA-TLX is used to measure the cognitive workload as the dependent variable.

This questionnaire asks the participants to rate the perceived mental, physical, and temporal demands as well as the performance, effort, and frustration. The German translation of the NASA-TLX is taken from Lehsing and Seifert [213].

The remote driving task in the user study is to cover as much distance as possible while avoiding obstacles and staying on the track. With uncoupled shared control, the remote operators are assisted in obstacle avoidance. This should reduce the number of collisions and subsequent stops. From this, it is expected that the performance of the remote operators increases. Consequently, the second hypothesis is that

*through uncoupled shared control, the performance in remote driving is improved.*

As the dependent variable, which is compared across the three control modes, a dedicated remote driving performance score is analyzed. This is a function of the covered distance, the number of collisions with obstacles, and the number of track departures.

Third, given the primary objective of the uncoupled shared control designs to enhance safety, it is hypothesized that

*through uncoupled shared control, the safety in remote driving is improved.*

To evaluate this hypothesis, the safety is assessed in two different ways. As an objective dependent variable, the number of collisions is counted and compared across the three control modes. As a subjective dependent variable on a scale from 1 to 5, the participants answer if they feel safer with an uncoupled shared control design of choice. This question is asked after the participants experienced both uncoupled shared control designs.

In order to tackle the second research question, additional dependent variables are operationalized and compared between SVC and SSVC. This analysis also includes the cognitive workload and its individual items, assessed through the NASA-TLX. In addition, the helpfulness of the applicable feedback modalities, as well as the uncoupled shared control design features are evaluated. Also, the study participants are asked how well they can control the vehicle with the respective control mode. Furthermore, parts of the standardized user experience questionnaire [214] are answered and evaluated. The German translation for this has been taken from Hinderks et al. [215]. Finally, after having experienced both uncoupled shared control designs, the question of which design is preferred is asked.

### 5.1.2 Study Design

Figure 5.1 shows an overview of the study design. First, each participant is given a general introduction to the study. This is followed by a technical introduction to the teleoperation system. After this, each participant teleoperates the vehicle with each of the three control modes. The order of the modes is evenly swapped between the participants. Finally, the study is concluded. In the following, each part of the study is described in more detail.

#### General Introduction

In the general introduction, the motivation for vehicle teleoperation and the study are explained to the participants. In this part, an informed consent form is signed and a codeword for the pseudonymization of the data is generated. Furthermore, it is communicated that the study can be aborted at any time.

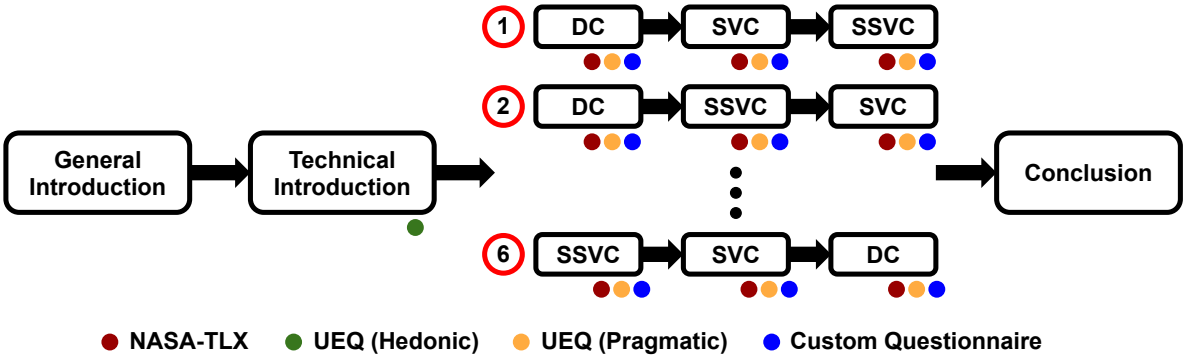


Figure 5.1: Overview of the experimental user study design. The design consists of four parts. The first, second, and fourth parts are the same for all participants. In the third part of the scored teleoperation drives, the order of the modes direct control (DC), shared velocity control (SVC), and shared steering and velocity control (SSVC) is evenly swapped between the participants. As depicted by the colored circles, four questionnaires are being answered over the course of the study. These are the NASA-Task Load Index (NASA-TLX), the parts of the hedonic and pragmatic quality of the user experience questionnaire (UEQ) as well as a custom questionnaire.

## Technical Introduction

In order to make the study participants familiar with the teleoperation system, a technical introduction is carried out. This includes the remote operator control interface, consisting of a steering wheel to steer, as well as gas and brake pedals. The latter is used to increase and decrease the desired velocity. To get used to this interface, the participants start by controlling the model in the `Vehicle Sim` package, which was introduced in Subsection 3.4.2, in a virtual environment without obstacles. During this, visible in Figure 3.8 and 3.10, the elements of the visual interface, such as the lanes, projecting the vehicle motion, as well as gear and velocity display, are explained. After this, a recording from the actual vehicle being teleoperated is played back. Based on this, the participants can get an impression of the visual interface, when the visual elements are overlaid with the video stream. Afterward, the participants start to teleoperate the actual vehicle without uncoupled shared control on the study course. First, they are given three minutes. As unexperienced remote operators need to get used to set a constant desired velocity with pedals, the velocity was limited to 3 m/s in this first test drive. Second, the participants are instructed to set and get used to higher velocities, the course layout of the study as well as the lateral motion capabilities of the vehicle. For this, a second, unassisted test drive of three minutes without velocity restriction is carried out. Finally, the technical introduction is concluded with a questionnaire. Having used the given teleoperation system for the first time, the participants answer the categories stimulation and novelty of the hedonic quality of the user experience, assessed through the user experience questionnaire. In this context, stimulation means that the system “is interesting, exciting and motivating” [215]. Novelty refers to the system being “innovative, inventive and creatively designed” [215].

## Scored Teleoperation Drives

After the completion of the technical introduction, the participants are prepared for the scored teleoperation drives. With the control mode, i.e., DC, SVC, or SSVC, as the independent variable, the participants are given three times five minutes to teleoperate the vehicle on the circular course with the objective to maximize the score. By evenly swapping the order of the modes, as shown in Figure 5.1, there are six different combinations. This compensates for the effects that result from the order in which the modes occurred.

As is communicated to the participants, the score is the covered distance. However, counted by a referee, the number of collisions and track departures results in a reduction of 30 m per occurrence. This rather high

penalty, which is equivalent to about one lap on the track, is intended to let participants make an appropriate compromise between safety and speed.

Whenever the participants teleoperate the vehicle together with an uncoupled shared control design, respective features such as correction of the steering angle or the velocity commands, as well as haptic or visual feedback are explained and shown in previously recorded demonstration videos. Test drives with the uncoupled shared control designs are not performed as the intuitiveness of the uncoupled shared control designs should also be evaluated.

After each scored teleoperation drive, the participants are asked to answer three questionnaires. First, the cognitive workload is collected through the raw NASA-TLX. Second, the categories efficiency, perspicuity, and dependability of the pragmatic quality of the user experience are assessed through the user experience questionnaire. In this context, efficiency means that tasks with the system can be performed “fast, efficient and in a pragmatic way” [215]. Perspicuity means that the system “is easy to understand, clear, simple, and easy to learn” [215]. Finally, dependability describes that the interaction with the system is predictable and supportive [215]. For consistency, the participants are also asked to answer this questionnaire after the teleoperation drive with DC. However, in this case, it should be answered for the complete teleoperation system and not for the particular uncoupled shared control design. Finally, a third custom questionnaire on the controllability, safety feeling, as well as helpfulness of applicable system features and feedback modalities is answered. Partially, the questions are depending on the mode. For example, the question on the helpfulness of the haptic feedback only has to be answered for the SSVC design. At the end of this questionnaire, there is also space for free-text comments on what was perceived positively as well as what could be improved in the past teleoperation drive.

#### Conclusion

At the end of the study, the participants have the option to give free-text comments on the study in general.

### 5.1.3 Teleoperation System Setup

In Section 3.4, an introduction to the teleoperation system at the Institute of Automotive Technology was given. In this section, hardware and software, which are used in the presented study, are described.

The software with the integrated uncoupled shared control designs, as described in Subsection 3.4.1 and 3.4.3, is used. The parameters of the vehicle, as well as solver settings, are available in Section A.1 in the appendix. With the objective to provoke activity, i.e., the need for interventions of the uncoupled shared control approaches, an artificial transmission delay is introduced. As a value known to have a significant negative effect on remote driving performance, this is up to 180 ms high [60]. In addition, in order to avoid the known effect that remote operators get used to a constant latency [216], it is made variable as it would be the case in a system with variable network conditions and no dedicated mitigation technique such as buffering. Each signal to and from the remote operator is delayed. This includes the control commands, visual and haptic feedback from the uncoupled shared control design, and videos from the vehicle. The data relevant to the control loop of the uncoupled shared control approach are not transmitted via the network. Hence, the state feedback and the list of detected objects are not delayed.

The teleoperated vehicle in the presented user study is the 1:10-scale vehicle testbed, introduced in Subsection 3.4.2 and shown in Figure 5.2. From its stereo camera, only the video from the left camera is transmitted and visualized to the remote operator. Obstacle detection is done by clustering the point clouds of the onboard LiDAR sensor. For transmission, a separate router is set up to host Wi-Fi, which the vehicle PC connects to.

Figure 5.2: Picture of the 1:10-scale vehicle testbed teleoperated in the experimental user study. On board, it is equipped with a 2D LiDAR sensor, a stereo camera, and an NVIDIA Jetson Xavier NX with six cores.

The remote operator desk with a Fanatec gaming wheel and pedals, introduced in Subsection 3.4.2, is used in the presented user study. Displaying an actual video feed from the vehicle, it is shown in Figure 5.3. As there is only one front-facing camera on the vehicle, only the center monitor of the setup is used during the teleoperation. During the study, the right monitor displays the questionnaires. The left monitor is turned off. The PC running the software of the operator side is connected to the same router as the vehicle PC but through a wired connection.


Figure 5.3: Picture of the remote operator desk used in the experimental user study. It is equipped with a Fanatec gaming wheel and pedals, three monitors mounted in a circular shape and a seat.

### 5.1.4 Course Setup

Shown in the picture in Figure 5.4, the course setup is a circuit with a length of approximately 30 m. On both sides, the bounds of the course are laid with cables. Placed partially on the inside, and partially on the outside of the circuit, foam cubes with edge lengths of 50 cm are used as obstacles. For reproducibility, the locations are marked on the ground below the cubes.

Figure 5.4: Picture of the course setup for the experimental user study. Foam cubes are used as obstacles. Around these, cables are used to mark the bounds of the course.

The course is at a vehicle hall at the Institute of Automotive Technology. Entering and exiting through two gates, the course is partially indoors and partially outdoors. The driving direction is counter-clockwise. Chicanes are set up on the straights and blocking obstacles are often placed right after a turn. As a whole, this makes up a challenging course that should provoke errors from the study participants and therefore require interventions of the uncoupled shared control approaches.

### 5.1.5 Testing Methodology for Significant Differences

Throughout the presentation of the study results, the following testing methodology for statistically significant differences from Field et al. [217] is adopted. For all tests, a significance level $p$ of 0.05 is used. In case a Bonferroni correction is applied, this level is reduced as required. To begin with, it is determined if parametric tests are applicable. For this, the data of each mode are tested for normality through the Shapiro-Wilk test, which is reported with the corresponding test statistic $W$. Testing for homogeneity of the data across the modes, this is followed by a Levene test, which is reported with corresponding test statistic $F$ [217, p. 166-204]. If data are normal and homogeneous, the assumptions for parametric tests are fulfilled and an analysis of variance, in short ANOVA, which is reported with the corresponding test statistic $F$, is conducted [217, p. 391-461]. If its result indicates a statistically significant difference, pairwise t-tests with a Bonferroni correction follow [217, p. 368-388]. These are reported with the corresponding effect size $r$. If the assumptions are not fulfilled, a non-parametric Friedman's ANOVA, which is reported with corresponding test statistic $\chi^2$, is performed [217, p. 686-692]. Again, if this indicates a statistically significant difference, it is followed by non-parametric, pairwise Wilcoxon signed-rank tests with a Bonferroni correction [217, p. 655-666]. Also, these are reported with the corresponding effect size $r$.

Following Fritz et al. [218], the effect sizes in the pairwise tests are interpreted as follows. If $r$ is below 0.1, there is no effect. Between 0.1 and 0.3, the effect is small. Between 0.3 and 0.5, it is medium. Above 0.5, the effect is deemed large.

## 5.2 Results

The study has been carried out in July and August 2022. For each participant, the complete experiment took approximately 60 to 70 minutes. A total of 32 participants took part. From these, 30 (93.8 %) were male and two (6.2 %) female. The median age was 26 years, with the youngest participant being 22 and the oldest being 40 years old. All participants were in possession of a driver's license, driving a minimum of 250 and a maximum of 30 000 km per year. The median traveled per year was 11 000 km. None of the participants had previous experience with a comparable teleoperation system. Only a few participants reported having driven a driving simulator before.

In the following sections, the results are presented. For the most part, these are color-coded by using red for DC, green for SVC, and blue for SSVC. First, the user experience, as rated with DC, is shown. Thereby, the representation of results through boxplots is introduced. After this, two sample teleoperation drives with SVC and SSVC are shown. This is followed by a brief analysis of learning effects across the three scored teleoperation drives. Then, the main study results are reported. First, results concerned with the three hypotheses and differences between DC and uncoupled shared control are analyzed. Second, with the objective to answer the question of what is the most suited uncoupled shared control design for remote driving, a comparison between SVC and SSVC is carried out. It is noted that only the results are presented in the following. Their interpretation is included in the discussion in the next chapter.

### 5.2.1 User Experience with Direct Control

In Figure 5.5, the user experience ratings of the participants for the teleoperation system with DC are shown as boxplots. In one box, the median and mean values are shown as a line and a cross, respectively. Excluding outliers, depicted as dots, the range between the minimum and maximum values is shown. The box represents the 25th and the 75th percentiles. This boxplot representation is used for several other results from the presented user study.

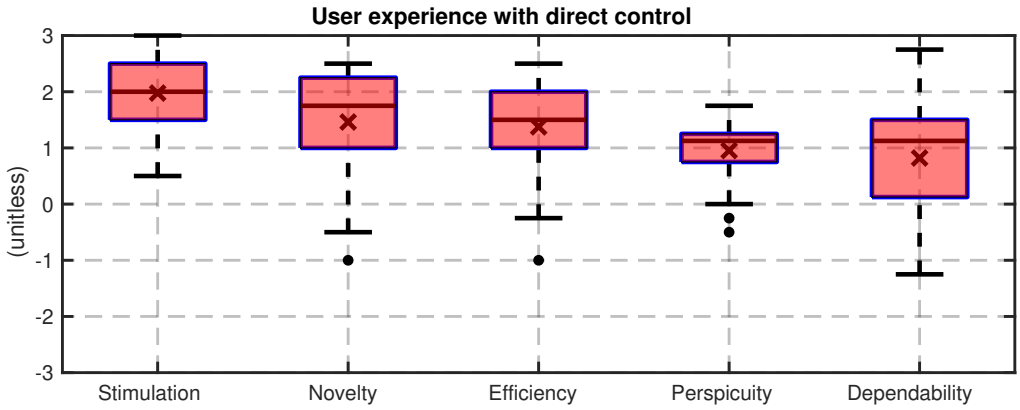


Figure 5.5: User experience of the teleoperation system with direct control, assessed through the user experience questionnaire. The scale ranges from -3 for a poor to +3 for a good user experience.

As described in Subsection 5.1.2, the categories of the hedonic quality, i.e., stimulation and novelty, were assessed after the technical introduction. Given that the study participants were selected to not have previous experience with a comparable teleoperation system, the ratings for stimulation and novelty, with mean values of 1.98 and 1.46, are above 0.8 and thus positive [215]. The pragmatic quality, i.e., efficiency, perspicuity, and dependability, was assessed after the scored teleoperation drive with DC. With mean ratings of 0.82 for dependability, 1.38 for efficiency, and 0.95 for perspicuity, these ratings of the teleoperation system are also positive.

### 5.2.2 Sample Teleoperation Drives with SVC and SSVC

In this section, sample teleoperation drives with SVC and SSVC are presented. To begin with, it is validated that the computation times of the approaches on the new target platform are acceptable. In Figure 5.6, the computation times are shown. For SSVC, three samples with a maximum of 66 ms are above 50 ms. In contrast to the results from the simulative validation, presented in Chapter 4, the SVC approach is running faster than the SSVC approach. Its maximum computation time is 19 ms. Overall, the computation times are higher, compared to those of the simulative validation. This is expected as the controlled system is not behaving exactly as predicted through the kinematic vehicle model. Nevertheless, it is shown that both controllers are capable to run at the target rate of 20 Hz consistently. The exceptions of the SSVC approach are deemed neglectable.

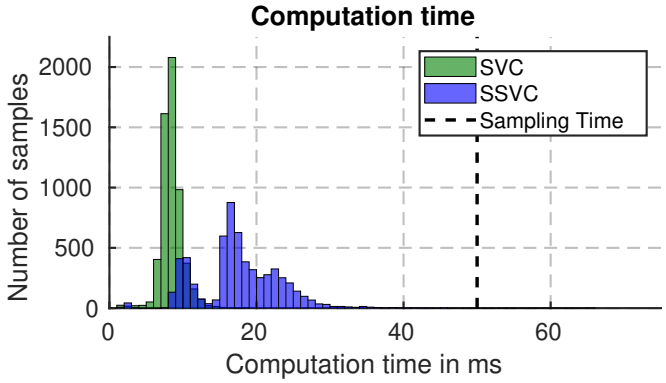


Figure 5.6: Computation times of the shared velocity control (SVC) and the shared steering and velocity control (SSVC) approaches in the sample teleoperation drives. With a maximum of 66 ms, three samples from the SSVC approach are above the sampling time of 50 ms. The maximum computation time with SVC is 19 ms.

From one study participant, the velocity and steering angle over time are shown, together with the respective interventions of the SVC and SSVC approaches in Figure 5.7 and 5.8, respectively. In the case of SVC, several interventions can be observed in the tracking of the desired velocity. In one instance around 95 s, the vehicle is slowed down significantly. In another instance at 120 s, it is stopped completely. For the drive with SSVC, in particular, in the steering angle, interventions are also visible. In contrast to this, the velocity is tracked more consistently. The vehicle is never brought to a complete stop.

Finally, for demonstrating the uncoupled shared control designs as well as DC in action, videos from the author of the present work performing remote driving are available[1,2,3]. It is noted that these videos are not a recording from the teleoperation drives presented in Figure 5.7 and 5.8.

[1] Video from the author performing remote driving with DC: https://youtu.be/oY-a-6BItjg
[2] Video from the author performing remote driving with SVC: https://youtu.be/yXRfVOLSFuM
[3] Video from the author performing remote driving with SSVC: https://youtu.be/aiOSsajcSfM

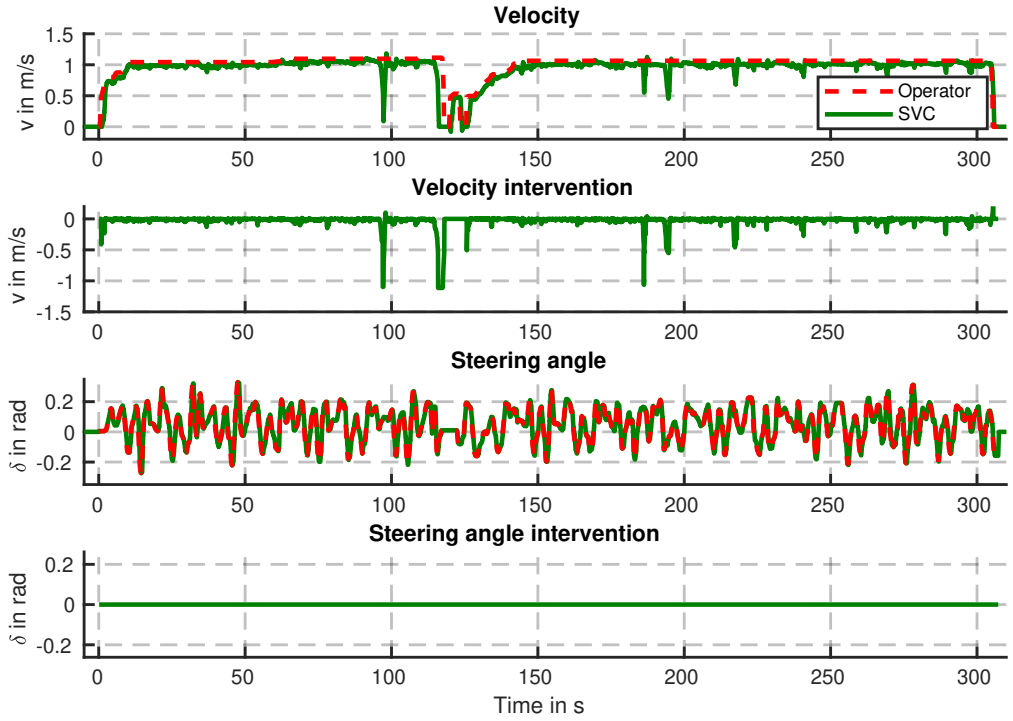


Figure 5.7: Velocity and steering angle with interventions of a teleoperation drive with shared velocity control (SVC).

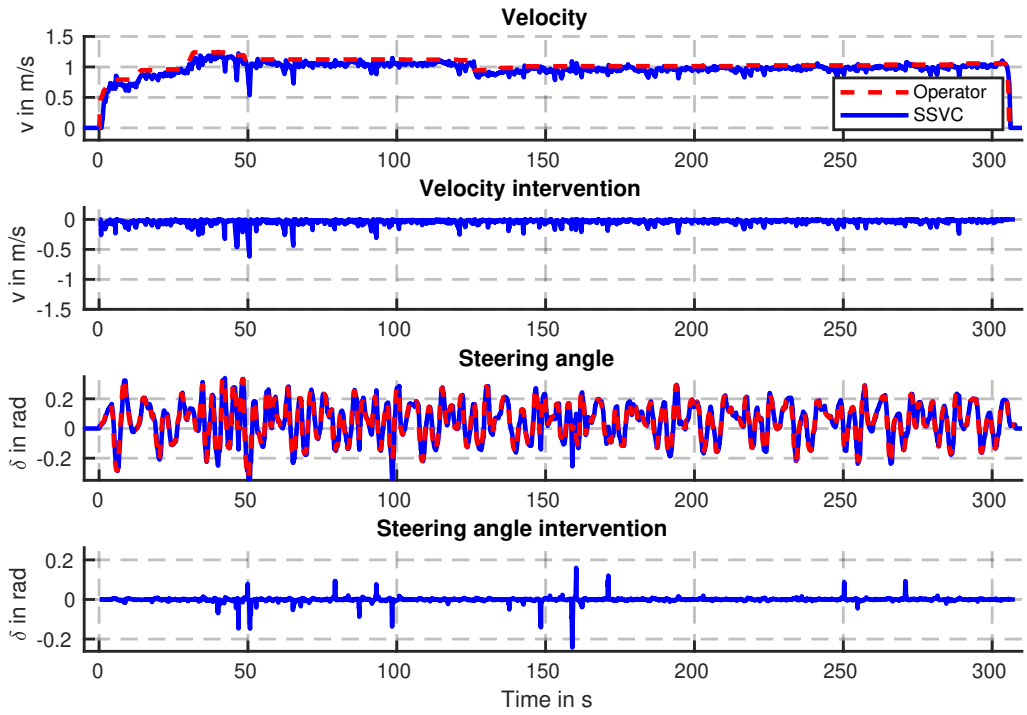


Figure 5.8: Velocity and steering angle with interventions of a teleoperation drive with shared steering and velocity control (SSVC).

### 5.2.3 Learning Effects

Before the presentation of the main study results, a brief analysis of learning effects across the three teleoperation drives, independent of the control mode, is carried out. The focus is on the rated controllability of the system as well as the individual items of the cognitive workload. The color coding uses different gray scales for the first, second, and third teleoperation drives, respectively.

## Controllability

The controllability per teleoperation drive is shown in Figure 5.9. With the mean ratings rising from 3.19 to 3.63, an increasing trend is visible.

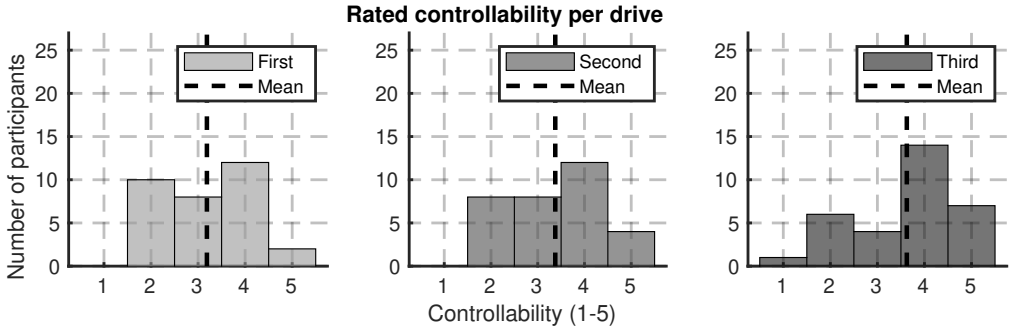


Figure 5.9: Controllability per teleoperation drive. Tests do not indicate significant differences.

Statistical tests, which complete results are also reported in Subsection A.2.1 in the appendix, are performed. As the data are not normal for all drives, a non-parametric Friedman's ANOVA is carried out. Despite the initial observation of learning effects, the result does not yield a significant difference in the controllability across the teleoperation drives.

## Items of Cognitive Workload

The results for the individual items of the cognitive workload per teleoperation drive are shown in Figure 5.10. In several items, trends are observable. For instance, the performance increases, and the temporal demand decreases across the three drives. For completeness, the mean cognitive workload per drive is shown in Figure A.1 in the appendix. However, as no clear trend can be observed, it is not analyzed further.

With the complete test results for this section reported in Subsection A.2.1 in the appendix, statistical tests are performed. As the data of the drives are not normal for all workload items, it is continued with non-parametric tests. Friedman's ANOVA does not indicate significant differences across the drives in the physical demand, the effort, as well as the frustration. However, with $p < 0.05$, the test results yield significant differences in the mental demand with $\chi^2(2) = 6.36$, the temporal demand with $\chi^2(2) = 8.54$, as well as the rated performance with $\chi^2(2) = 8.92$.

Pairwise Wilcoxon signed-rank tests with a Bonferroni correction follow for the items, which indicated significant differences. In the case of the mental demand, with $p < 0.017$, the result yields a significant decrease between the first and the third teleoperation drive. With $r = 0.43$, the effect size is medium. With $p < 0.01$, the test indicates a significant increase in the performance between the first and third teleoperation drive. With $r = 0.53$, the effect size is large. Finally, with $p < 0.01$, the results yield significant decreases in the temporal demand between the first and the second, as well as between the first and the third teleoperation drive. With $r = 0.47$ and $r = 0.50$, the effect sizes are medium in both cases.

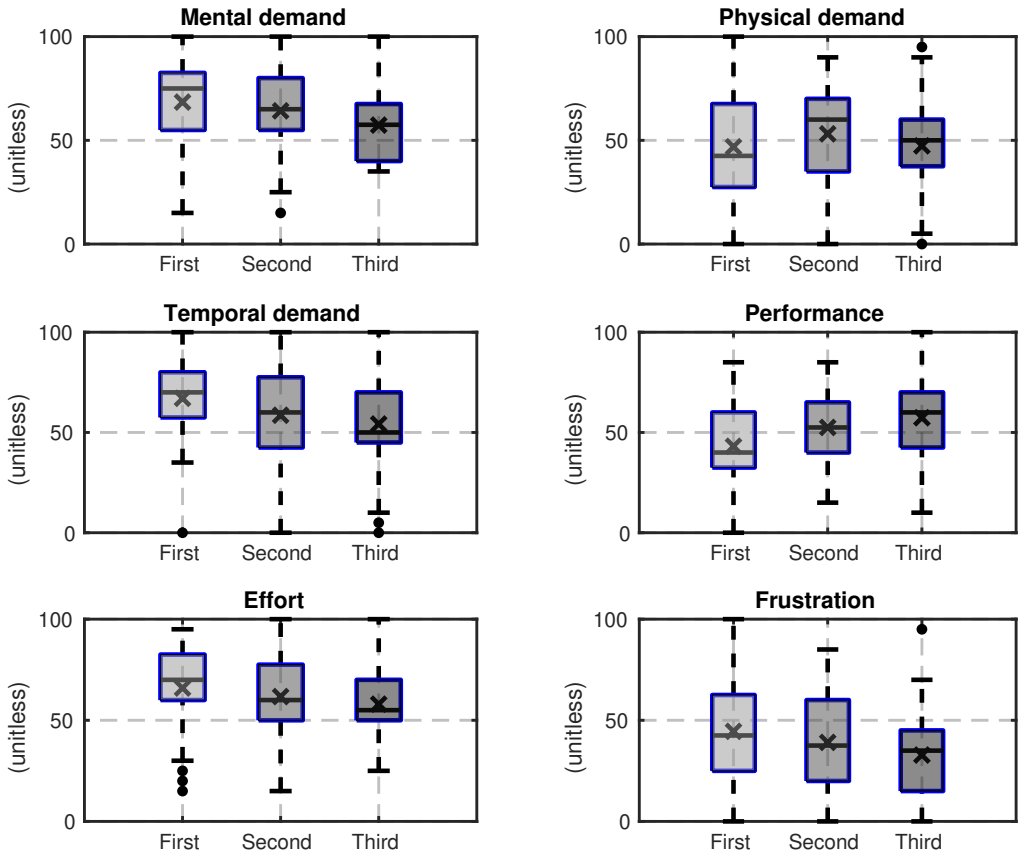


Figure 5.10: Items of the cognitive workload per teleoperation drive assessed through the NASA-TLX. Tests yield significant differences in the mental demand between the first and the third teleoperation drive. The same applies to the performance. The temporal demand is significantly different between the first and the second, as well as the first and the third teleoperation drive. For the items of physical demand, effort, and frustration, no significant differences are found.

In the results presented in the following, learning effects were compensated by swapping the order of the modes. Nevertheless, from the test results, it has been found that learning effects were present in the mental demand, temporal demand, and rated performance.

### 5.2.4 Hypothesis 1: Cognitive Workload

It was hypothesized that uncoupled shared control affects the cognitive workload of remote operators when performing remote driving. For this analysis, the cognitive workload, calculated as the mean from the items of the NASA-TLX, is evaluated. The results are shown in Figure 5.11. It can be observed that, compared to DC with a mean cognitive workload of 54.9, the mean of SVC with 51.0 is lower. With 56.1, the mean of SSVC is higher.

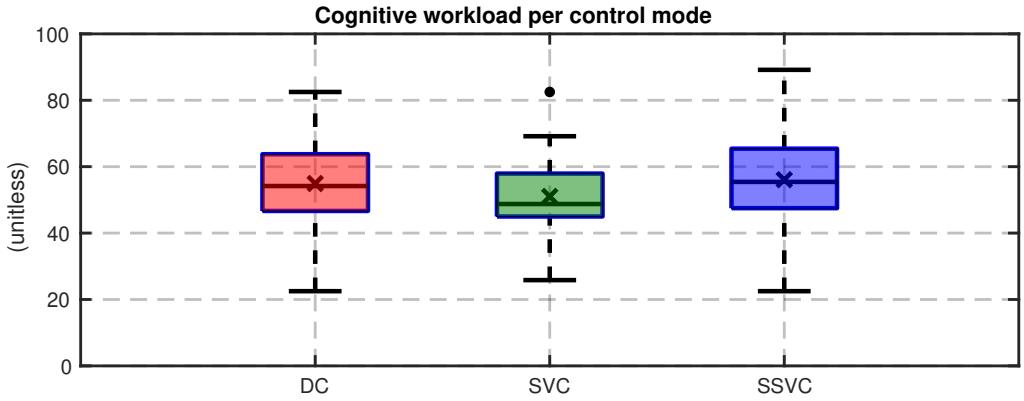


Figure 5.11: Mean cognitive workload with direct control (DC), shared velocity control (SVC), and shared steering and velocity control (SSVC) assessed through the NASA-TLX. Tests do not indicate significant differences.

The data are tested for significant differences. The complete test results are given in Subsection A.2.2 in the appendix. To begin with, the data are tested for the assumptions made by parametric tests. The Shapiro-Wilk test and the Levene test indicate normality and homogeneity of the data for all control modes. In consequence, it is continued with a parametric ANOVA. Despite the initial observations, with $p > 0.05$ and $F(2,93) = 2.16$, this test does not yield a significant difference in the cognitive workload across the control modes.

As described in Subsection 5.1.1, two effects were expected related to the cognitive workload. These were a decrease in the cognitive workload through the assistance, but also a potential increase due to disturbances through uncoupled shared control. As the results in this section showed, these effects seem to balance each other. In consequence, the first hypothesis that the cognitive workload is affected through uncoupled shared control is rejected.

### 5.2.5 Hypothesis 2: Remote Operator Performance

The second hypothesis was that the remote operators' performance in remote driving improves through uncoupled shared control. As explained in the study design, the score is calculated from the covered distance in each teleoperation drive minus the number of collisions and track departures times 30 m. To begin with, the outcomes of the covered distances per mode are shown in Figure 5.12. It is observed that the covered distance of DC with a mean of 338.4 m is larger in comparison to SVC with a mean of 292.9 m and SSVC with a mean of 265.1 m.

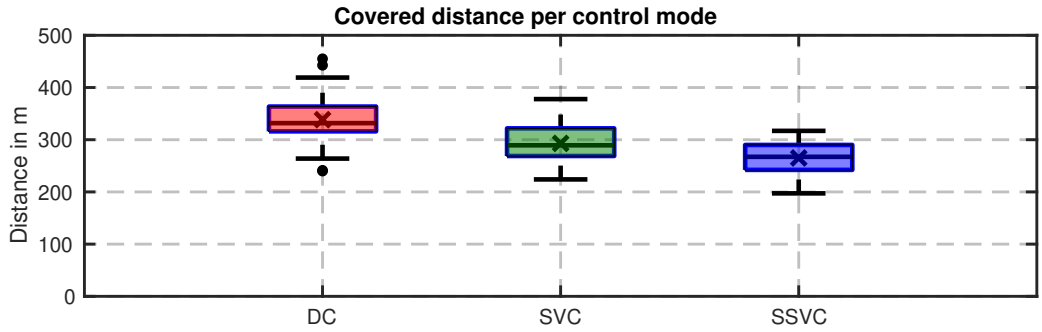


Figure 5.12: Covered distance with direct control (DC), shared velocity control (SVC), and shared steering and velocity control (SSVC).

Second, the number of collisions per mode is shown in Figure 5.13. With a mean of 1.34, the number of collisions with DC is higher as compared to 0.19 with SVC and 0.63 with SSVC.

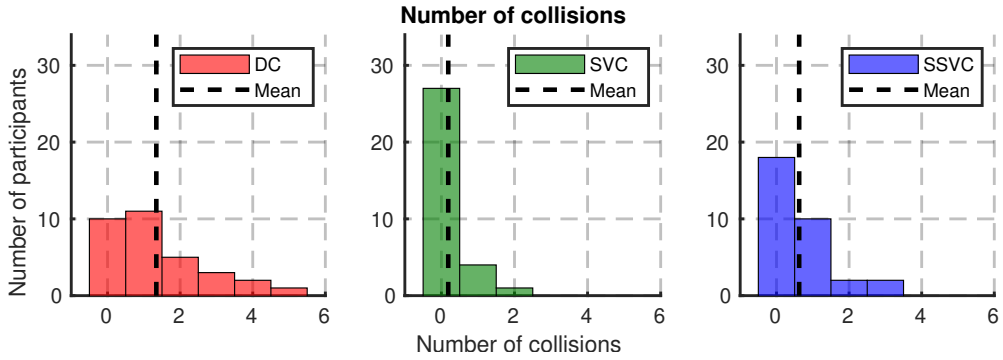


Figure 5.13: Number of collisions with direct control (DC), shared velocity control (SVC), and shared steering and velocity control (SSVC).

As the third contributor to the performance score, the number of track departures is shown in Figure 5.14. With rare exceptions of one and two track departures, the majority of participants managed to keep the vehicle on the course consistently with DC and SVC. In contrast to this, there are an average of 0.78 track departures per drive with SSVC. This reveals one issue with the capability of this approach to override the steering angle. As it is not aware of the track bounds, the model predictive control solution may be in a local minimum which is at the wrong side of an obstacle. In consequence, if the remote operator does not brake in time, the vehicle can be led off the track in some cases.

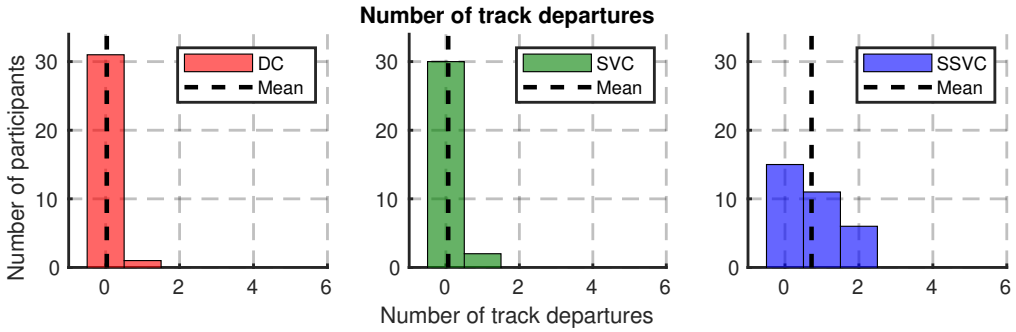


Figure 5.14: Number of track departures with direct control (DC), shared velocity control (SVC), and shared steering and velocity control (SSVC).

Finally, from these data, the performance score is computed for each participant. The results are shown in Figure 5.15. First observations indicate that the scores with SVC, with a mean of 291.1 m, and SSVC, with a mean of 243.5 m, are lower than the scores with DC, with a mean of 297.1 m.

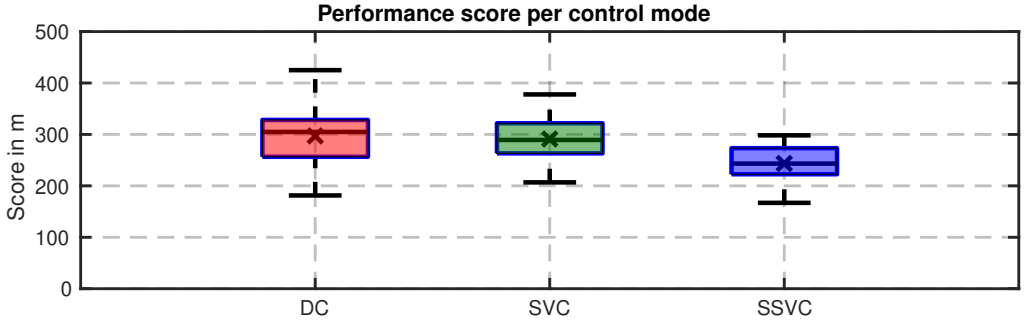


Figure 5.15: Performance score with direct control (DC), shared velocity control (SVC), and shared steering and velocity control (SSVC). Tests yield that the score with SSVC is significantly lower in comparison to the scores with DC and SVC.

These observations are followed by statistical tests, which complete test results are reported in Subsection A.2.3 in the appendix. As the Levene test indicates significant non-homogeneity of the score data across the modes, the assumptions for parametric tests are not fulfilled. In consequence, a Friedman's ANOVA is conducted. With $p$ < 1e-4 and $\chi^2(2) = 22.75$, this test indicates significant differences across the modes. This is followed by pairwise Wilcoxon signed-rank tests with a Bonferroni correction. With $p$ < 1e-4, the performance score with SSVC is significantly lower compared to DC as well as SVC. With $r = 0.77$ and $r = 0.79$, the effect sizes in both tests are large. With $p > 0.05$, there is no significant difference between the performance scores with DC and SVC. With $r = 0.09$, the effect size in this test is neglectable.

Through uncoupled shared control, it was expected and thus hypothesized that the performance of the remote operators increases. However, the presented statistical analysis showed that this is not the case. It was even found that the performance with SSVC is significantly lower in comparison to the other two control modes. In consequence, the second hypothesis is rejected. In addition, the issue with SSVC, not being aware of the track bounds, has been revealed.

### 5.2.6 Hypothesis 3: Safety

Third, it was hypothesized that safety is increased with uncoupled shared control. For this, two metrics are analyzed. Objectively, the effect of uncoupled shared control on the number of collisions is assessed. Subjectively, the agreement of the study participants to the question, if the perceived safety with an uncoupled shared control approach of choice is increased, is analyzed.

First, the number of collisions is analyzed. For this, the results were already shown in Figure 5.13. The total number of collisions was 43 with DC, six with SVC, and 20 with SSVC. It is noted that, in theory, the uncoupled shared control approaches should be capable to avoid all collisions. However, given the limitations of the obstacle detection method and unmodelled dynamics of the 1:10-scale vehicle testbed, not all collisions could be avoided in the presented user study. Nevertheless, it is concluded that the uncoupled shared control designs effectively improve the safety of the vehicle by assisting in the task of collision avoidance. Second, the study participants' responses to the question, if the perceived safety is increased with an uncoupled shared control approach of choice, are analyzed. The scale of the agreement ranged from 1 to 5. The original responses are shown in Figure A.2 in the appendix. For the analysis in this section, the responses are summarized, as shown in Figure 5.16. Responses greater and smaller than three are taken as agreement and disagreement, respectively. A response equal to three is taken as neutral. Three participants reported not feeling safer with uncoupled shared control. Four participants responded to be neutral. With 25 participants, the majority reported an increase in the perceived safety feeling with uncoupled shared control.

In conclusion, from an objective and a subjective perspective, the presented analysis shows that uncoupled shared control makes remote driving safer. In consequence, the third hypothesis is accepted.

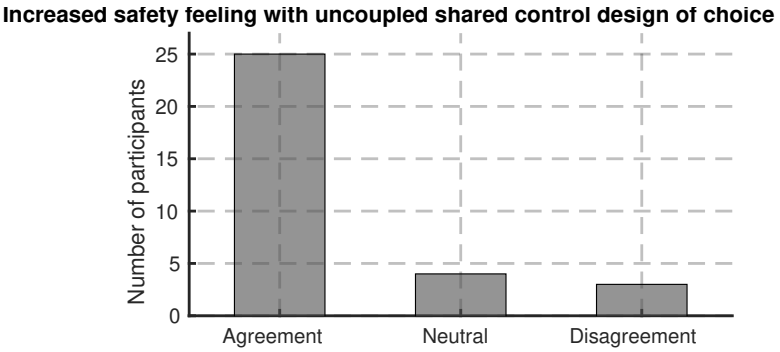


Figure 5.16: Summarized agreement to an increase in the perceived safety feeling with an uncoupled shared control design of choice.

### 5.2.7 Comparison of SVC and SSVC

To answer the second research question, which asked about what is the most suited uncoupled shared control design variant for remote driving, the two uncoupled shared control designs, SVC and SSVC, are compared. The comparison is carried out with respect to several measures. To begin with, the cognitive workload, assessed through the NASA-TLX, and its individual items are compared. This is followed by an analysis of the participants' opinions on the helpfulness of the applicable feedback modalities. Then, the rated controllability, as well as the pragmatic quality of the user experience with the uncoupled shared control designs are compared. Finally, the rated helpfulness of the respective uncoupled shared control design features and the participants' preference for an uncoupled shared control design are analyzed. As no hypotheses, which explicitly compare the SVC and SSVC designs, have been formulated, the statistical tests in this section are performed exploratively. If applicable, the results with DC for the respective measures are provided for reference and completeness. However, given the focus in this section to compare SVC and SSVC, they are not discussed in more detail.

## Items of Cognitive Workload

In Subsection 5.2.4, the mean cognitive workload has already been analyzed. This did not indicate a significant difference between SVC and SSVC. In this section, the analysis is continued by comparing the individual items of the cognitive workload. The participants' ratings are shown in Figure 5.17. As the Shapiro-Wilk test indicates that the items effort and frustration are not normal, the analysis is continued with non-parametric tests. The complete test results are given in Subsection A.2.5 in the appendix.

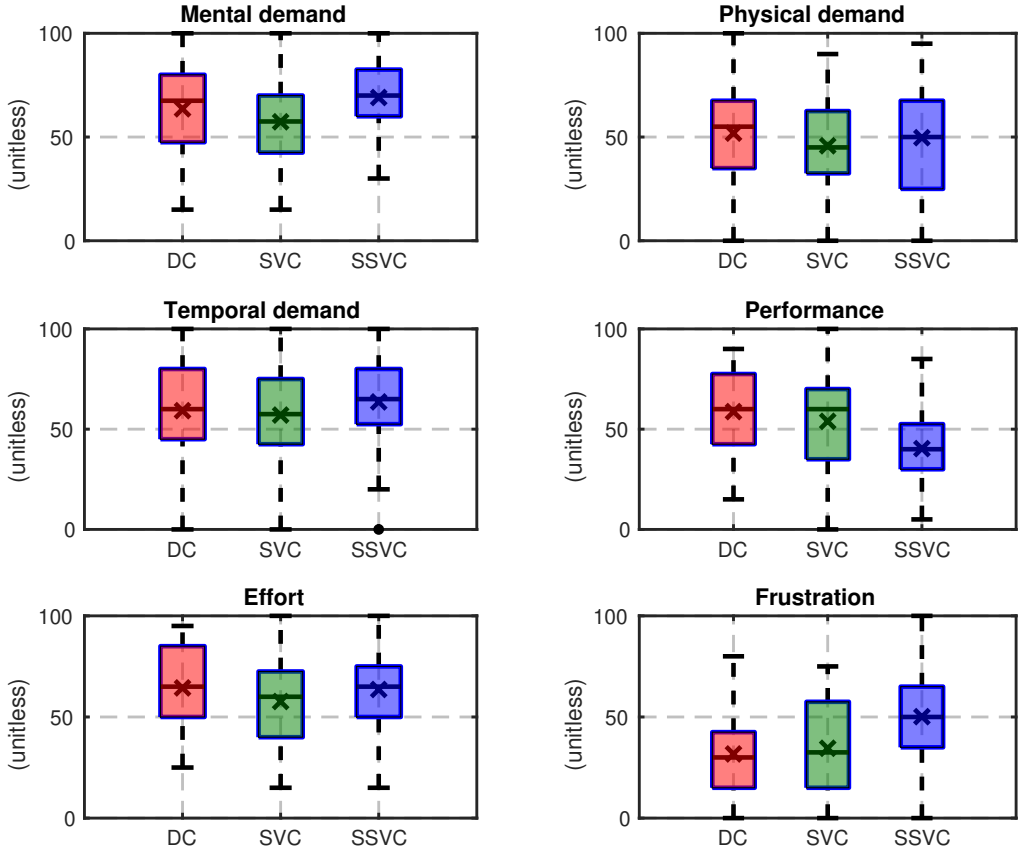


Figure 5.17: Items of the cognitive workload with direct control (DC), shared velocity control (SVC), and shared steering and velocity control (SSVC) assessed through the NASA-TLX. Tests yield significant differences in the performance between SSVC in comparison to DC as well as SVC. The frustration with SSVC is also significantly different in comparison to DC as well as SVC. For the items mental demand, physical demand, temporal demand, and effort, no significant differences are found.

To begin with, Friedman's ANOVA does not indicate significant differences for the items mental demand, physical demand, temporal demand, and effort.

However, with $p$ < 1e-3 and $\chi^2(2) = 14.05$, Friedman's ANOVA indicates statistically significant differences in the performance between the control modes. With $p$ < 1e-3 and $p$ < 0.01, post-hoc Wilcoxon signed-rank tests with a Bonferroni correction yield that the rated performance with DC and SVC is significantly higher in comparison with SSVC. With $r = 0.68$ and $r = 0.46$, there are large and medium effects, respectively.

The analysis of the rated frustration yields similar results. With $p$ < 0.01 and $\chi^2(2) = 10.52$, Friedman's ANOVA yields that there are statistically significant differences between the control modes. With $p$ < 1e-3 and $p$ < 0.01, post-hoc Wilcoxon signed-rank tests with a Bonferroni correction reveal that these differences are between SSVC and DC as well as SVC. With $r = 0.59$ and $r = 0.53$, both effects are large.

## Visual and Haptic Feedback

In this section, the participants' ratings of the helpfulness of the provided feedback modalities are analyzed. In addition, some of the received comments are summarized.

As described in Subsection 3.2.3 and 3.3.3, the visual feedback for the uncoupled shared control designs consists of visual elements, which are overlaid with the video stream. In the case of SVC, a colored polygon is used to visualize the trajectory tree. In the case of SSVC, a colored polygon is used to show the current trajectory plan of the approach. On a scale from 1 to 5, the participants' ratings of the helpfulness of the visual feedback for both approaches are shown in Figure 5.18. With a mean of 3.9 for SVC and 3.5 for SSVC, the majority of the participants rated the visual feedback in both designs as helpful.

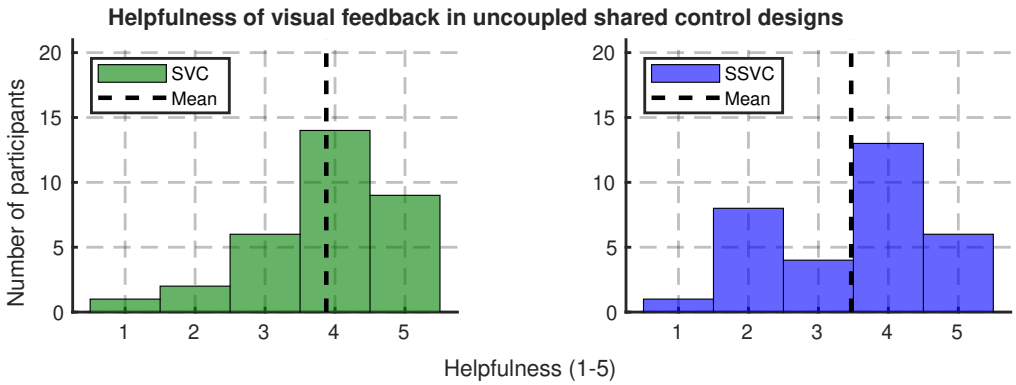


Figure 5.18: Helpfulness of the visual feedback in the shared velocity control (SVC) design and the shared steering and velocity control (SSVC) design. With a mean of 3.9 for SVC and 3.5 for SSVC, the majority of the participants rated the visual feedback in both designs as helpful.

Several comments on the visual feedback of the SVC design were received. These included the consensus that the visual feedback improves the capability of predictive driving, the understanding of the reactions of the SVC approach, as well as the capability to estimate the distance to obstacles. Improvement suggestions included the use of different polygon shapes or arrows, additional colors, and the inversion of the display, i.e., only coloring the space that is not drivable. It was also mentioned that it would be helpful to improve the clarity of the display to communicate if the system will brake partially or completely.

Also, several comments mentioned the visual feedback of the SSVC design. In these, it was stated that it enables predictive driving, improves lane keeping performance, and helps to understand the decisions of the system. It was also mentioned that the polygon would probably be helpful alone, even without the active intervention of the SSVC approach. Improvement suggestions included that the clarity of the coloring could be improved. Potentially, the intervention could be visualized earlier.

The white lines in the visual feedback, computed based on the current steering wheel angle of the vehicle, represented an element that was present in all teleoperation drives. Its helpfulness was explicitly asked for and rated by the participants after the teleoperation drive with DC. The answers are shown in Figure A.3 in the appendix. With a mean of 3.9, this element was also perceived as helpful by the majority of the participants.

As presented in Subsection 3.3.3, also haptic feedback was provided in the SSVC design. Its rated helpfulness is shown in Figure 5.19. With a mean of 3.5, the majority of participants also perceived this as helpful. Comments mentioned that it is intuitive and important to understand when the SSVC approach intervenes in steering. Some participants stated that the haptic feedback could have been stronger.

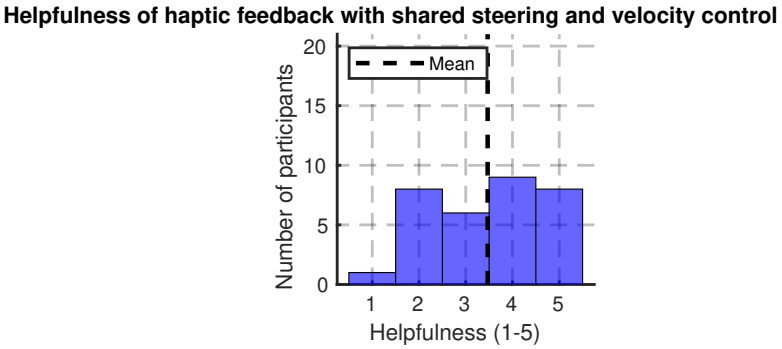


Figure 5.19: Helpfulness of the haptic feedback in the shared steering and velocity control design. With a mean of 3.5, the majority of participants also perceived this as helpful.

## Controllability

After each teleoperation drive, the participants were asked to subjectively rate the controllability of the teleoperation system. Again from 1 to 5, the answers could range from poor to good controllability. The responses of the participants are shown in Figure 5.20. The mean rating for DC is 3.6. With 3.8, the mean rating for SVC is higher. With 2.8, the mean rating for SSVC is lower.

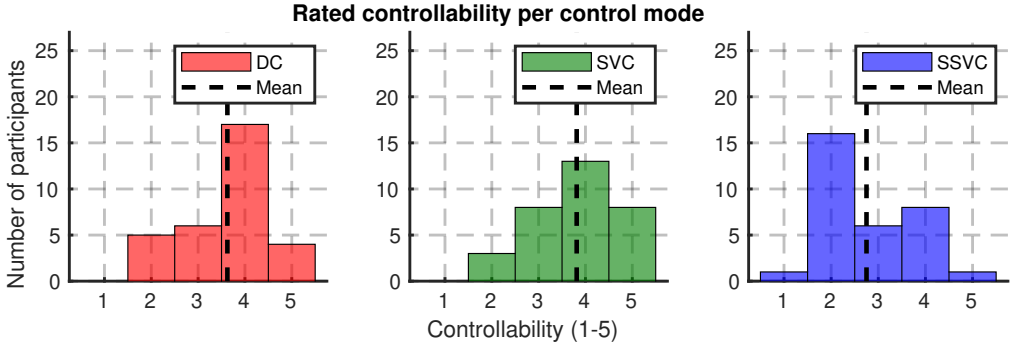


Figure 5.20: Controllability with direct control (DC), shared velocity control (SVC), and shared steering and velocity control (SSVC). Tests yield that the controllability with SVC is rated significantly higher in comparison to SSVC.

Statistical tests are carried out for the comparison of SVC and SSVC. The complete test statistics are reported in Subsection A.2.5 in the appendix. As the data of all modes are not normal, non-parametric tests are performed. With $p$ < 1e-4 and $\chi^2(2) = 20.17$, Friedman's ANOVA indicates significant differences. With $p$ < 1e-3, the result of a post-hoc Wilcoxon signed-rank test with a Bonferroni correction yields that the controllability with SVC is rated significantly higher in comparison to SSVC. With $r = 0.64$, the effect is large.

## Pragmatic Quality of User Experience

After each teleoperation drive with an uncoupled shared control design, the participants were asked to rate the three categories of the pragmatic user experience quality on a scale from -3 to +3. The answers are summarized in Figure 5.21. It can be observed that the user experience of SVC is rated higher in all three categories.

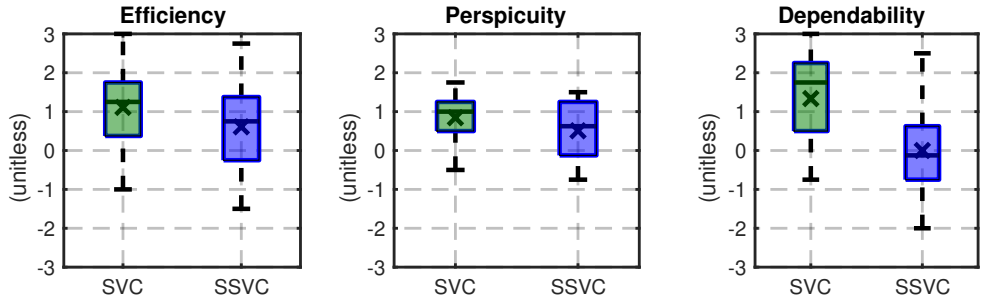


Figure 5.21: Pragmatic quality of the user experience with shared velocity control (SVC), and shared steering and velocity control (SSVC). Tests yield that the user experience with SVC is rated significantly higher in comparison to SSVC in all three categories. The scale ranges from -3 for a poor to +3 for a good user experience.

Statistical tests, which complete results are reported in Subsection A.2.5 in the appendix, are carried out. As the data are not normal for all modes, non-parametric Wilcoxon signed-rank tests are performed for the comparison of SVC and SSVC. With $p < 0.05$, the tests yield significantly greater efficiency and perspicuity with SVC. With $r = 0.37$ and $r = 0.40$, the effect sizes are medium. With $p <$ 1e-4, the dependability with SVC is significantly greater as compared to SSVC. With $r = 0.71$, the effect is large.

## Uncoupled Shared Control Design Features

After each teleoperation drive with uncoupled shared control, the participants were asked to rate the helpfulness of the respective features of the design. As the names suggest, those features were the overriding of the velocity in the case of SVC, as well as the overriding of steering and velocity in the case of SSVC. Again, the rated helpfulness could range from 1 to 5. Also, if related comments were received, these are summarized in this section.

In Figure 5.22, the results are shown for the velocity overriding feature in both designs. With mean ratings of 4.0 with SVC and 3.5 with SSVC, the feature is rated as helpful overall.

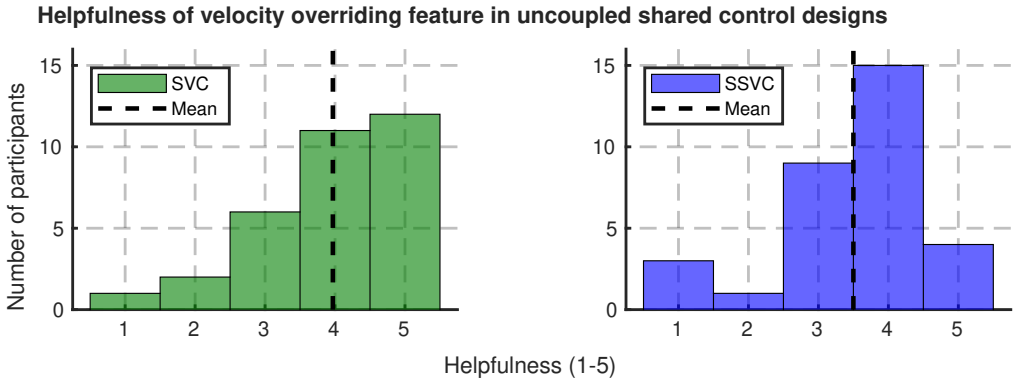


Figure 5.22: Helpfulness of the velocity overriding feature in the shared velocity control (SVC) design, as well as the shared steering and velocity control (SSVC) design. With mean ratings of 4.0 with SVC and 3.5 with SSVC, the feature is rated as helpful overall.

In comments, participants' feedback on the SVC included that the system improves safety through automatic and smooth braking, effectively reducing the workload when controlling the velocity. Improvement suggestions were to decrease the deceleration potential and frequency of the system braking. Furthermore, it has been noted that automatic reacceleration of the vehicle after braking through the system is critical, especially in turns.

The rated helpfulness of the steering overriding feature in the SSVC design is shown in Figure 5.23. With a mean of 2.8, a value below the middle of the scale at 3.0, it is not rated as helpful by the study participants.

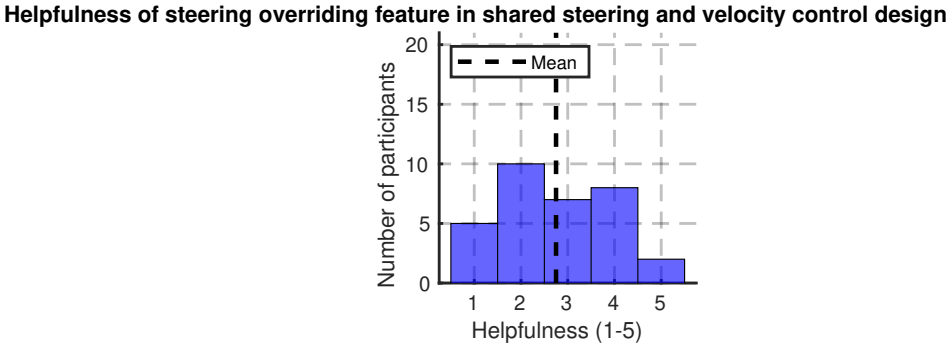


Figure 5.23: Helpfulness of the steering overriding feature in the shared steering and velocity control design. With a mean of 2.8, it is not rated as helpful on average.

In comments, participants reported that minor steering interventions were helpful as they avoided collisions without stopping. It was noted that the SSVC design restricts less than the SVC design, enabling more effective driving at speeds up to 4 km/h. Beyond that larger steering interventions often destabilized and disturbed, when trying to follow the own intentions. Also, it was mentioned that it was difficult to predict when the system intervenes. This partially increased the stress level. Finally, it was suggested that the system should reduce the velocity when a steering intervention occurs. Also, the approach should be made aware of the track boundaries as it would avoid departures of the course.

## Preferred Uncoupled Shared Control Design

Finally, after the second teleoperation drive with an uncoupled shared control design, the participants were asked which uncoupled shared control design was preferred. Originally, the answers could range from 1 to 5, where 1 and 5 corresponded to a strong preference for the SVC and SSVC design, respectively. The original ratings are shown in Figure A.4 in the appendix. Similar to the procedure in Subsection 5.2.6, the answers are summarized for clarity in this section. The results are shown in Figure 5.24. With 23 out of 32, the majority of the study participants reported preferring the SVC design. Only 9 answered to have a preference for the SSVC design. No participants were undecided.

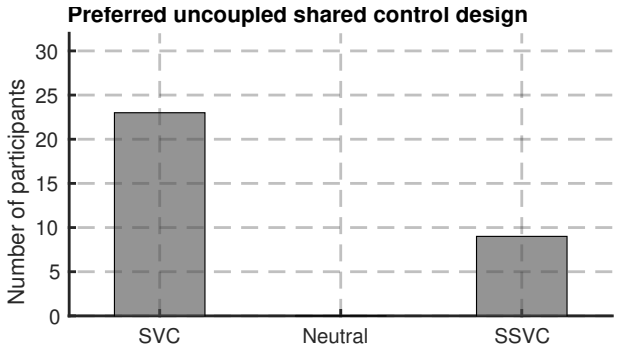


Figure 5.24: Summarized responses of the preferred uncoupled shared control design. With 23 out of 32, the majority of the participants prefer shared velocity control (SVC) over shared steering and velocity control (SSVC).

# 6 Discussion

After the presentation of the results from the experimental user study, they are discussed in this chapter. First, with the goal to provide answers to the first research question, the effects of uncoupled shared control on remote driving in comparison to direct control are described. This is followed by the discussion on the second research question, which asked what is the most suited uncoupled shared control design for remote driving. After this, the limitations of the user study as well as uncoupled shared control, in general, are elaborated. Finally, the chapter concludes with a brief discussion on regulatory topics, following up on the challenges of teleoperation that have been outlined in Subsection 1.2.3 in the introduction.

## 6.1 Effects of Uncoupled Shared Control

In this section, based on the results from the experimental user study, the effects of uncoupled shared control on remote driving in comparison to direct control are discussed in response to the first research question. In addition, a comparison with results from the work by Anderson [158] is incorporated for some aspects. As already described in Subsection 2.2.2, this work evaluated an uncoupled shared control design that could correct the remote operator's steering control actions. The evaluation was carried out in a user study with teleoperation experiments and 20 participants. In two different modes, "unshared" and "shared", i.e., direct control and shared steering control, the participants' task was to traverse a course with static obstacles as fast as possible. In the present work, the shared steering control design variant was not considered as it yields the limitation of being incapable of avoiding collisions through braking, which is required in, for example, dead ends. However, as these were not part of the course setup, a comparison of shared steering control to the present user study, which considered SVC and SSVC, is possible to some extent.

In the present work, first, it was hypothesized that uncoupled shared control affects the cognitive workload of remote operators in the remote driving task. Two effects were expected. On the one hand, the uncoupled shared control designs have the potential to reduce cognitive workload as they assist in collision avoidance. On the other hand, the interventions may disturb as the uncoupled shared control approaches deviate from the remote operators' intentions. Analyzing the individual items of the cognitive workload, it became apparent that direct control and SVC are consistently rated comparably. However, effects are visible with SSVC, with performance and frustration being rated significantly lower and higher, respectively. Nevertheless, as these effects balanced each other, no difference was found in the mean cognitive workload of SSVC either. In consequence, the results in Subsection 5.2.4 rejected the first hypothesis.

Second, it was hypothesized that uncoupled shared control improves the performance of the remote driving task, which was covering as much distance as possible without colliding or leaving the track. For reference, the considered performance score, reported by Anderson, improved by a factor of 1.4 with uncoupled shared control, in comparison to direct control [158, p. 113]. These results are in contradiction to the results in the present work. In Subsection 5.2.5, it was shown that the achieved score with the SVC design is only comparable with direct control. In the case of SSVC, it was even found that the participants' performance score was significantly lower. Surprisingly, the hypothesis had to be rejected. Analyzing the individual

variables that make up the score, i.e., the covered distance as well as the number of collisions and track departures, there are implications of a variable tradeoff between speed and accuracy, in particular with SSVC. Also, when comparing against the results in [158], it is concluded that different results are to be expected for different uncoupled shared control systems and user study settings.

Third, it was hypothesized that uncoupled shared control increases safety in remote driving. As reported in Subsection 5.2.6, the remote operators' perceived level of safety did increase. With 1.34 collisions per drive, the results showed that direct control yielded the highest number of collisions. Through uncoupled shared control, this could be reduced to 0.63 with SSVC and 0.19 with SVC. This is in line with the results reported by Anderson. These yielded a reduction of the number of collisions per run from 0.41 with direct control to 0.11 with uncoupled shared control [158, p. 109-110]. It is noted that, in theory, all collisions should be avoidable. However, in the present work, there were some limitations to the technical system performance. For instance, there were unmodelled actuation delays. In addition, depending on whether one or two sides of an obstacle were visible, the LiDAR-based detection algorithm outputs inconsistent obstacle dimensions. This leads to one limitation of uncoupled shared control in general, which is the assumed functionality of the perception of the automated driving system. This will be discussed further in Section 6.4.

Several effects through uncoupled shared control have been identified. Due to balancing positive and negative effects, the mean cognitive workload was found to be unaffected. Surprisingly, the performance of remote operators did not improve through uncoupled shared control. In the case of SSVC, it was even reduced as the approach deviated from the remote operators' intentions in some instances. On the positive side, there are general improvements in vehicle safety as well as the remote operators' perception of safety.

## 6.2 Most Suited Uncoupled Shared Control Design

In Subsection 5.2.7, several results from the experimental user study were presented, comparing SVC and SSVC. In this section, these results are used in order to respond to the second research question, which asked about the most suited uncoupled shared control design for remote driving.

To begin with, the mean cognitive workload did not yield a significant difference between the control modes. However, when comparing SVC and SSVC, there are some observations to be made in the individual items of the cognitive workload. It was found that the frustration and the performance with SVC are rated significantly lower and significantly higher, respectively. This indicates a clear disadvantage of SSVC, which likely originated from the undesirable steering interventions of the SSVC in some cases. This resulted in the avoidance of an obstacle on the wrong side, which led the vehicle off the track. In general, this indicates that the application of SSVC may not have been ideal in the tight driving course. This potentially represents a limitation of the presented user study and will be discussed further in Section 6.3.

As found, the performance score is different when comparing SVC and SSVC. Although the covered distance with both designs is comparable, SSVC was more heavily penalized, especially given the number of track departures. This led to the result that the score with SVC is significantly better in comparison to the score with SSVC.

Both uncoupled shared control designs have proven to enhance the safety of the vehicle by effectively reducing the number of collisions. Although this metric was even better with SVC, it is noted that all collisions should be avoidable if previously mentioned technical shortcomings are resolved. Considering this, no recommendation can be given on the better uncoupled shared control design in terms of collision avoidance.

The applicable feedback modalities in both uncoupled shared control designs were consistently rated helpful by the study participants. This, as well as received comments, confirmed that the feedback for the

communication from the automation to the remote operator represents an important aspect of uncoupled shared control. Hence, it should be designed with care. Several comments from the study participants already gave suggestions for possible improvements, which will be included in the outlook for future work in the following chapter.

The study results suggest that the SVC design offers improved controllability and user experience compared to SSVC. This indicates that participants perceived SVC as more intuitive and reliable. It is assumed that the lack of knowledge regarding track boundaries in the SSVC design also contributed to its lower ratings.

The helpfulness of the uncoupled shared control design features, i.e., overriding of the steering or velocity commands, has been rated as mixed. In both designs, the majority of the study participants rated the overriding of the desired velocity for collision avoidance as helpful. Likely as a more conservative intervention, braking of the vehicle is deemed more acceptable. The opinions on the feature of SSVC to override the steering angle were rather neutral to negative, likely due to the intervention being too aggressive in some instances. This underlines that steering interventions are a feature, which is likely to only be accepted in cases where the uncoupled shared control approach is well aware of the remote operator's intentions.

Finally, when directly asked which uncoupled shared control design they preferred, 23 out of 32 participants stated being in favor of SVC. Only nine preferred SSVC. No neutral, i.e., undecided, responses were given.

In conclusion, the majority of the presented results from the experimental user study indicate that the SVC design is superior and preferred by the participants, highlighting its advantages in several measures. However, it is important to acknowledge the limitations of this study, which may have influenced certain findings. The following section will discuss these limitations in detail, providing insights into the factors that may have impacted the results.

## 6.3 Limitations of the User Study

There are several findings and recommendations from the results of the presented user study. However, such an experiment also comes with limitations. These are elaborated and discussed in this section.

In the present work, the evaluation of the uncoupled shared control designs has been carried out with the participants operating a teleoperation system with an actual vehicle, and not a driving simulator. This gives the results better comparability with real-world scenarios and thus more relevance. However, the teleoperated vehicle was not of full size, but only a testbed at a scale of 1:10. Given this, it is likely that the participants were always aware that the actual risk and taken damage, in case of collisions, were limited. This represents one limitation or, in simple terms, an influencing factor on the results. The teleoperation likely would have been more conservative if the vehicle had been full size.

Given the objective to cover as much distance as possible in a given time, the general setting of the study was motivating the participants to remotely drive the vehicle at high speeds. As described in the study design in Subsection 5.1.2, the purpose was to evaluate the performance of the uncoupled shared control designs under extreme conditions. To some extent, this should be noted as a limitation of the presented study. A racing setting would not be reasonable for actual remote driving circumstances. In these, achieving the highest speed would not have a high priority. However, remote operators should not drive arbitrarily slow either. Speed and accuracy will need to be traded off in some way, but not as drastically as in the presented user study. In addition, it is noted that the study setup, with static obstacles and a circular course, did not represent a reasonable fail case of an automated driving system. A more versatile setup as well as the consideration of dynamic obstacles is something to be considered in future work.

The number of collisions with obstacles was used as a measure to quantify safety. For the setting of the study with higher speeds, this was reasonable. However, for actual remote driving, not a single collision would be acceptable. Instead, other metrics such as the time-to-collision should be taken into account. Also, the consideration of lane departures should be discussed. Although it led to a penalty on the performance score in the user study, it was not considered an unsafe action. In reality, this may be different, and uncoupled shared control approaches should possibly be designed to also avoid it.

In the technical introduction, the participants were given six minutes of driving. Based on this, it was assumed that the participants had the chance to get to know the teleoperation system and the course of the track well enough. Nevertheless, as the results in Subsection 5.2.3 showed, learning effects could still be identified. For instance, as part of the cognitive workload, several items show an observable trend. Also, the rated controllability indicates learning effects, increasing from a mean of 3.19 to 3.63 over the course of the three scored teleoperation drives. It can be assumed that these variable learning effects between the control modes could have been avoided by training the participants for longer. It also remains an open question how the results would have turned out with experienced remote operators performing remote driving on a regular basis. Nevertheless, it is noted that parts of these effects were been mitigated through randomization of the order of modes.

As described before, one further limitation of the user study was that the application of SSVC in the tight driving setting was not ideal. It can be assumed that, if the space would have been wider and multiple obstacles would not follow each other closely, the risk of the SSVC design taking over and deviating far from the remote operators' intentions, would have been much lower. In this case, it is possible that some of the assessed metrics would have been more in favor of SSVC.

Several circumstances indicate the limitations of the presented user study. First, while the setup came close to an actual teleoperation system, a full-size vehicle could have been used. This would have made the actual risk, which is perceived by the participants, more reasonable. Second, the participants' willingness to take more risks was potentially skewed as the performance score could be improved by driving at higher speeds. Third, it has been noted that the assessment of safety would be different in actual remote driving scenarios. Fourth, some learning effects were identified, which could have been avoided through more training. Fifth and last, it was noted that the application of SSVC in a different setting may have led to different results. In conclusion, while the recommendations, which were derived from the study results, are clear, they should be taken with care and may be different for a different vehicle teleoperation system or other remote driving circumstances.

## 6.4 Limitations of Uncoupled Shared Control

In the present work, uncoupled shared control has been introduced as an enabler of remote driving. However, it also comes with certain limitations, which are discussed in this section.

The application of vehicle teleoperation has been presented as a fallback for certain fail cases of the automated driving system. However, uncoupled shared control, as a remote driving concept, makes assumptions about certain parts of the automated driving system being available. In particular, the core assumption of uncoupled shared control for obstacle avoidance is that the perception of the automated driving system is functional and capable of detecting obstacles. Hence, if the perception module requires assistance, the teleoperation system should be complemented by at least the perception modification concept, which was introduced in Subsection 2.1.1.

In uncoupled shared control, the automation is capable of overriding the control actions from the remote operator in the interest of safety. The assumption is that it is the remote operator who makes mistakes and

needs to be safeguarded. In consequence, the automation in uncoupled shared control has to be fully reliable. This raises concerns in case of automation failure. This is a research topic in itself in the field of shared control. For instance, in the work from Bhardwaj et al. [162], this has been studied through the introduction of cases in which the automation failed to intervene appropriately. Similarly, from this different perspective, Huang et al. [219] encourage shared control as it enables “the human driver [...] to compensate for the automation system’s degraded performance and to ensure the safety of the [...] system.”. This describes the use case of shared control in exactly the opposite way. Overall, considering potential automation fail cases, the minimal requirement should be the introduction of an emergency stop button for the remote operator through which the vehicle can be brought to a safe stop at all times.

The workload in remote driving is generally high. As has been justified, uncoupled shared control is meant to represent a fallback for the automated driving system in fail cases at the tactical level of the dynamic driving task. Not representing a direct limitation of uncoupled shared control, it is noted that some fail cases could also be addressed through remote assistance concepts. As the interaction in remote assistance is not continuous, it is assumed that this imposes a lower cognitive workload on the remote operators. As this needs to be studied, it will be noted as an item for future work in the outlook in the next chapter.

To summarize, although shared control has been presented as a teleoperation concept that holds great promises, it makes certain assumptions, which potentially limit its applicability. For instance, it is assumed that the perception of the automated driving system and the automation of the uncoupled shared control approach are fully reliable. Only then, safety can be ensured. In addition, in remote assistance, there possibly exist alternative solutions to resolve automated driving system fail cases at the tactical level of the dynamic driving task. Finally, it has to be noted that certain challenges of remote driving, such as the complete connection loss between the remote operator and the vehicle, will persist despite shared control. These will continue to require a specific solution.

## 6.5 Regulation

In the summary of several acts on automated driving [93–95] in Subsection 1.2.3, regulation has been introduced as a challenge of remote driving. In this section, the topic is revisited.

Two remote assistance concepts, which were described in Subsection 2.1.1, are deemed compliant. On the one hand, remote clearance of maneuver proposals from the remote operator through the automated driving system is described. This translates to the compliance of the collaborative path planning concept. On the other hand, the proposal of a maneuver from the remote operator to the automated driving system is allowed as well. In this case, the automated driving system should validate the proposed maneuver and only execute it in case it is deemed feasible and safe. This means that the concept of path guidance is also compliant.

Given this, remote driving in the form of direct control is not permitted under current regulations. However, based on the concepts and findings of the present work, shared control may qualify as a compliant remote driving concept that holds the potential to meet the necessary safety requirements. From a regulatory perspective, shared control can be interpreted as the remote operator proposing maneuvers at a higher frequency. In the event that an unsafe control action is commanded, the shared control approach, as a part of the automated driving system, can reject and safeguard against its execution.

Finally, within this context, it is important to acknowledge that the considerations for vehicle teleoperation extend beyond regulatory aspects and encompass societal perspectives as well. The impact of shared control on the acceptance of vehicle teleoperation remains an open question that warrants separate investigation. A possible approach to explore this aspect could involve building upon the research conducted by Keller et al. [220], who examined the acceptability of teleoperation among railway passengers.

# 7 Conclusion and Outlook

In the present work, vehicle teleoperation has been introduced as a fallback for highly-automated, driverless vehicles that require remote support in fail cases at the tactical level of the dynamic driving task. While direct control is a simple solution, it comes with inherent risks, which arise from different challenges such as latency, reduced situational awareness, and unstable connectivity. For this purpose, uncoupled shared control has been introduced as a remote driving concept that aims to safeguard against unsafe control actions from the remote operator.

In the state of the art, an overview has been given of remote assistance and remote driving concepts. The latter included shared control, which was introduced as the particular focus of the present work. Thereby, it was derived that uncoupled shared control for the use case of obstacle avoidance is able to mitigate the safety concerns of direct control under certain assumptions. For instance, shared control relies on a functional perception of the automated driving system. Based on this, the first research question was derived, asking what the effects of uncoupled shared control are in comparison to direct control as a remote driving concept. Also, from the overview of uncoupled shared control design variants in the literature, the second research question was derived, asking what the most suited uncoupled shared control design is for remote driving.

The derivation of research questions was followed by the presentation of the methodology to tackle them. First, as it is not capable of keeping the vehicle safe in some scenarios, shared steering control has been excluded in the present work. The other two uncoupled shared control design variants, namely SVC and SSVC, were considered. For these, two design concepts were proposed and described. These made use of model-based trajectory planning and model predictive control techniques as well as visual and haptic feedback in order to communicate the intentions and interventions from the uncoupled shared control approaches to the remote operator. The vehicle teleoperation system at the Institute of Automotive Technology and the integration of the uncoupled shared control approaches therein were described. After this, a simulative validation in two scenarios was presented, validating and comparing the characteristics of the two approaches in case of dynamic and unsafe control actions from a simulated remote operator.

Finally, to evaluate the designs experimentally, an experimental user study was conducted with 32 participants. Therein, to answer the first research question, direct control was compared against SVC and SSVC. The results were multifaceted. First, they yielded that the choice of the control mode has no effect on the mean cognitive workload. Second, contrary to what was originally hypothesized, the performance is not higher with uncoupled shared control. Third, it was shown that safety increases with uncoupled shared control. In addition, SVC and SSVC were compared in various metrics. In response to the second research question, the results of, for example, controllability and user experience recommended that SVC is the most suited uncoupled shared control design for remote driving. However, these results were accompanied by some limitations, which were highlighted in the discussion. Proposing uncoupled shared control as a compliant maneuver proposal concept for vehicle teleoperation, the discussion also included a follow-up on the regulatory issues from the introduction.

Based on the present work, several points for future work can be been identified. In summary, these are concerned with the reconsideration of the study design, improvements to the presented uncoupled shared control designs as well as extensions to the shared control framework, and research on social matters.

The study design used in the present work has been an approach to evaluate and compare the uncoupled shared control designs in extreme conditions. In future work, different study setups should be considered. For instance, actual scenarios should not require overly frequent overriding actions through the uncoupled shared control design. Also, as discussed, the operationalization of safety could be different, with metrics such as time-to-collision being calculated. Additionally, an objective measure of the controllability of the teleoperation system would be valuable.

The presented uncoupled shared control designs have the potential for improvement in various ways. While the following suggestions are not exhaustive, they offer a glimpse into possible future directions. One recommendation is to address the conflict between the remote operator and the automation by preventing SVC from automatically re-accelerating after a braking intervention. This has surprised some participants, especially when they take turns. For the SSVC approach, it was suggested that the velocity should be decreased if the system intervenes in the steering angle. This would help in stabilizing the vehicle after the intervention. Moreover, the study results highlighted the importance of feedback for communication from the automation to the remote operator in uncoupled shared control. Therefore, incorporating haptic pedals may facilitate communication of intervention in the velocity control. Additionally, the haptic feedback on the steering wheel can be predictive rather than purely reactive during an actual intervention. Study participants also made various suggestions regarding visual feedback, such as improving clarity when the SVC is about to stop the vehicle.

Additional technical refinements can be explored for uncoupled shared control. One of the primary areas of focus should be on validating the uncoupled shared control approaches in the presence of dynamic obstacles. It is anticipated that the operability of SVC would be significantly constrained as maintaining the safety of the vehicle becomes more challenging while assuming hazardous steering actions from the remote operator. Also, the shared control approaches can make use of more extensive models to predict the actions of the remote operators. Furthermore, as highlighted in the introduction of the shared control use cases, the potential of control resumption between the automation and the remote operator, and vice versa, motivate further investigation. Performing the handover, while the vehicle is in motion, can substantially increase the productivity of the teleoperation interaction.

Also, several greater extensions of the shared control framework are conceivable. For example, the uncoupled shared control design could incorporate data from a remote operator monitoring system. This could be used to respond when the remote operator becomes drowsy. Also on the subject of deployment, thought must be given to how a remote operator desk for remote driving is integrated into a remote control center. In this context, another user study should also be considered. In this, it would be valuable to teleoperate a full-size vehicle in driving scenarios, which represent more likely fail cases for an automated driving system.

The presented study compared uncoupled shared control with direct control to determine the effects of uncoupled shared control. However, there are still open questions regarding the comparison of uncoupled shared control with other vehicle teleoperation concepts, such as collaborative path planning and path guidance. These also address fail cases of an automated driving system at the tactical level of the dynamic driving task, making use of a functional perception. Possibly, these concepts have a lower cognitive workload for the remote operator but may lack the flexibility to respond quickly to dynamic traffic situations. In contrast, uncoupled shared control may have an advantage in this regard. However, a targeted study is needed to explore these comparisons in more detail.

Finally, there is a question about the societal acceptance of remote operation of automated vehicles. To address this, surveys can be conducted to gather opinions on this matter before the technology is ready for widespread use. It remains to be seen whether uncoupled shared control can help increase the acceptance of remote driving or teleoperation more generally.

# List of Figures

# List of Tables

# Bibliography


[1] World Health Organization. „Road traffic injuries," 2022. Available: https://www.who.int/news-room/fact-sheets/detail/road-traffic-injuries [visited on 02/15/2023].

[2] S. Tsugawa, T. Yatabe, T. Hirose and S. Matsumoto, „An automobile with artificial intelligence," in *Proceedings of the 6th International Joint Conference on Artificial Intelligence - Volume 2*, 1979, 893–895.

[3] E. Dickmanns, „The development of machine vision for road vehicles in the last decade," in *Intelligent Vehicle Symposium, 2002. IEEE*, 2002, pp. 268–281. DOI: 10.1109/IVS.2002.1187962.

[4] S. Thrun, M. Montemerlo, H. Dahlkamp, D. Stavens, A. Aron, J. Diebel, P. Fong, J. Gale, M. Halpenny, G. Hoffmann, et al., „Stanley: The robot that won the DARPA Grand Challenge," *Journal of Field Robotics*, vol. 23, no. 9, pp. 661–692, 2006, DOI: 10.1002/rob.20147.

[5] C. Urmson, C. Baker, J. Dolan, P. Rybski, B. Salesky, W. Whittaker, D. Ferguson and M. Darms, „Autonomous Driving in Traffic: Boss and the Urban Challenge," *AI Magazine*, vol. 30, no. 2, p. 17, 2009, DOI: 10.1609/aimag.v30i2.2238.

[6] E. Guizzo. „How Google's Self-Driving Car Works," 2011. Available: https://spectrum.ieee.org/how-google-self-driving-car-works [visited on 02/26/2023].

[7] Waymo. „History of Waymo," 2023. Available: https://waymo.com/company/#story [visited on 02/26/2023].

[8] K. Burnett, A. Schimpe, S. Samavi, M. Gridseth, C. W. Liu, Q. Li, Z. Kroeze and A. P. Schoellig, „Building a Winning Self-Driving Car in Six Months," in *2019 International Conference on Robotics and Automation (ICRA)*, 2019, pp. 9583–9589. DOI: 10.1109/ICRA.2019.8794029.

[9] J. Betz, T. Betz, F. Fent, M. Geisslinger, A. Heilmeier, L. Hermansdorfer, T. Herrmann, S. Huch, P. Karle, M. Lienkamp, et al., „TUM autonomous motorsport: An autonomous racing software for the Indy Autonomous Challenge," *Journal of Field Robotics*, 2022, DOI: 10.1002/rob.22153.

[10] D. Holland-Letz, M. Kässer, B. Kloss and T. Müller. „Mobility's future: An investment reality check," 2021. Available: https://www.mckinsey.com/industries/automotive-and-assembly/our-insights/mobilitys-future-an-investment-reality-check [visited on 02/15/2023].

[11] Cruise. „About Cruise," 2023. Available: https://getcruise.com/about/ [visited on 04/08/2023].

[12] M. Herger. „Waymo and Cruise Expand Service Areas and Hours for their Robotaxi Fleets," 2022. Available: https://thelastdriverlicenseholder.com/2022/12/20/waymo-and-cruise-expand-service-areas-and-hours-for-their-robotaxi-fleets/ [visited on 02/15/2023].

[13] M. Chafkin. „Even After $100 Billion, Self-Driving Cars Are Going Nowhere," 2022. Available: https://www.bloomberg.com/news/features/2022-10-06/even-after-100-billion-self-driving-cars-are-going-nowhere [visited on 02/15/2023].

[14] Gatik. „About Gatik," 2023. Available: https://gatik.ai/about/ [visited on 02/15/2023].

[15] Aurora. „Aurora Horizon," 2023. Available: https://aurora.tech/aurora-horizon [visited on 02/15/2023].

[16] Waabi. „Introducing the Waabi Driver,“ 2023. Available: https://waabi.ai/introducing-the-waabi-driver/ [visited on 02/15/2023].

[17] SAE International, „SAE J3016: Taxonomy and Definitions for Terms Related to Driving Automation Systems for On-Road Motor Vehicles,“ 2021.

[18] J.-M. Georg, J. Feiler, F. Diermeyer and M. Lienkamp, „Teleoperated Driving, a Key Technology for Automated Driving? Comparison of Actual Test Drives with a Head Mounted Display and Conventional Monitors,“ in *2018 21st International Conference on Intelligent Transportation Systems (ITSC)*, 2018, pp. 3403–3408. DOI: 10.1109/ITSC.2018.8569408.

[19] S. Neumeier, N. Gay, C. Dannheim and C. Facchi, „On the way to autonomous vehicles teleoperated driving,“ *AmE 2018: Automotive meets Electronics - 9. GMM-Fachtagung*, pp. 49–54, 2018, ISBN: 9783800745241.

[20] C. Kettwich, A. Schrank, H. Avsar and M. Oehl, „What if the Automation Fails? – A Classification of Scenarios in Teleoperated Driving,“ in *13th International Conference on Automotive User Interfaces and Interactive Vehicular Applications*, 2021, pp. 92–96. DOI: 10.1145/3473682.3480271.

[21] D. Majstorović, S. Hoffmann, F. Pfab, A. Schimpe, M.-M. Wolf and F. Diermeyer, „Survey on Teleoperation Concepts for Automated Vehicles,“ in *2022 IEEE International Conference on Systems, Man, and Cybernetics (SMC)*, 2022, pp. 1290–1296. DOI: 10.1109/SMC53654.2022.9945267.

[22] R. Hoeger, H. Zeng, A. Hoess, T. Kranz, S. Boverie, M. Strauss, E. Jakobsson, A. Beutner, A. Bartels, T.-B. To, et al., „Highly automated vehicles for intelligent transport (HAVEit) - Deliverable D61.1 - Final Report,“ 2011. Available: https://cordis.europa.eu/docs/projects/cnect/4/212154/080/deliverables/001-HAVEit212154D611FinalReportPublished.pdf.

[23] M. W. Spong, S. Hutchinson and M. Vidyasagar, *Robot Modeling and Control, 2nd Edition*, Wiley, 2020, ISBN: 978-1-119-52404-5.

[24] B. Paden, M. Cap, S. Z. Yong, D. Yershov and E. Frazzoli, „A Survey of Motion Planning and Control Techniques for Self-Driving Urban Vehicles,“ *IEEE Transactions on Intelligent Vehicles*, vol. 1, no. 1, pp. 33–55, 2016, DOI: 10.1109/TIV.2016.2578706.

[25] A. Tampuu, T. Matiisen, M. Semikin, D. Fishman and N. Muhammad, „A Survey of End-to-End Driving: Architectures and Training Methods,“ *IEEE Transactions on Neural Networks and Learning Systems*, vol. 33, no. 4, pp. 1364–1384, 2022, DOI: 10.1109/TNNLS.2020.3043505.

[26] T. M. Gasser and D. Westhoff, „BASt-study: Definitions of automation and legal issues in Germany,“ 2012. Available: https://onlinepubs.trb.org/onlinepubs/conferences/2012/Automation/presentations/Gasser.pdf.

[27] D. Bogdoll, S. Orf, L. Töttel and J. M. Zöllner, „Taxonomy and Survey on Remote Human Input Systems for Driving Automation Systems,“ in *Future of Information and Communication (FICC)* 2022, pp. 94–108, DOI: 10.1007/978-3-030-98015-3_6. Available: https://link.springer.com/10.1007/978-3-030-98015-3_6.

[28] Centre for Connected & Automated Vehicles, „Connected and automated vehicles - Vocabulary,“ Technical Report, BSI Flex 1890 v4.0:2022-03, 2022. Available: https://www.bsigroup.com/globalassets/localfiles/en-gb/cav/cav_voc.pdf.

[29] Centre for Connected and Autonomous Vehicles, „Guidelines for developing and assessing control systems for automated vehicles,“ Technical Report, BSI PAS 1880:2, 2022. Available: https://www.bsigroup.com/globalassets/localfiles/en-gb/cav/pas-1880---guidelines-for-developing-and-assessing-control-systems-for-automated-vehicles.pdf.

[30] S. Lu, R. Zhong and W. Shi, „Teleoperation Technologies for Enhancing Connected and Autonomous Vehicles," in *2022 IEEE 19th International Conference on Mobile Ad Hoc and Smart Systems (MASS)*, 2022, pp. 435–443. DOI: 10.1109/MASS56207.2022.00068.

[31] R. Gogna. „Teleoperations for Collaborative Vehicle Guidance," Patent No. WO2021211322A1, 2021.

[32] A. L. K. Lockwood, R. Gogna, G. Linscott, P. Orecchio, D. Xie, A. G. Rege and J. S. Levinson. „Predictive teleoperator situational awareness," Patent No. US10976732B2, 2021.

[33] Zoox. „How Zoox Uses TeleGuidance to Provide Remote Assistance to its Autonomous Vehicles," 2020. Available: https://youtu.be/NKQHuutVx78 [visited on 04/08/2023].

[34] Cruise. „Cruise Under the Hood 2021: From Self-Driving R&D to Self-Driving Reality," 2021. Available: https://youtu.be/YnhYeTWvfB0?t=433 [visited on 04/08/2023].

[35] B. Rech, S. Gläser, M. Engel, H.-J. Günther, T. Buburuzan, S. Kleinau, B. Lehmann and J. Hartog. „Method for remotely controlling a plurality of driverless self-driving systems, control station for remotely controlling the self-driving systems, and system," Patent No. WO2018171991A1, 2018.

[36] R. Bellan. „DriveU.auto to power remote piloting of EasyMile's autonomous shuttles, Coco's sidewalk robots," 2022. Available: https://techcrunch.com/2022/01/04/driveu-auto-to-power-remote-piloting-of-easymiles-autonomous-shuttles-cocos-sidewalk-robots/ [visited on 02/22/2023].

[37] EasyMile. „SAFESTREAM project to accelerate autonomous driving to SAE Level 4 in public transport in Germany launched," 2023. Available: https://easymile.com/news/safestream-project-accelerate-autonomous-driving-sae-level-4-public-transport-germany-launched [visited on 02/22/2023].

[38] Ottopia Technologies. „How Ottopia uses differente Remote Assistance Techniques to operate Autonomous Vehicles," 2019. Available: https://youtu.be/IIkLSwaTJg8 [visited on 04/08/2023].

[39] S. Abuelsamid. „Ottopia To Provide Remote Assistance For Motional Robotaxis," 2021. Available: https://www.forbes.com/sites/samabuelsamid/2021/07/28/ottopia-to-provide-remote-assistance-for-motional-robotaxis/ [visited on 02/22/2023].

[40] Motional. „Motional's Remote Vehicle Assistance (RVA)," 2022. Available: https://youtu.be/pyoHeEcgHFA [visited on 04/08/2023].

[41] Handelsblatt. „VW und Fernride testen in Wolfsburg ferngesteuerte Lkw," 2022. Available: https://www.handelsblatt.com/technik/it-internet/automatisiertes-fahren-vw-und-fernride-testen-in-wolfsburg-ferngesteuerte-lkw/28278722.html [visited on 04/08/2023].

[42] W. Pluta. „Vay darf in Hamburg ohne Sicherheitspersonal telefahren," 2022. Available: https://www.golem.de/news/mobilitaetsdienst-vay-darf-in-hamburg-ohne-sicherheitspersonal-telefahren-2212-170700.html [visited on 02/22/2023].

[43] J.-M. Georg, J. Feiler, S. Hoffmann and F. Diermeyer, „Sensor and Actuator Latency during Teleoperation of Automated Vehicles," in *2020 IEEE Intelligent Vehicles Symposium (IV)*, 2020, pp. 760–766. DOI: 10.1109/IV47402.2020.9304802.

[44] T. Sheridan, „Space teleoperation through time delay: review and prognosis," *IEEE Transactions on Robotics and Automation*, vol. 9, no. 5, pp. 592–606, 1993, DOI: 10.1109/70.258052.

[45] F. E. Chucholowski, M. Sauer and M. Lienkamp, „Evaluation of Display Methods for Teleoperation of Road Vehicles," *Journal of Unmanned System Technology*, vol. 3, no. 3, pp. 80–85, 2016, DOI: 10.21535/just.v3i3.38.

[46] G Graf, Y Abdelrahman, H Xu, Y Abdrabou, D Schitz, H Hußmann and F Alt, „The Predictive Corridor : A Virtual Augmented Driving Assistance System for Teleoperated Autonomous Vehicles," in *International Conference on Artificial Reality and Telexistence and Eurographics Symposium on Virtual Environments (ICAT-EGVE)*, 2020, DOI: 10.2312/egve.20201260.

[47] G. Graf, H. Xu, D. Schitz and X. Xu, „Improving the Prediction Accuracy of Predictive Displays for Teleoperated Autonomous Vehicles," in *2020 6th International Conference on Control, Automation and Robotics (ICCAR)*, 2020, pp. 440–445. DOI: 10.1109/ICCAR49639.2020.9108011.

[48] Y. Sato, S. Kashihara and T. Ogishi, „Implementation and Evaluation of Latency Visualization Method for Teleoperated Vehicle," in *2021 IEEE Intelligent Vehicles Symposium (IV)*, 2021, pp. 1–7. DOI: 10.1109/IV48863.2021.9575817.

[49] J. Prakash, M. Vignati, D. Vignarca, E. Sabbioni and F. Cheli. „"Predictive Display with Perspective Projection of Surroundings in Vehicle Teleoperation to Account Time-delays"," 2022. arXiv: 2211.11918. Available: http://arxiv.org/abs/2211.11918.

[50] F. E. Chucholowski, „Eine vorausschauende Anzeige zur Teleoperation von Straßenfahrzeugen," PhD thesis, Technical University of Munich, 2015.

[51] A. Hosseini and M. Lienkamp, „Predictive safety based on track-before-detect for teleoperated driving through communication time delay," in *2016 IEEE Intelligent Vehicles Symposium (IV)*, 2016, pp. 165–172. DOI: 10.1109/IVS.2016.7535381.

[52] A. Hosseini, F. Richthammer and M. Lienkamp, „Predictive Haptic Feedback for Safe Lateral Control of Teleoperated Road Vehicles in Urban Areas," in *2016 IEEE 83rd Vehicular Technology Conference (VTC Spring)*, 2016, pp. 1–7. DOI: 10.1109/VTCSpring.2016.7504430.

[53] M. Moniruzzaman, A. Rassau, D. Chai and S. M. S. Islam, „High Latency Unmanned Ground Vehicle Teleoperation Enhancement by Presentation of Estimated Future through Video Transformation," *Journal of Intelligent & Robotic Systems*, vol. 106, no. 2, p. 48, 2022, ISBN: 0123456789. DOI: 10.1007/s10846-022-01749-3.

[54] A. Belogolovy, D. Dasalukunte, R. Dorrance, E. Stupachenko and X. Zhang. „"Low latency communication over commercially available LTE and remote driving"," 2022. arXiv: 2209.09794. Available: http://arxiv.org/abs/2209.09794.

[55] H. Nagakura, Y. Hatori and Y. Uchimura, „Tele-driving including time-varying delay based on MPC with stability constraints," in *IECON 2021 – 47th Annual Conference of the IEEE Industrial Electronics Society*, 2021, pp. 1–6. DOI: 10.1109/IECON48115.2021.9589762.

[56] A. Kousaridas, A. Schimpe, S. Euler, X. Vilajosana, M. Fallgren, G. Landi, F. Moscatelli, S. Barmpounakis, F. Vázquez-Gallego, R. Sedar, et al., „5G Cross-Border Operation for Connected and Automated Mobility: Challenges and Solutions," *Future Internet*, vol. 12, no. 1, p. 5, 2019, DOI: 10.3390/fi12010005.

[57] H. Kim, „5G Vertical Trials, Use Cases and Scenarios," in *2022 IEEE International Conference on Internet of Things and Intelligence Systems (IoTaIS)*, 2022, pp. 81–86. DOI: 10.1109/IoTaIS56727.2022.9975928.

[58] G. Kakkavas, K. N. Nyarko, C. Lahoud, D. Kuhnert, P. Kuffner, M. Gabriel, S. Ehsanfar, M. Diamanti, V. Karyotis, K. MoBner, et al., „Teleoperated Support for Remote Driving over 5G Mobile Communications," in *2022 IEEE International Mediterranean Conference on Communications and Networking (MeditCom)*, 2022, pp. 280–285. DOI: 10.1109/MeditCom55741.2022.9928745.

[59] S. Li, Y. Zhang, S. Edwards and P. T. Blythe, „Exploration into the Needs and Requirements of the Remote Driver When Teleoperating the 5G-Enabled Level 4 Automated Vehicle in the Real World—A Case Study of 5G Connected and Automated Logistics," *Sensors*, vol. 23, no. 2, p. 820, 2023, DOI: 10.3390/s23020820.

[60] L. H. Frank, J. G. Casali and W. W. Wierwille, „Effects of Visual Display and Motion System Delays on Operator Performance and Uneasiness in a Driving Simulator," *Human Factors: The Journal of the Human Factors and Ergonomics Society*, vol. 30, no. 2, pp. 201–217, 1988, DOI: 10.1177/001872088803000207.

[61] S. Neumeier, P. Wintersberger, A.-K. Frison, A. Becher, C. Facchi and A. Riener, „Teleoperation: The Holy Grail to Solve Problems of Automated Driving? Sure, but Latency Matters," in *Proceedings of the 11th International Conference on Automotive User Interfaces and Interactive Vehicular Applications*, 2019, pp. 186–197. DOI: 10.1145/3342197.3344534.

[62] O. Musicant, A. Botzer and S. Shoval, „Effects of simulated time delay on teleoperators' performance in inter-urban conditions," *Transportation Research Part F: Traffic Psychology and Behaviour*, vol. 92, no. December 2022, pp. 220–237, 2022, DOI: 10.1016/j.trf.2022.11.007.

[63] DriveU.auto. „Teleoperation Interfaces: Challenges and guidelines for Autonomous Vehicles Research Summary," 2022. Available: https://driveu.auto/blog/teleoperation-interfaces-challenges-and-guidelines-for-autonomous-vehicles-research-summary/ [visited on 04/08/2023].

[64] R. Chellali and K. Baizid, „What Maps and What Displays for Remote Situation Awareness and ROV Localization?," in *Lecture Notes in Computer Science (including subseries Lecture Notes in Artificial Intelligence and Lecture Notes in Bioinformatics)*. vol. 6772 LNCS 2011, pp. 364–372, ISBN: 9783642216688. DOI: 10.1007/978-3-642-21669-5_43. Available: http://link.springer.com/10.1007/978-3-642-21669-5_43.

[65] C. Mutzenich, S. Durant, S. Helman and P. Dalton, „Updating our understanding of situation awareness in relation to remote operators of autonomous vehicles," *Cognitive Research: Principles and Implications*, vol. 6, no. 1, p. 9, 2021, DOI: 10.1186/s41235-021-00271-8.

[66] X. Shen, Z. J. Chong, S. Pendleton, G. M. James Fu, B. Qin, E. Frazzoli and M. H. Ang, „Teleoperation of On-Road Vehicles via Immersive Telepresence Using Off-the-shelf Components," in *Advances in Intelligent Systems and Computing* 2016, pp. 1419–1433, ISBN: 9783319083377. DOI: 10.1007/978-3-319-08338-4_102. Available: http://link.springer.com/10.1007/978-3-319-08338-4_102.

[67] A. Hosseini and M. Lienkamp, „Enhancing telepresence during the teleoperation of road vehicles using HMD-based mixed reality," in *2016 IEEE Intelligent Vehicles Symposium (IV)*, 2016, pp. 1366–1373. DOI: 10.1109/IVS.2016.7535568.

[68] Y. Luo, J. Wang, R. Shi, H.-N. Liang and S. Luo, „In-Device Feedback in Immersive Head-Mounted Displays for Distance Perception During Teleoperation of Unmanned Ground Vehicles," *IEEE Transactions on Haptics*, vol. 15, no. 1, pp. 79–84, 2022, DOI: 10.1109/TOH.2021.3138590.

[69] J.-M. Georg and F. Diermeyer, „An Adaptable and Immersive Real Time Interface for Resolving System Limitations of Automated Vehicles with Teleoperation," in *2019 IEEE International Conference on Systems, Man and Cybernetics (SMC)*, 2019, pp. 2659–2664. DOI: 10.1109/SMC.2019.8914306.

[70] T. Tang, J. Kurkowski and M. Lienkamp, „Teleoperated Road Vehicles: A Novel Study on the Effect of Blur on Speed Perception," *International Journal of Advanced Robotic Systems*, vol. 10, no. 9, p. 333, 2013, DOI: 10.5772/56735.

[71] Nanyang Technological University. „NTU Singapore develops high-fidelity teleoperation for heavy-duty vehicles," 2021. Available: https://www.ntu.edu.sg/news/detail/remote-controlled-road-sweeper-tests-begin-in-sentosa/ntu-singapore-develops-high-fidelity-teleoperation-for-heavy-duty-vehicles [visited on 03/01/2023].

[72] V. Linkov and M. Vanžura, „Situation Awareness Measurement in Remotely Controlled Cars," *Frontiers in Psychology*, vol. 12, no. April, 2021, DOI: 10.3389/fpsyg.2021.592930.

[73] G. Graf, H. Palleis and H. Hussmann, „A Design Space for Advanced Visual Interfaces for Teleoperated Autonomous Vehicles," in *Proceedings of the International Conference on Advanced Visual Interfaces*, 2020, pp. 1–3. DOI: 10.1145/3399715.3399942.

[74] G. Graf and H. Hussmann, „User Requirements for Remote Teleoperation-based Interfaces," in *12th International Conference on Automotive User Interfaces and Interactive Vehicular Applications*, 2020, pp. 85–88. DOI: 10.1145/3409251.3411730.

[75] C. Kettwich, A. Schrank and M. Oehl, „Teleoperation of Highly Automated Vehicles in Public Transport: User-Centered Design of a Human-Machine Interface for Remote-Operation and Its Expert Usability Evaluation," *Multimodal Technologies and Interaction*, vol. 5, no. 5, p. 26, 2021, DOI: 10.3390/mti5050026.

[76] K. Doki, K. Suzuki, Y. Funabora, S. Doki and Y. Yano, „Operator Assistance for Remote Driving with Augmented Image based on Gaze Information," in *2022 IEEE 31st International Symposium on Industrial Electronics (ISIE)*, 2022, pp. 1094–1099. DOI: 10.1109/ISIE51582.2022.9831663.

[77] S. Neumeier, E. A. Walelgne, V. Bajpai, J. Ott and C. Facchi, „Measuring the Feasibility of Teleoperated Driving in Mobile Networks," in *2019 Network Traffic Measurement and Analysis Conference (TMA)*, 2019, pp. 113–120. DOI: 10.23919/TMA.2019.8784466.

[78] M. Akselrod, N. Becker, M. Fidler and R. Luebben, „4G LTE on the Road - What Impacts Download Speeds Most?," in *2017 IEEE 86th Vehicular Technology Conference (VTC-Fall)*, 2017, pp. 1–6. DOI: 10.1109/VTCFall.2017.8288296.

[79] F. Jomrich, A. Herzberger, T. Meuser, B. Richerzhagen, R. Steinmetz and C. Wille, „Cellular Bandwidth Prediction for Highly Automated Driving - Evaluation of Machine Learning Approaches based on Real-World Data," in *Proceedings of the 4th International Conference on Vehicle Technology and Intelligent Transport Systems*, 2018, pp. 121–132. DOI: 10.5220/0006692501210132.

[80] R. Parasuraman, S. Caccamo, F. Baberg, P. Ogren and M. Neerincx, „A New UGV Teleoperation Interface for Improved Awareness of Network Connectivity and Physical Surroundings," *Journal of Human-Robot Interaction*, vol. 6, no. 3, p. 48, 2017, DOI: 10.5898/JHRI.6.3.Parasuraman.

[81] M. Boban, M. Giordani and M. Zorzi, „Predictive Quality of Service: The Next Frontier for Fully Autonomous Systems," *IEEE Network*, vol. 35, no. 6, pp. 104–110, 2021, DOI: 10.1109/MNET.001.2100237.

[82] H. Schippers, C. Schuler, B. Sliwa and C. Wietfeld, „System Modeling and Performance Evaluation of Predictive QoS for Future Tele-Operated Driving," in *2022 IEEE International Systems Conference (SysCon)*, 2022, pp. 1–8. DOI: 10.1109/SysCon53536.2022.9773810.

[83] A. M. Mohamed, N. AbdelBaki and T. Arafa, „Feasibility Study of Using Predictive LTE Connection Selection from Multi-Operator for Teleoperated Vehicles," in *2022 International Conference on Computer and Applications (ICCA)*, 2022, pp. 1–6. DOI: 10.1109/ICCA56443.2022.10039521.

[84] 5G Automotive Association. „White Paper: Making 5G Proactive and Predictive for the Automotive Industry," 2020. Available: https://5gaa.org/content/uploads/2020/01/5GAA_White-Paper_Proactive-and-Predictive_v04_8-Jan.-2020-003.pdf [visited on 03/02/2023].

[85] S. Neumeier, V. Bajpai, M. Neumeier, C. Facchi and J. Ott, „Data Rate Reduction for Video Streams in Teleoperated Driving," *IEEE Transactions on Intelligent Transportation Systems*, vol. 23, no. 10, pp. 19145–19160, 2022, DOI: 10.1109/TITS.2022.3171718.

[86] M. E. Dehshalie, F. Prignoli, P. Falcone and M. Bertogna, „Model-based selective image downsampling in remote driving applications," in *2022 IEEE 25th International Conference on Intelligent Transportation Systems (ITSC)*, 2022, pp. 3225–3230. DOI: 10.1109/ITSC55140.2022.9922590.

[87] Y. Sato, S. Kashihara and T. Ogishi, „Robust Video Transmission System Using 5G/4G Networks for Remote Driving," in *2022 IEEE Intelligent Vehicles Symposium (IV)*, 2022, pp. 616–622. DOI: 10.1109/IV51971.2022.9827313.

[88] T. Tang, P. Vetter, S. Finkl, K. Figel and M. Lienkamp, „Teleoperated Road Vehicles – The "Free Corridor" as a Safety Strategy Approach," *Applied Mechanics and Materials*, vol. 490-491, pp. 1399–1409, 2014, ISBN: 9783038350019. DOI: 10.4028/www.scientific.net/AMM.490-491.1399.

[89] S. Hoffmann and F. Diermeyer, „Systems-theoretic Safety Assessment of Teleoperated Road Vehicles," in *Proceedings of the 7th International Conference on Vehicle Technology and Intelligent Transport Systems*, 2021, pp. 446–456. DOI: 10.5220/0010438904460456.

[90] P. A. Linne and J. Andersson, „Regulating Road Vehicle Teleoperation: Back to the Near Future," in *2021 IEEE Intelligent Vehicles Symposium Workshops (IV Workshops)*, 2021, pp. 135–140. DOI: 10.1109/IVWorkshops54471.2021.9669226.

[91] Department for Transport of the United Kingdom. „Code of Practice: automated vehicle trialling (Updated 28 January 2022)," 2022. Available: https://www.gov.uk/government/publications/trialling-automated-vehicle-technologies-in-public/code-of-practice-automated-vehicle-trialling.

[92] Swedish Ministry of Infrastructure. „Decree (2017:309) on experimental operations with automated vehicles," 2017. Available: https://rkrattsbaser.gov.se/sfst?bet=2017:309.

[93] Deutsches Bundesministerium für Digitales und Verkehr (BMDV). „Autonome-Fahrzeuge-Genehmigungs- und-Betriebs-Verordnung - AFGBV," 2022. Available: http://www.gesetze-im-internet.de/afgbv/__1.html.

[94] Deutsches Bundesministerium für Digitales und Verkehr (BMDV). „Straßenverkehrsgesetz (StVG) zuletzt geändert am 20.12.2022," 2022. Available: https://www.gesetze-im-internet.de/stvg/BJNR004370909.html.

[95] Europäische Union (EU). „Durchführungsverordnung (EU) 2022/1426 der Kommission," 2022. Available: https://eur-lex.europa.eu/legal-content/DE/TXT/?uri=celex:32022R1426.

[96] F. Flemisch, A. Schieben, J. Kelsch and C. Löper, „Automation spectrum, inner / outer compatibility and other potentially useful human factors concepts for assistance and automation," 2008.

[97] A. Schimpe, D. Majstorović and F. Diermeyer, „Steering Action-aware Adaptive Cruise Control for Teleoperated Driving," in *2022 IEEE International Conference on Systems, Man, and Cybernetics (SMC)*, 2022, pp. 988–993. DOI: 10.1109/SMC53654.2022.9945081.

[98] A. Schimpe and F. Diermeyer, „Steer with Me: A Predictive, Potential Field-Based Control Approach for Semi-Autonomous, Teleoperated Road Vehicles," in *2020 IEEE 23rd International Conference on Intelligent Transportation Systems (ITSC)*, 2020, pp. 1–6. DOI: 10.1109/ITSC45102.2020.9294702.

[99] A. Schimpe, S. Hoffmann and F. Diermeyer, „Adaptive Video Configuration and Bitrate Allocation for Teleoperated Vehicles," in *2021 IEEE Intelligent Vehicles Symposium Workshops (IV Workshops)*, 2021, pp. 148–153. DOI: 10.1109/IVWorkshops54471.2021.9669258.

[100] A. Schimpe, J. Feiler, S. Hoffmann, D. Majstorović and F. Diermeyer, „Open Source Software for Teleoperated Driving," in *2022 International Conference on Connected Vehicle and Expo (ICCVE)*, 2022, pp. 1–6. DOI: 10.1109/ICCVE52871.2022.9742859.

[101] J. Feiler, S. Hoffmann and D. F. Diermeyer, „Concept of a Control Center for an Automated Vehicle Fleet," in *2020 IEEE 23rd International Conference on Intelligent Transportation Systems (ITSC)*, 2020, pp. 1–6. DOI: 10.1109/ITSC45102.2020.9294411.

[102] C. Kettwich and A. Dreßler, „Requirements of Future Control Centers in Public Transport," in *12th International Conference on Automotive User Interfaces and Interactive Vehicular Applications*, 2020, pp. 69–73. DOI: 10.1145/3409251.3411726.

[103] O. Amador, M. Aramrattana and A. Vinel, „A Survey on Remote Operation of Road Vehicles," *IEEE Access*, vol. 10, no. December 2022, pp. 130135–130154, 2022, DOI: 10.1109/ACCESS.2022.3229168.

[104] F. Flemisch, D. Abbink, M. Itoh, M.-P. Pacaux-Lemoine and G. Weßel, „Shared control is the sharp end of cooperation: Towards a common framework of joint action, shared control and human machine cooperation," *IFAC-PapersOnLine*, vol. 49, no. 19, pp. 72–77, 2016, DOI: 10.1016/j.ifacol.2016.10.464.

[105] A. Hosseini, T. Wiedemann and M. Lienkamp, „Interactive path planning for teleoperated road vehicles in urban environments," in *17th International IEEE Conference on Intelligent Transportation Systems (ITSC)*, 2014, pp. 400–405. DOI: 10.1109/ITSC.2014.6957723.

[106] D. Schitz, S. Bao, D. Rieth and H. Aschemann, „Shared Autonomy for Teleoperated Driving: A Real-Time Interactive Path Planning Approach," in *2021 IEEE International Conference on Robotics and Automation (ICRA)*, 2021, pp. 999–1004. DOI: 10.1109/ICRA48506.2021.9561918.

[107] D. Majstorović and F. Diermeyer, „Dynamic Collaborative Path Planning for Remote Assistance of highly-automated Vehicles," in *Submission to IEEE International Automated Vehicle Validation Conference 2023*, 2023.

[108] A. Schimpe, A. Pfadler and L. Montero Bayo, „Tele-operated Driving - Overview & Achievements," 5GCroCo Web-Seminar, 2022. Available: https://5gcroco.eu/images/templates/rsvario/images/5GCroCo_Webinar__ToD.pdf.

[109] D. Schitz, G. Graf, D. Rieth and H. Aschemann, „Interactive Corridor-Based Path Planning for Teleoperated Driving," in *2021 7th International Conference on Mechatronics and Robotics Engineering (ICMRE)*, 2021, pp. 174–179. DOI: 10.1109/ICMRE51691.2021.9384848.

[110] A. Björnberg. „Shared Control for Vehicle Teleoperation with a Virtual Environment Interface," Master's thesis in Systems, Control and Robotics, 2020.

[111] J. Feiler and F. Diermeyer, „The Perception Modification Concept to Free the Path of An Automated Vehicle Remotely," in *Proceedings of the 7th International Conference on Vehicle Technology and Intelligent Transport Systems*, 2021, pp. 405–412. DOI: 10.5220/0010433304050412.

[112] J. P. Feiler, „Modifizierung der maschinellen Wahrnehmung mittels Teleoperation," PhD thesis, Technical University of Munich, 2023. Available: https://mediatum.ub.tum.de/1687818.

[113] S. Bensoussan and M. Parent, „Computer-aided teleoperation of an urban vehicle," in *1997 8th International Conference on Advanced Robotics. Proceedings. ICAR'97*, 1997, pp. 787–792. DOI: 10.1109/ICAR.1997.620271.

[114] O. Bodell and E. Gulliksson. „Teleoperation of Autonomous Vehicle With 360° Camera Feedback," Master's thesis in Systems, Control and Mechatronics, 2016.

[115] B. Ross, J. Bares, D. Stager, L. Jackel and M. Perschbacher, „An Advanced Teleoperation Testbed," in *Field and Service Robotics*. vol. 42 Berlin, Heidelberg: Springer Berlin Heidelberg, 2007, pp. 297–304, ISBN: 9783540754039. DOI: 10.1007/978-3-540-75404-6_28. Available: http://link.springer.com/10.1007/978-3-540-75404-6_28.

[116] M. Gafert, A. G. Mirnig, P. Fröhlich and M. Tscheligi, „TeleOperationStation: XR-Exploration of User Interfaces for Remote Automated Vehicle Operation," in *CHI Conference on Human Factors in Computing Systems Extended Abstracts*, 2022, pp. 1–4. DOI: 10.1145/3491101.3519882.

[117] A. Dosovitskiy, G. Ros, F. Codevilla, A. López and V. Koltun, „CARLA: An open urban driving simulator," in *Proc. of 1st Annual Conference on Robot Learning (CoRL)*, 2017, pp. 1–16.

[118] M. Hofbauer, C. B. Kuhn, G. Petrovic and E. Steinbach, „TELECARLA: An Open Source Extension of the CARLA Simulator for Teleoperated Driving Research Using Off-the-Shelf Components," in *2020 IEEE Intelligent Vehicles Symposium (IV)*, 2020, pp. 335–340. DOI: 10.1109/IV47402.2020.9304676.

[119] S. Gnatzig, F. Chucholowski, T. Tang and M. Lienkamp, „A System Design for Teleoperated Road Vehicles," in *Proceedings of the 10th International Conference on Informatics in Control, Automation and Robotics*, 2013, pp. 231–238. DOI: 10.5220/0004475802310238.

[120] J. S. Kay and C. E. Thorpe, „Operator Interface Design Issues in a Low-Bandwidth and High-Latency Vehicle Teleoperation System," in *SAE Technical Papers*, 1995, DOI: 10.4271/951485.

[121] S. Gnatzig, F. Schuller and M. Lienkamp, „Human-machine interaction as key technology for driverless driving - A trajectory-based shared autonomy control approach," in *2012 IEEE RO-MAN: The 21st IEEE International Symposium on Robot and Human Interactive Communication*, 2012, pp. 913–918. DOI: 10.1109/ROMAN.2012.6343867.

[122] S. Hoffmann, D. Majstorović and F. Diermeyer, „Safe Corridor: A Trajectory-Based Safety Concept for Teleoperated Road Vehicles," in *2022 International Conference on Connected Vehicle and Expo (ICCVE)*, 2022, pp. 1–6. DOI: 10.1109/ICCVE52871.2022.9742770.

[123] I. Jatzkowski, T. Stolte, R. Graubohm and P. M. Maurer, „Integration of a Vehicle Operating Mode Management into UNICAR agil's Automotive Service-oriented Software Architecture," *30th Aachen Colloquium Sustainable Mobility 2021*, pp. 595–614, 2021.

[124] Q. Zhang, Z. Xu, Y. Wang, L. Yang, X. Song and Z. Huang. „"Predicted Trajectory Guidance Control Framework of Teleoperated Ground Vehicles Compensating for Delays"," 2022. arXiv: 2212.02706. Available: http://arxiv.org/abs/2212.02706.

[125] G. Li, Q. Li, C. Yang, Y. Su, Z. Yuan and X. Wu, „The Classification and New Trends of Shared Control Strategies in Telerobotic Systems: A Survey," *IEEE Transactions on Haptics*, vol. XX, no. Xx, pp. 1–17, 2023, DOI: 10.1109/TOH.2023.3253856.

[126] J. Vreeswijk, A. Habibovic, O. Madland and F. Hooft, „Remote Support for Automated Vehicle Operations," 2023, pp. 149–164, ISBN: 9783319609331. DOI: 10.1007/978-3-031-11112-9_12. Available: https://link.springer.com/10.1007/978-3-031-11112-9_12.

[127] T. B. Sheridan and W. L. Verplank, „Human and computer control of undersea teleoperators," *Massachusetts Inst of Tech Cambridge Man-Machine Systems Lab*, 1978.

[128] G. Hirzinger, B. Brunner, J. Dietrich and J. Heindl, „ROTEX-the first remotely controlled robot in space," in *Proceedings of the 1994 IEEE International Conference on Robotics and Automation*, 1994, pp. 2604–2611. DOI: 10.1109/ROBOT.1994.351121.

[129] G. Hirzinger, K. Landzettel, B. Brunner, M. Fischer, C. Preusche, D. Reintsema, A. Albu-Schäffer, G. Schreiber and B.-M. Steinmetz, „DLR's robotics technologies for on-orbit servicing," *Advanced Robotics*, vol. 18, no. 2, pp. 139–174, 2004, DOI: 10.1163/156855304322758006.

[130] K. Goodrich, P. Schutte, F. Flemisch and R. Williams, „Application of the H-Mode, A Design and Interaction Concept for Highly Automated Vehicles, to Aircraft," in *2006 ieee/aiaa 25TH Digital Avionics Systems Conference*, 2006, pp. 1–13. DOI: 10.1109/DASC.2006.313781.

[131] R. Li, Y. Li, S. E. Li, E. Burdet and B. Cheng, „Driver-automation indirect shared control of highly automated vehicles with intention-aware authority transition," in *2017 IEEE Intelligent Vehicles Symposium (IV)*, 2017, pp. 26–32. DOI: 10.1109/IVS.2017.7995694.

[132] F. O. Flemisch, C. A. Adams, S. R. Conway, K. H. Goodrich, M. T. Palmer and P. C. Schutte, „The H-Metaphor as a Guideline for Vehicle Automation and Interaction," vol. L-18448, 2003.

[133] F. Flemisch, D. A. Abbink, M. Itoh, M.-P. Pacaux-Lemoine and G. Weßel, „Joining the blunt and the pointy end of the spear: towards a common framework of joint action, human–machine cooperation, cooperative guidance and control, shared, traded and supervisory control," *Cognition, Technology & Work*, vol. 21, no. 4, pp. 555–568, 2019, ISBN: 0123456789. DOI: 10.1007/s10111-019-00576-1.

[134] SAE International. „Survey Shows Public Enthusiasm About Self-Driving Cars,“ 2019. Available: https://www.sae.org/news/press-room/2019/11/sae-international-survey-shows-public-enthusiasm-about-self-driving-cars [visited on 03/07/2023].

[135] M. Marcano, S. Diaz, J. Perez and E. Irigoyen, „A Review of Shared Control for Automated Vehicles: Theory and Applications,“ *IEEE Transactions on Human-Machine Systems*, vol. 50, no. 6, pp. 475–491, 2020, DOI: 10.1109/THMS.2020.3017748.

[136] L. Saleh, P. Chevrel, F. Claveau, J.-F. Lafay and F. Mars, „Shared Steering Control Between a Driver and an Automation: Stability in the Presence of Driver Behavior Uncertainty,“ *IEEE Transactions on Intelligent Transportation Systems*, vol. 14, no. 2, pp. 974–983, 2013, DOI: 10.1109/TITS.2013.2248363.

[137] K. Yang, Y. Liu, X. Na, X. He, Y. Liu, J. Wu, S. Nakano and X. Ji, „Preview-scheduled steering assistance control for co-piloting vehicle: a human-like methodology,“ *Vehicle System Dynamics*, vol. 58, no. 4, pp. 518–544, 2020, DOI: 10.1080/00423114.2019.1590607.

[138] A.-T. Nguyen, C. Sentouh and J.-C. Popieul, „Sensor Reduction for Driver-Automation Shared Steering Control via an Adaptive Authority Allocation Strategy,“ *IEEE/ASME Transactions on Mechatronics*, vol. 23, no. 1, pp. 5–16, 2018, DOI: 10.1109/TMECH.2017.2698216.

[139] M. Flad, L. Frohlich and S. Hohmann, „Cooperative Shared Control Driver Assistance Systems Based on Motion Primitives and Differential Games,“ *IEEE Transactions on Human-Machine Systems*, vol. 47, no. 5, pp. 711–722, 2017, DOI: 10.1109/THMS.2017.2700435.

[140] T. Wada, K. Sonoda, T. Okasaka and T. Saito, „Authority transfer method from automated to manual driving via haptic shared control,“ in *2016 IEEE International Conference on Systems, Man, and Cybernetics (SMC)*, 2016, pp. 002659–002664. DOI: 10.1109/SMC.2016.7844641.

[141] T. Saito, T. Wada and K. Sonoda, „Control Authority Transfer Method for Automated-to-Manual Driving Via a Shared Authority Mode,“ *IEEE Transactions on Intelligent Vehicles*, vol. 3, no. 2, pp. 198–207, 2018, DOI: 10.1109/TIV.2018.2804167.

[142] S. Cutlip, Y. Wan, N. Sarter and R. B. Gillespie, „The Effects of Haptic Feedback and Transition Type on Transfer of Control Between Drivers and Vehicle Automation,“ *IEEE Transactions on Human-Machine Systems*, vol. 51, no. 6, pp. 613–621, 2021, DOI: 10.1109/THMS.2021.3107255.

[143] D. Maggi, „Safe and Seamless Transfer of Control Authority Exploring Haptic Shared Control during Handovers,“ PhD thesis, University of Leeds, 2022.

[144] K. Sonoda, K. Okada, K. Sato, G. Abe and T. Wada, „Does Shared Mode Improve Steering and Vehicle Motions During Control Transition From Automated to Manual Driving in Real Passenger Car?,“ *IEEE Access*, vol. 10, no. July, pp. 85880–85890, 2022, DOI: 10.1109/ACCESS.2022.3197885.

[145] F. Flemisch, M. Heesen, J. Kelsch, J. Schindler, C. Preusche and J. Dittrich, „Shared and cooperative movement control of intelligent technical systems: Sketch of the design space of haptic-multimodal coupling between operator, co-automation, base system and environment,“ *IFAC Proceedings Volumes*, vol. 43, no. 13, pp. 304–309, 2010, DOI: 10.3182/20100831-4-FR-2021.00054.

[146] M. Mulder, „Haptic Gas Pedal Feedback for Active Car-Following Support,“ PhD thesis, Delft University of Technology, 2007, ISBN: 9789085592662. Available: https://repository.tudelft.nl/islandora/object/uuid%3A008d10dc-3aa1-4b29-b445-579278543057.

[147] H. Jamson, D. L. Hibberd and N. Merat, „The Design of Haptic Gas Pedal Feedback to Support Eco-Driving,“ in *Proceedings of the 7th International Driving Symposium on Human Factors in Driver Assessment, Training, and Vehicle Design : driving assessment 2013*, 2013, pp. 264–270. DOI: 10.17077/drivingassessment.1499.

[148] M. Corno, „Design, Analysis, and Validation of a Haptic-Based Driver Support System for Traction Control," *IEEE Transactions on Intelligent Transportation Systems*, vol. 14, no. 4, pp. 1849–1859, 2013, DOI: 10.1109/TITS.2013.2268316.

[149] R. Li, Y. Li, S. E. Li, C. Zhang, E. Burdet and B. Cheng, „Indirect Shared Control for Cooperative Driving Between Driver and Automation in Steer-by-Wire Vehicles," *IEEE Transactions on Intelligent Transportation Systems*, vol. 22, no. 12, pp. 7826–7836, 2021, DOI: 10.1109/TITS.2020.3010620.

[150] W. Wang, X. Na, D. Cao, J. Gong, J. Xi, Y. Xing and F.-Y. Wang, „Decision-making in driver-automation shared control: A review and perspectives," *IEEE/CAA Journal of Automatica Sinica*, vol. 7, no. 5, pp. 1–19, 2020, DOI: 10.1109/JAS.2020.1003294.

[151] D. D. Salvucci and R. Gray, „A Two-Point Visual Control Model of Steering," *Perception*, vol. 33, no. 10, pp. 1233–1248, 2004, DOI: 10.1068/p5343.

[152] M. Treiber, A. Hennecke and D. Helbing, „Congested traffic states in empirical observations and microscopic simulations," *Physical Review E*, vol. 62, no. 2, pp. 1805–1824, 2000, DOI: 10.1103/PhysRevE.62.1805.

[153] J. Kelsch, F. Flemisch, C. Löper, A. Schieben and J. Schindler, „Links oder rechts, schneller oder langsamer? Grundlegende Fragestellungen beim Cognitive Systems Engineering von hochautomatisierter Fahrzeugführung," *Cognitive Systems Engineering in der Fahrzeug- und Prozessführung*, pp. 227–240, 2006, ISBN: 3-932182-51-0.

[154] M. Baltzer, E. Altendorf, S. Meier and F. Flemisch, „Mediating the Interaction between Human and Automation during the Arbitration Processes in Cooperative Guidance and Control of Highly Automated Vehicles: Base concept and First Study," in *Advances in Human Aspects of Transportation: Part I*, 2014, DOI: 10.54941/ahfe100647.

[155] A. Enes and W. Book, „Blended Shared Control of Zermelo's navigation problem," in *Proceedings of the 2010 American Control Conference*, 2010, pp. 4307–4312. DOI: 10.1109/ACC.2010.5530818.

[156] M. Allain, S. Konduri, H. Maske, P. Pagilla and G. Chowdhary, „Blended Shared Control of a Hydraulic Excavator," *IFAC-PapersOnLine*, vol. 50, no. 1, pp. 14928–14933, 2017, DOI: 10.1016/j.ifacol.2017.08.2541.

[157] S. J. Anderson, S. C. Peters, T. E. Pilutti and K. Iagnemma, „An optimal-control-based framework for trajectory planning, threat assessment, and semi-autonomous control of passenger vehicles in hazard avoidance scenarios," *International Journal of Vehicle Autonomous Systems*, vol. 8, no. 2/3/4, p. 190, 2010, DOI: 10.1504/IJVAS.2010.035796.

[158] S. Anderson, „Constraint-Based Navigation for Safe, Shared Control of Ground Vehicles," PhD thesis, Massachusetts Institute of Technology, 2013. Available: https://dspace.mit.edu/handle/1721.1/79314.

[159] M. Li, H. Cao, X. Song, Y. Huang, J. Wang and Z. Huang, „Shared Control Driver Assistance System Based on Driving Intention and Situation Assessment," *IEEE Transactions on Industrial Informatics*, vol. 14, no. 11, pp. 4982–4994, 2018, DOI: 10.1109/TII.2018.2865105.

[160] M. Li, X. Song, H. Cao, J. Wang, Y. Huang, C. Hu and H. Wang, „Shared control with a novel dynamic authority allocation strategy based on game theory and driving safety field," *Mechanical Systems and Signal Processing*, vol. 124, pp. 199–216, 2019, DOI: 10.1016/j.ymssp.2019.01.040.

[161] A. Bhardwaj, A. H. Ghasemi, Y. Zheng, H. Febbo, P. Jayakumar, T. Ersal, J. L. Stein and R. B. Gillespie, „Who's the boss? Arbitrating control authority between a human driver and automation system," *Transportation Research Part F: Traffic Psychology and Behaviour*, vol. 68, pp. 144–160, 2020, DOI: 10.1016/j.trf.2019.12.005.

[162] A. Bhardwaj, Y. Lu, S. Pan, N. Sarter and R. B. Gillespie, „Comparing Coupled and Decoupled Steering Interface Designs for Emergency Obstacle Evasion," *IEEE Access*, vol. 9, pp. 116857–116868, 2021, DOI: 10.1109/ACCESS.2021.3106225.

[163] M. Yue, C. Fang, H. Zhang and J. Shangguan, „Adaptive authority allocation-based driver-automation shared control for autonomous vehicles," *Accident Analysis & Prevention*, vol. 160, no. July, p. 106301, 2021, DOI: 10.1016/j.aap.2021.106301.

[164] J. Liu, H. Guo, W. Shi, Q. Dai and J. Zhang, „Driver-automation shared steering control considering driver neuromuscular delay characteristics based on stackelberg game," *Green Energy and Intelligent Transportation*, vol. 1, no. 2, p. 100027, 2022, DOI: 10.1016/j.geits.2022.100027.

[165] S. M. Erlien, S. Fujita and J. C. Gerdes, „Shared Steering Control Using Safe Envelopes for Obstacle Avoidance and Vehicle Stability," *IEEE Transactions on Intelligent Transportation Systems*, vol. 17, no. 2, pp. 441–451, 2016, DOI: 10.1109/TITS.2015.2453404.

[166] A. Balachandran, M. Brown, S. M. Erlien and J. C. Gerdes, „Predictive Haptic Feedback for Obstacle Avoidance Based on Model Predictive Control," *IEEE Transactions on Automation Science and Engineering*, vol. 13, no. 1, pp. 26–31, 2016, DOI: 10.1109/TASE.2015.2498924.

[167] A. Gray, Y. Gao, T. Lin, J. K. Hedrick and F. Borrelli, „Stochastic predictive control for semi-autonomous vehicles with an uncertain driver model," in *16th International IEEE Conference on Intelligent Transportation Systems (ITSC 2013)*, 2013, pp. 2329–2334. DOI: 10.1109/ITSC.2013.6728575.

[168] W. Guo, H. Cao, S. Zhao, M. Li, B. Yi and X. Song, „A data-driven model-based shared control strategy considering drivers' adaptive behavior in driver-automation interaction," *Proceedings of the Institution of Mechanical Engineers, Part D: Journal of Automobile Engineering*, p. 095440702211048, 2022, DOI: 10.1177/09544070221104888.

[169] Y. Chen, Y. Song, L. Shi and J. Gao, „Stochastic model predictive control for driver assistance control of intelligent vehicles considering uncertain driving environment," *Journal of Vibration and Control*, vol. 29, no. 3-4, pp. 758–771, 2023, DOI: 10.1177/10775463211052353.

[170] A. Seppänen, J. Vepsäläinen, R. Ojala and K. Tammi, „Comparison of Semi-autonomous Mobile Robot Control Strategies in Presence of Large Delay Fluctuation," *Journal of Intelligent & Robotic Systems*, vol. 106, no. 1, p. 28, 2022, ISBN: 0123456789. DOI: 10.1007/s10846-022-01711-3.

[171] L. Yan, X. Wu, M. Xu and M. Wang, „Cooperative Steering Control System for Robust Obstacle Avoidance in Cluttered Off-Road Environments," in *2022 6th CAA International Conference on Vehicular Control and Intelligence (CVCI)*, 2022, pp. 1–6. DOI: 10.1109/CVCI56766.2022.9965092.

[172] W. Huang, Y. Zhou, J. Li and C. Lv, „Potential Hazard-Aware Adaptive Shared Control for Human-Robot Cooperative Driving in Unstructured Environment," in *2022 17th International Conference on Control, Automation, Robotics and Vision (ICARCV)*, 2022, pp. 405–410. DOI: 10.1109/ICARCV57592.2022.10004306.

[173] B. Asadi and A. Vahidi, „Predictive Cruise Control: Utilizing Upcoming Traffic Signal Information for Improving Fuel Economy and Reducing Trip Time," *IEEE Transactions on Control Systems Technology*, vol. 19, no. 3, pp. 707–714, 2011, DOI: 10.1109/TCST.2010.2047860.

[174] H. Chu, L. Guo, B. Gao, H. Chen, N. Bian and J. Zhou, „Predictive Cruise Control Using High-Definition Map and Real Vehicle Implementation," *IEEE Transactions on Vehicular Technology*, vol. 67, no. 12, pp. 11377–11389, 2018, DOI: 10.1109/TVT.2018.2871202.

[175] M. Althoff, S. Maierhofer and C. Pek, „Provably-Correct and Comfortable Adaptive Cruise Control," *IEEE Transactions on Intelligent Vehicles*, vol. 6, no. 1, pp. 159–174, 2021, DOI: 10.1109/TIV.2020.2991953.

[176] S. Magdici and M. Althoff, „Adaptive Cruise Control with Safety Guarantees for Autonomous Vehicles," *IFAC-PapersOnLine*, vol. 50, no. 1, pp. 5774–5781, 2017, DOI: 10.1016/j.ifacol.2017.08.418.

[177] B. van Arem, C. J. G. van Driel and R. Visser, „The Impact of Cooperative Adaptive Cruise Control on Traffic-Flow Characteristics," *IEEE Transactions on Intelligent Transportation Systems*, vol. 7, no. 4, pp. 429–436, 2006, DOI: 10.1109/TITS.2006.884615.

[178] K. S. Schweidel, S. M. Koehler, V. R. Desaraju and M. Baric, „Driver-in-the-Loop Contingency MPC with Invariant Sets," in *2022 European Control Conference (ECC)*, 2022, pp. 808–813. DOI: 10.23919/ECC55457.2022.9838190.

[179] D. Schitz, G. Graf, D. Rieth and H. Aschemann, „Model-Predictive Cruise Control for Direct Teleoperated Driving Tasks," in *2021 European Control Conference (ECC)*, 2021, pp. 1808–1813. DOI: 10.23919/ECC54610.2021.9655187.

[180] J. Storms, K. Chen and D. Tilbury, „A shared control method for obstacle avoidance with mobile robots and its interaction with communication delay," *The International Journal of Robotics Research*, vol. 36, no. 5-7, pp. 820–839, 2017, DOI: 10.1177/0278364917693690.

[181] W. Schwarting, J. Alonso-Mora, L. Pauli, S. Karaman and D. Rus, „Parallel autonomy in automated vehicles: Safe motion generation with minimal intervention," in *2017 IEEE International Conference on Robotics and Automation (ICRA)*, 2017, pp. 1928–1935. DOI: 10.1109/ICRA.2017.7989224.

[182] W. Schwarting, J. Alonso-Mora, L. Paull, S. Karaman and D. Rus, „Safe Nonlinear Trajectory Generation for Parallel Autonomy With a Dynamic Vehicle Model," *IEEE Transactions on Intelligent Transportation Systems*, vol. 19, no. 9, pp. 2994–3008, 2018, DOI: 10.1109/TITS.2017.2771351.

[183] T. Weiskircher, Q. Wang and B. Ayalew, „Predictive Guidance and Control Framework for (Semi-)Autonomous Vehicles in Public Traffic," *IEEE Transactions on Control Systems Technology*, vol. 25, no. 6, pp. 2034–2046, 2017, DOI: 10.1109/TCST.2016.2642164.

[184] D. Tran, J. Du, W. Sheng, D. Osipychev, Y. Sun and H. Bai, „A Human-Vehicle Collaborative Driving Framework for Driver Assistance," *IEEE Transactions on Intelligent Transportation Systems*, vol. 20, no. 9, pp. 3470–3485, 2019, DOI: 10.1109/TITS.2018.2878027.

[185] Y. Cho, H. Yun, J. Lee, A. Ha and J. Yun, „GoonDAE: Denoising-Based Driver Assistance for Off-Road Teleoperation," *IEEE Robotics and Automation Letters*, vol. 8, no. 4, pp. 2405–2412, 2023, DOI: 10.1109/LRA.2023.3250008.

[186] R. Rajamani, *Vehicle Dynamics and Control*, (Mechanical Engineering Series), Boston, MA, Springer US, p. 544, 2012, ISBN: 978-1-4614-1432-2. DOI: 10.1007/978-1-4614-1433-9. arXiv: arXiv:1011.1669v3. Available: https://link.springer.com/10.1007/978-1-4614-1433-9.

[187] J. Kabzan, M. I. Valls, V. J. F. Reijgwart, H. F. C. Hendrikx, C. Ehmke, M. Prajapat, A. Bühler, N. Gosala, M. Gupta, R. Sivanesan, et al., „AMZ Driverless: The full autonomous racing system," *Journal of Field Robotics*, vol. 37, no. 7, rob.21977, 2020, DOI: 10.1002/rob.21977.

[188] H. B. Pacejka and E. Bakker, „THE MAGIC FORMULA TYRE MODEL," *Vehicle System Dynamics*, vol. 21, no. sup001, pp. 1–18, 1992, DOI: 10.1080/00423119208969994.

[189] E. Hairer, S. P. Nørsett and G. Wanner, *Solving Ordinary Differential Equations I*, (Springer Series in Computational Mathematics). vol. 8, Berlin, Heidelberg, Springer Berlin Heidelberg, 1993, ISBN: 978-3-540-56670-0. DOI: 10.1007/978-3-540-78862-1. Available: http://link.springer.com/10.1007/978-3-540-78862-1.

[190] E. F. Camacho and C. Bordons, *Model Predictive control*, (Advanced Textbooks in Control and Signal Processing), London, Springer London, p. 405, 2007, ISBN: 978-1-85233-694-3. DOI: 10.1007/978-0-85729-398-5. arXiv: arXiv:1011.1669v3. Available: http://link.springer.com/10.1007/978-0-85729-398-5.

[191] J. B. Rawlings, D. Q. Mayne and M. Diehl, *Model predictive control: theory, computation, and design - 2nd Edition*, Nob Hill Publishing, 2017.

[192] N. Dang, T. Brüdigam, M. Leibold and M. Buss, „Combining Event-Based Maneuver Selection and MPC Based Trajectory Generation in Autonomous Driving," *Electronics*, vol. 11, no. 10, p. 1518, 2022, DOI: 10.3390/electronics11101518.

[193] T. Brüdigam, „Safety and Efficiency in Model Predictive Control for Systems with Uncertainty," PhD thesis, Technical University of Munich, 2022.

[194] S. Boyd and L. Vandenberghe, *Convex Optimization*, Cambridge University Press, pp. 135–186, 2004, ISBN: 9780521833783. DOI: 10.1017/CBO9780511804441. Available: https://www.cambridge.org/core/product/identifier/9780511804441/type/book.

[195] Mercedes-Benz. „MBUX Augmented Reality Head-up-Display," 2023. Available: https://www.mercedes-benz.de/passengercars/mercedes-benz-cars/models/eqs/saloon-v297/equipment.pi.html/mercedes-benz-cars/models/eqs/saloon-v297/equipment/individualization/mbux-ar-hud [visited on 01/27/2023].

[196] Volkswagen. „AR Head-up-Display," 2023. Available: https://www.volkswagen.de/de/elektrofahrzeuge/id-technologie/id-augmented-reality-navigation.html [visited on 01/27/2023].

[197] G. Sharma, H. Yasuda and M. Kuehner. „"Continuous Visual Feedback of Risk for Haptic Lateral Assistance"," 2023. arXiv: 2301.10933. Available: http://arxiv.org/abs/2301.10933.

[198] R. Verschueren, G. Frison, D. Kouzoupis, J. Frey, N. van Duijkeren, A. Zanelli, B. Novoselnik, T. Albin, R. Quirynen and M. Diehl, „acados—a modular open-source framework for fast embedded optimal control," *Mathematical Programming Computation*, vol. 14, no. 1, pp. 147–183, 2022, DOI: 10.1007/s12532-021-00208-8.

[199] S. Saparia, A. Schimpe and L. Ferranti, „Active Safety System for Semi-Autonomous Teleoperated Vehicles," in *2021 IEEE Intelligent Vehicles Symposium Workshops (IV Workshops)*, 2021, pp. 141–147. DOI: 10.1109/IVWorkshops54471.2021.9669239.

[200] A. Schimpe, J. Feiler, S. Hoffmann and D. Majstorović. „GitHub | TUM FTM Teleoperated Driving Software," 2021. Available: https://github.com/TUMFTM/teleoperated_driving [visited on 04/16/2023].

[201] M. Quigley, B. Gerkey, K. Conley, J. Faust, T. Foote, J. Leibs, E. Berger, R. Wheeler and A. Ng, „ROS: an open-source Robot Operating System," in *ICRA Workshop on Open Source Software*, 2009, pp. 1–6. DOI: 10.1109/IECON.2015.7392843.

[202] A. Schimpe. „GitHub | tod_video," 2021. Available: https://github.com/TUMFTM/tod_perception/tree/master/tod_video [visited on 04/16/2023].

[203] A. Schimpe, J. Feiler, S. Hoffmann, D. Majstorović and F. Diermeyer. „Demonstrations of Open Source Software for Teleoperated Driving," 2021. Available: https://youtu.be/bQZLCOpOAQc [visited on 04/16/2023].

[204] M. O'Kelly, V. Sukhil, H. Abbas, J. Harkins, C. Kao, Y. V. Pant, R. Mangharam, D. Agarwal, M. Behl, P. Burgio, et al. „"F1/10: An Open-Source Autonomous Cyber-Physical Platform"," 2019. arXiv: 1901.08567. Available: https://arxiv.org/abs/1901.08567.

[205] G. Rong, B. H. Shin, H. Tabatabaee, Q. Lu, S. Lemke, M. Mozeiko, E. Boise, G. Uhm, M. Gerow, S. Mehta, et al., „LGSVL Simulator: A High Fidelity Simulator for Autonomous Driving," in *2020 IEEE 23rd International Conference on Intelligent Transportation Systems (ITSC)*, 2020, pp. 1–6. DOI: 10.1109/ITSC45102.2020.9294422.

[206] D. Majstorović and F. Diermeyer, „Driverless road-marking Machines: Ma(r)king the Way towards the Future of Mobility," in *2022 IEEE International Conference on Systems, Man, and Cybernetics (SMC)*, 2022, pp. 1297–1303. DOI: 10.1109/SMC53654.2022.9945440.

[207] T. Woopen et al., „UNICAR agil - Disruptive Modular Architectures for Agile , Automated Vehicle Concepts,“ *27. Aachen Colloquium Automobile and Engine Technology*, pp. 663–694, 2018.

[208] A. Schimpe. „GitHub | tod_shared_control,“ 2023. Available: https://github.com/TUMFTM/tod_control/tree/master/tod_shared_control [visited on 05/17/2023].

[209] MathWorks. „MATLAB,“ 2023. Available: https://de.mathworks.com/products/matlab.html [visited on 05/03/2023].

[210] P. T. Boggs and J. W. Tolle, „Sequential Quadratic Programming,“ *Acta Numerica*, vol. 4, no. January, pp. 1–51, 1995, DOI: 10.1017/S0962492900002518.

[211] G. Frison and M. Diehl, „HPIPM: a high-performance quadratic programming framework for model predictive control,“ *IFAC-PapersOnLine*, vol. 53, no. 2, pp. 6563–6569, 2020, DOI: 10.1016/j.ifacol.2020.12.073.

[212] S. Hart, „Task Load Index (NASA-TLX) V 1.0,“ 1986, DOI: 10.1007/978-3-319-57111-9_1256.

[213] C. Lehsing and K. Seifert. „German translation of NASA-TLX,“ Available: https://www.keithv.com/software/nasatlx/nasatlx_german.html [visited on 07/01/2022].

[214] B. Laugwitz, T. Held and M. Schrepp, „Construction and Evaluation of a User Experience Questionnaire,“ in *Lecture Notes in Computer Science (including subseries Lecture Notes in Artificial Intelligence and Lecture Notes in Bioinformatics)*. vol. 5298 LNCS 2008, pp. 63–76, ISBN: 3540893490. DOI: 10.1007/978-3-540-89350-9_6. Available: http://link.springer.com/10.1007/978-3-540-89350-9_6.

[215] A. Hinderks, M. Schrepp and J. Thomaschewski. „User Experience Questionnaire,“ 2018. Available: https://www.ueq-online.org/ [visited on 07/01/2022].

[216] R. Liu, D. Kwak, S. Devarakonda, K. Bekris and L. Iftode, „Investigating Remote Driving over the LTE Network,“ in *Proceedings of the 9th International Conference on Automotive User Interfaces and Interactive Vehicular Applications*, 2017, pp. 264–269. DOI: 10.1145/3122986.3123008.

[217] A. Field, J. Miles and Z. Field, *Discovering statistics using R*, Great Britain: Sage Publications Ltd., 2012.

[218] C. O. Fritz, P. E. Morris and J. J. Richler, „Effect size estimates: Current use, calculations, and interpretation.“ *Journal of Experimental Psychology: General*, vol. 141, no. 1, pp. 2–18, 2012, DOI: 10.1037/a0024338.

[219] C. Huang, C. Lv, P. Hang, Z. Hu and Y. Xing, „Human–Machine Adaptive Shared Control for Safe Driving Under Automation Degradation,“ *IEEE Intelligent Transportation Systems Magazine*, vol. 14, no. 2, pp. 53–66, 2022, DOI: 10.1109/MITS.2021.3065382.

[220] K. Keller, C. Zimmermann, J. Zibuschka and O. Hinz, „Trust is Good, Control is Better - Customer Preferences Regarding Control in Teleoperated and Autonomous Taxis,“ in *Proceedings of the Annual Hawaii International Conference on System Sciences*, 2021, pp. 1849–1858. DOI: 10.24251/HICSS.2021.225.

# Prior Publications

During the development of this dissertation, publications and student theses were written in which partial aspects of this work were presented.

## Conferences, Periodicals; Scopus/Web of Science listed (peer-reviewed)

[21] D. Majstorović, S. Hoffmann, F. Pfab, A. Schimpe, M.-M. Wolf and F. Diermeyer, „Survey on Teleoperation Concepts for Automated Vehicles," in *2022 IEEE International Conference on Systems, Man, and Cybernetics (SMC)*, 2022, pp. 1290–1296. DOI: 10.1109/SMC53654.2022.9945267.

[97] A. Schimpe, D. Majstorović and F. Diermeyer, „Steering Action-aware Adaptive Cruise Control for Teleoperated Driving," in *2022 IEEE International Conference on Systems, Man, and Cybernetics (SMC)*, 2022, pp. 988–993. DOI: 10.1109/SMC53654.2022.9945081.

[98] A. Schimpe and F. Diermeyer, „Steer with Me: A Predictive, Potential Field-Based Control Approach for Semi-Autonomous, Teleoperated Road Vehicles," in *2020 IEEE 23rd International Conference on Intelligent Transportation Systems (ITSC)*, 2020, pp. 1–6. DOI: 10.1109/ITSC45102.2020.9294702.

[99] A. Schimpe, S. Hoffmann and F. Diermeyer, „Adaptive Video Configuration and Bitrate Allocation for Teleoperated Vehicles," in *2021 IEEE Intelligent Vehicles Symposium Workshops (IV Workshops)*, 2021, pp. 148–153. DOI: 10.1109/IVWorkshops54471.2021.9669258.

[100] A. Schimpe, J. Feiler, S. Hoffmann, D. Majstorović and F. Diermeyer, „Open Source Software for Teleoperated Driving," in *2022 International Conference on Connected Vehicle and Expo (ICCVE)*, 2022, pp. 1–6. DOI: 10.1109/ICCVE52871.2022.9742859.

[199] S. Saparia, A. Schimpe and L. Ferranti, „Active Safety System for Semi-Autonomous Teleoperated Vehicles," in *2021 IEEE Intelligent Vehicles Symposium Workshops (IV Workshops)*, 2021, pp. 141–147. DOI: 10.1109/IVWorkshops54471.2021.9669239.

## Journals, Conferences, Periodicals, Reports, Conference Proceedings and Poster, etc.; not Scopus/Web of Science listed

[108] A. Schimpe, A. Pfadler and L. Montero Bayo, „Tele-operated Driving - Overview & Achievements," 5GCroCo Web-Seminar, 2022. Available: https://5gcroco.eu/images/templates/rsvario/images/5GCroCo_Webinar__ToD.pdf.

A. Schimpe, „Presentation on Open Source Software for Teleoperated Driving," 2022. Available: https://mediatum.ub.tum.de/node?id=1693635.

## Non-thesis-relevant publications; Scopus/Web of Science listed (peer-reviewed)

[8] K. Burnett, A. Schimpe, S. Samavi, M. Gridseth, C. W. Liu, Q. Li, Z. Kroeze and A. P. Schoellig, „Building a Winning Self-Driving Car in Six Months," in *2019 International Conference on Robotics and Automation (ICRA)*, 2019, pp. 9583–9589. DOI: 10.1109/ICRA.2019.8794029.

[56] A. Kousaridas, A. Schimpe, S. Euler, X. Vilajosana, M. Fallgren, G. Landi, F. Moscatelli, S. Barmpounakis, F. Vázquez-Gallego, R. Sedar, et al., „5G Cross-Border Operation for Connected and Automated Mobility: Challenges and Solutions," *Future Internet*, vol. 12, no. 1, p. 5, 2019, DOI: 10.3390/fi12010005.

D. Hetzer, M. Muehleisen, A. Kousaridas, S. Barmpounakis, S. Wendt, K. Eckert, A. Schimpe, J. Löfhede and J. Alonso-Zarate, „5G connected and automated driving: use cases, technologies and trials in cross-border environments," *EURASIP Journal on Wireless Communications and Networking*, vol. 2021, no. 1, p. 97, 2021, DOI: 10.1186/s13638-021-01976-6.

P. Kontopoulos, S. Barmpounakis, M. Muehleisen, F. Gardes, R. Sedar, F. Vazquez-Gallego, R. Casellas, F. Moscatelli, X. Vilajosana, A. Schimpe, et al., „Service Performance Measurement Methods for 5g Connected and Automated Mobility Use Cases," *SSRN Electronic Journal*, pp. 1–11, 2022, DOI: 10.2139/ssrn.4040705.

## Thesis-relevant open-source software

[200] A. Schimpe, J. Feiler, S. Hoffmann and D. Majstorović. „GitHub | TUM FTM Teleoperated Driving Software," 2021. Available: https://github.com/TUMFTM/teleoperated_driving [visited on 04/16/2023].

[202] A. Schimpe. „GitHub | tod_video," 2021. Available: https://github.com/TUMFTM/tod_perception/tree/master/tod_video [visited on 04/16/2023].

[208] A. Schimpe. „GitHub | tod_shared_control," 2023. Available: https://github.com/TUMFTM/tod_control/tree/master/tod_shared_control [visited on 05/17/2023].

# Supervised Student Theses

The following student theses were written within the framework of the dissertation under the supervision of the author in terms of content, technical and scientific support as well as under relevant guidance of the author. In the following, the bachelor, semester and master theses relevant and related to this dissertation are listed. Many thanks to the authors of these theses for their extensive support within the framework of this research project.

C. S. Bétous, „Game-Theoretic Modelling of the Human-Machine Interaction in a Shared Control Approach for Semi-Autonomous, Teleoperated Vehicles," Master's Thesis, Technical University of Munich, 2021.

H. Kang, „Adaptive Driver-Trajectory Prediction for Shared Control of Semi-automated Vehicles," Master's Thesis, Technical University of Munich, 2022.

P. Pitschi, „Model Predictive Control for Shared Control at the Limits of Driving Dynamics," Semester Thesis, Technical University of Munich, 2022.

S. Saparia, „Active Safety Control for Semi-Autonomous, Teleoperated Road Vehicles," Master's Thesis, Delft University of Technology, 2020.

Y. Wang, „Deep Learning-based Imitation Learning of Shared Control Interactions," Semester Thesis, Technical University of Munich, 2022.

# Appendix

# A Appendix

## A.1 Vehicle Parameters and Solver Settings

The parameters of the **passenger vehicle** are given as follows.

- Distance from center of mass to front axle: $l_\mathrm{f}$ = 1.45 m
- Distance from center of mass to rear axle: $l_\mathrm{r}$ = 1.56 m
- Maximum steering angle: $\delta_\mathrm{max}$ = 0.61 rad
- Distance from center of mass to front bumper: 2.41 m
- Distance from center of mass to rear bumper: 2.68 m
- Width from left to right edge: 2.18 m

The **solver settings in the simulative validation** are given as follows.

- Maximum number of SQP iterations: 15, tolerance for SQP convergence: 1e-2
- Maximum number of QP iterations: 100, tolerance for QP convergence: 1e-4
- `HPIPM` with `partial_condensing_hpipm` setting

The parameters of the **1:10-scale vehicle testbed** are given as follows.

- Distance from center of mass to front axle: $l_\mathrm{f}$ = 0.23 m
- Distance from center of mass to rear axle: $l_\mathrm{r}$ = 0.10 m
- Maximum steering angle: $\delta_\mathrm{max}$ = 0.34 rad
- Distance from center of mass to front bumper: 0.36 m
- Distance from center of mass to rear bumper: 0.24 m
- Width from left to right edge: 0.30 m

The **solver settings in the experimental user study** are given as follows.

- Maximum number of SQP iterations: 3, tolerance for SQP convergence: 1e-2
- Maximum number of QP iterations: 80, tolerance for QP convergence: 1e-4
- `HPIPM` with `partial_condensing_hpipm` setting

## A.2 Additional Data and Test Results from User Study

In the following, additional data and test results from the experimental user are reported.

### A.2.1 Learning Effects

In the following, additional data and test results for the learning effects from the user study are reported.

#### Controllability

The analyzed variables of the controllability per drive and test results for the assumptions of parametric tests are given in Table A.1. The results of tests for statistically significant differences are given in Table A.2.

Table A.1: Variables and assumptions for parametric tests of the controllability per drive.

| **Tested Mode** | **Median** | **Mean** | **Normal** (Shapiro-Wilk test) | **Homogeneous** (Levene test) |
|---|---|---|---|---|
| Controllability in first drive | 3 | 3.19 | No ($p$=0.0003, $W$=0.8454) | Yes ($p$=0.9061, $F$(2,93)=0.0987) |
| Controllability in second drive | 3.5 | 3.38 | No ($p$=0.0010, $W$=0.8679) | |
| Controllability in third drive | 4 | 3.63 | No ($p$=0.0008, $W$=0.8625) | |

Table A.2: Tests for statistically significant differences of the controllability between the drives.

| **Tested Modes** | **Significantly different** (All three modes: Friedman's ANOVA) |
|---|---|
| Controllability in first, second and third drive | No ($p$=0.4600, $\chi^2$(2)=1.5532) |

#### Mean Cognitive Workload

The mean cognitive workload per drive is shown in Figure A.1.

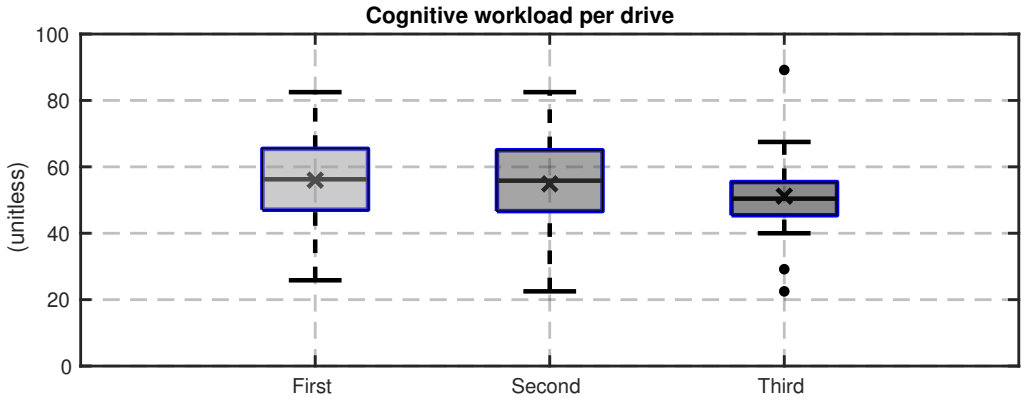


Figure A.1: Mean cognitive workload per teleoperation drive, assessed through the NASA-TLX.

## Items of Cognitive Workload

The analyzed variables of the items of the cognitive workload per drive and test results for the assumptions of parametric tests are given in Table A.3. The results of tests for significant differences are given in Table A.4.

Table A.3: Variables and assumptions for parametric tests of the items of the cognitive workload per drive.

| **Tested Mode** | **Median** | **Mean** | **Normal** (Shapiro-Wilk test) | **Homogeneous** (Levene test) |
|---|---|---|---|---|
| Mental demand in first drive | 75.0 | 68.4 | Yes ($p$=0.0942, $W$=0.9435) | Yes ($p$=0.8969, $F$(2,93)=0.1089) |
| Mental demand in second drive | 65.0 | 64.2 | Yes ($p$=0.1266, $W$=0.9480) | |
| Mental demand in the third drive | 57.5 | 57.3 | Yes ($p$=0.0636, $W$=0.9375) | |
| Physical demand in first drive | 42.5 | 46.9 | Yes ($p$=0.5822, $W$=0.9729) | Yes ($p$=0.3479, $F$(2,93)=1.0678) |
| Physical demand in second drive | 60.0 | 53.1 | Yes ($p$=0.1202, $W$=0.9472) | |
| Physical demand in third drive | 50.0 | 47.3 | Yes ($p$=0.5411, $W$=0.9715) | |
| Temporal demand in first drive | 70.0 | 67.0 | Yes ($p$=0.0554, $W$=0.9354) | Yes ($p$=0.5788, $F$(2,93)=0.5501) |
| Temporal demand in second drive | 60.0 | 58.6 | Yes ($p$=0.6038, $W$=0.9736) | |
| Temporal demand in third drive | 50.0 | 54.2 | Yes ($p$=0.4116, $W$=0.9666) | |
| Performance in first drive | 40.0 | 43.1 | Yes ($p$=0.2190, $W$=0.9564) | Yes ($p$=0.7917, $F$(2,93)=0.2341) |
| Performance in second drive | 52.5 | 52.5 | Yes ($p$=0.3717, $W$=0.9649) | |
| Performance in third drive | 60.0 | 57.3 | Yes ($p$=0.1543, $W$=0.9510) | |
| Effort in first drive | 70.0 | 65.9 | No ($p$=0.0131, $W$=0.9126) | Yes ($p$=0.8847, $F$(2,93)=0.1227) |
| Effort in second drive | 60.0 | 61.7 | Yes ($p$=0.4620, $W$=0.9686) | |
| Effort in third drive | 55.0 | 58.0 | Yes ($p$=0.6071, $W$=0.9737) | |
| Frustration in first drive | 42.5 | 44.5 | Yes ($p$=0.8993, $W$=0.9838) | Yes ($p$=0.6749, $F$(2,93)=0.3949) |
| Frustration in second drive | 37.5 | 39.1 | Yes ($p$=0.4377, $W$=0.9677) | |
| Frustration in third drive | 35.0 | 32.8 | Yes ($p$=0.0666, $W$=0.9382) | |

Table A.4: Tests for statistically significant differences of the items of the cognitive workload between the drives.

| **Tested Modes** | **Significantly different** (All three drives: Friedman's ANOVA, Pairwise: Wilcoxon signed-rank test) |
|---|---|
| Mental demand in first, second & third drive | Yes ($p$=0.0416, $\chi^2$(2)=6.3590) |
| Mental demand in first & second drive | No ($p$=0.6705, $r$=0.0752) |
| Mental demand in first & third drive | Yes ($p$=0.0158, $r$=0.4266) |
| Mental demand in second & third drive | No ($p$=0.0936, $r$=0.2964) |
| Physical demand in first, second & third drive | No ($p$=0.0973, $\chi^2$(2)=4.6609) |
| Temporal demand in first, second & third drive | Yes ($p$=0.0140, $\chi^2$(2)=8.5439) |
| Temporal demand in first & second drive | Yes ($p$=0.0083, $r$=0.4668) |
| Temporal demand in first & third drive | Yes ($p$=0.0052, $r$=0.4945) |
| Temporal demand in second & third drive | No ($p$=0.2834, $r$=0.1896) |
| Performance in first, second & third drive | Yes ($p$=0.0116, $\chi^2$(2)=8.9194) |
| Performance in first & second drive | No ($p$=0.0818, $r$=0.3077) |
| Performance in first & third drive | Yes ($p$=0.0028, $r$=0.5291) |
| Performance in second & third drive | No ($p$=0.2802, $r$=0.1909) |
| Effort in first, second & third drive | No ($p$=0.1821, $\chi^2$(2)=3.4068) |
| Frustration in first, second & third drive | No ($p$=0.0546, $\chi^2$(2)=5.8167) |

### A.2.2 Hypothesis 1: Cognitive Workload

The analyzed variables of the mean cognitive workload and test results for the assumptions of parametric tests are given in Table A.5. The results of tests for statistically significant differences are given in Table A.6.

Table A.5: Variables and assumptions for parametric tests of the mean cognitive workload per control mode.

| **Tested Mode** | **Median** | **Mean** | **Normal** (Shapiro-Wilk test) | **Homogeneous** (Levene test) |
|---|---|---|---|---|
| Mean cognitive workload with DC | 54.1667 | 54.9219 | Yes ($p$=0.6285, $W$=0.9744) | Yes ($p$=0.4337, $F$(2,93)=0.8430) |
| Mean cognitive workload with SVC | 48.7500 | 51.0417 | Yes ($p$=0.4512, $W$=0.9682) | |
| Mean cognitive workload with SSVC | 55.4167 | 56.0677 | Yes ($p$=0.5966, $W$=0.9734) | |

Table A.6: Tests for statistically significant differences of the mean cognitive workload between the control modes.

| **Tested Modes** | **Significantly different** (All three modes: ANOVA) |
|---|---|
| Mean cognitive workload with DC, SVC & SSVC | No ($p$=0.1240, $F$(2,93)=2.1592) |

### A.2.3 Hypothesis 2: Remote Operator Performance

The analyzed variables of the mean cognitive workload and test results for the assumptions of parametric tests are given in Table A.7. The results of tests for statistically significant differences are given in Table A.8.

Table A.7: Variables and assumptions for parametric tests of the performance score per control mode.

| **Tested Mode** | **Median** | **Mean** | **Normal** (Shapiro-Wilk test) | **Homogeneous** (Levene test) |
|---|---|---|---|---|
| Performance with DC | 304.86 | 297.10 | Yes ($p$=0.7714, $W$=0.9790) | No ($p$=0.0293, $F$(2,93)=3.6673) |
| Performance with SVC | 289.31 | 291.05 | Yes ($p$=0.9548, $W$=0.9867) | |
| Performance with SSVC | 243.28 | 243.50 | Yes ($p$=0.3413, $W$=0.9635) | |

Table A.8: Tests for statistically significant differences of the performance score between the control modes.

| **Tested Modes** | **Significantly different** (All three modes: Friedman's ANOVA, Pairwise: Wilcoxon signed-rank test) |
|---|---|
| Performance with DC, SVC & SSVC | Yes ($p$=1.2e-5, $\chi^2$(2)=22.75) |
| Performance with DC & SVC | No ($p$=0.6006, $r$=0.0926) |
| Performance with DC & SSVC | Yes ($p$=1.4e-5, $r$=0.7669) |
| Performance with SVC & SSVC | Yes ($p$=8.6e-6, $r$=0.7867) |

### A.2.4 Hypothesis 3: Safety

The agreement of the study participants to the question, if the perceived safety increased with an uncoupled shared control design of choice is shown in Figure A.2.

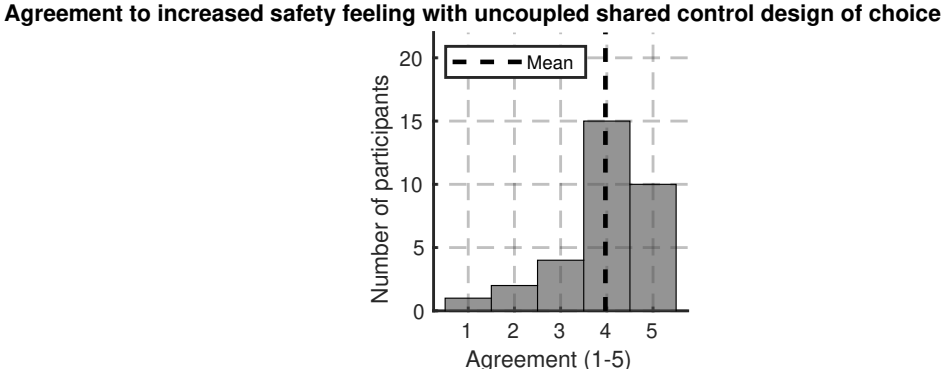


Figure A.2: Agreement to an increased safety feeling with the uncoupled shared control design of choice.

### A.2.5 Comparison of SVC and SSVC

In this section of the appendix, additional data and test results for the comparison between SVC and SSVC from the experimental user study, presented in Section 5.2, are reported.

## Items of Cognitive Workload

The analyzed variables of the items of the cognitive workload per mode and test results for the assumptions of parametric tests are given in Table A.9. The results of tests for statistically significant differences are given in Table A.10.

Table A.9: Variables and assumptions for parametric tests of the items of the cognitive workload per control mode.

| **Tested Mode** | **Median** | **Mean** | **Normal** (Shapiro-Wilk test) | **Homogeneous** (Levene test) |
|---|---|---|---|---|
| Mental demand with DC | 67.5 | 63.5938 | Yes ($p$=0.5232, $W$=0.9709) | Yes ($p$=0.2624, $F$(2,93)=1.3575) |
| Mental demand with SVC | 57.5 | 57.3438 | Yes ($p$=0.9189, $W$=0.9847) | |
| Mental demand with SSVC | 70.0 | 69.0625 | Yes ($p$=0.1025, $W$=0.9448) | |
| Physical demand with DC | 55.0 | 51.8750 | Yes ($p$=0.5084, $W$=0.9703) | Yes ($F$(2,93)=0.4420, $p$=0.6441) |
| Physical demand with SVC | 45.0 | 45.7812 | Yes ($p$=0.6410, $W$=0.9748) | |
| Physical demand with SSVC | 50.0 | 49.6875 | Yes ($p$=0.2825, $W$=0.9604) | |
| Temporal demand with DC | 60.0 | 59.2188 | Yes ($p$=0.3910, $W$=0.9658) | Yes ($F$(2,93)=0.7267, $p$=0.4863) |
| Temporal demand with SVC | 57.5 | 57.0312 | Yes ($p$=0.8229, $W$=0.9808) | |
| Temporal demand with SSVC | 65.0 | 63.5938 | Yes ($p$=0.1582, $W$=0.9514) | |
| Performance with DC | 60.0 | 58.7500 | Yes ($p$=0.1044, $W$=0.9451) | Yes ($F$(2,93)=0.5420, $p$=0.5834) |
| Performance with SVC | 60.0 | 53.9062 | Yes ($p$=0.7654, $W$=0.9788) | |
| Performance with SSVC | 40.0 | 40.3125 | Yes ($p$=0.3383, $W$=0.9634) | |
| Effort with DC | 65.0 | 64.3750 | No ($p$=0.0315, $W$=0.9266) | Yes ($p$=0.6929, $F$(2,93)=0.3684) |
| Effort with SVC | 60.0 | 57.6562 | Yes ($p$=0.9343, $W$=0.9855) | |
| Effort with SSVC | 65.0 | 63.5938 | Yes ($p$=0.6840, $W$=0.9762) | |
| Frustration with DC | 30.0 | 31.7188 | Yes ($p$=0.4135, $W$=0.9667) | Yes ($F$(2,93)=1.1805, $p$=0.3117) |
| Frustration with SVC | 32.5 | 34.5312 | No ($p$=0.0381, $W$=0.9296) | |
| Frustration with SSVC | 50.0 | 50.1562 | Yes ($p$=0.8262, $W$=0.9809) | |

Table A.10: Tests for statistically significant differences of the items of the cognitive workload between the control modes.

| **Tested Modes** | **Significantly different** (All three modes: Friedman's ANOVA, Pairwise: Wilcoxon signed-rank test) |
|---|---|
| Mental demand with DC, SVC & SSVC | No ($p$=0.0890, $\chi^2$(2)=4.8376) |
| Physical demand with DC, SVC & SSVC | No ($p$=0.4083, $\chi^2$(2)=1.7913) |
| Temporal demand with DC, SVC & SSVC | No ($p$=0.4270, $\chi^2$(2)=1.7018) |
| Performance with DC, SVC & SSVC | Yes ($p$=0.0009, $\chi^2$(2)=14.0484) |
| Performance with DC & SVC | No ($p$=0.4425, r=0.1358) |
| Performance with DC & SSVC | Yes ($p$=0.0001, $r$=0.6756) |
| Performance with SVC & SSVC | Yes ($p$=0.0098, $r$=0.4568) |
| Effort with DC, SVC & SSVC | No ($p$=0.0940, $\chi^2$(2)=4.7288) |
| Frustration with DC, SVC & SSVC | Yes ($p$=0.0052, $\chi^2$(2)=10.5167) |
| Frustration with DC & SVC | No ($p$=0.5708, $r$=0.1002) |
| Frustration with DC & SSVC | Yes ($p$=0.0009, $r$=0.5885) |
| Frustration with SVC & SSVC | Yes ($p$=0.0026, $r$=0.5322) |

## Visual and Haptic Feedback

The ratings of the study participants on the helpfulness of the visual feedback with DC are shown in Figure A.3.

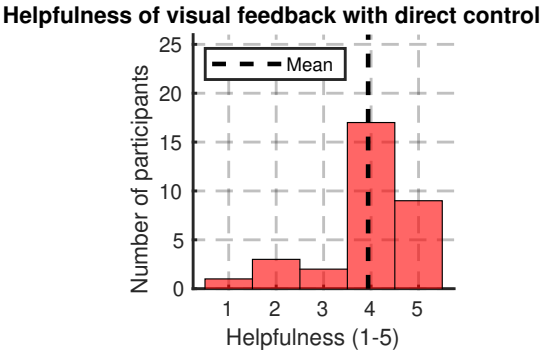


Figure A.3: Rated helpfulness of the visual feedback with direct control.

## Controllability

The analyzed variables of the controllability per mode and test results for the assumptions of parametric tests are given in Table A.11. The results of tests for statistically significant differences are given in Table A.12.

Table A.11: Variables and assumptions for parametric tests of the controllability per control mode.

| **Tested Mode** | **Median** | **Mean** | **Normal** (Shapiro-Wilk test) | **Homogeneous** (Levene test) |
|---|---|---|---|---|
| Controllability with DC | 4 | 3.63 | No ($p$=0.0002, $W$=0.8341) | Yes ($p$=0.6241, $F$(2,93)=0.4738) |
| Controllability with SVC | 4 | 3.81 | No ($p$=0.0001, $W$=0.8264) | |
| Controllability with SSVC | 2 | 2.75 | No ($p$=0.0012, $W$=0.8706) | |

Table A.12: Tests for statistically significant differences of the controllability between the control modes.

| **Tested Modes** | **Significantly different** (All three modes: Friedman's ANOVA, Pairwise: Wilcoxon signed-rank test) |
|---|---|
| Controllability with DC, SVC & SSVC | Yes ($p$=4.2e-5, $\chi^2$(2)=20.1702) |
| Controllability with DC & SVC | Yes ($p$=0.4420, $r$=0.1359 |
| Controllability with DC & SSVC | Yes ($p$=0.0005, $r$=0.6122) |
| Controllability with SVC & SSVC | Yes ($p$=0.0003, $r$=0.6383) |

## Pragmatic Quality of User Experience

The analyzed variables of the hedonic quality of the user experience per mode and test results for the assumptions of parametric tests are given in Table A.13. The results of tests for statistically significant differences are given in Table A.14.

Table A.13: Variables and assumptions for parametric tests of the pragmatic quality of the user experience per uncoupled shared control design.

| **Tested Mode** | **Median** | **Mean** | **Normal** (Shapiro-Wilk test) | **Homogeneous** (Levene test) |
|---|---|---|---|---|
| Efficiency with SVC | 1.25 | 1.11 | Yes ($p$=0.1033, $W$=0.9449) | Yes ($p$=0.9248, $F$(1,62)=0.0090) |
| Efficiency with SSVC | 0.75 | 0.61 | Yes ($p$=0.6594, $W$=0.9754) | |
| Perspicuity with SVC | 1.00 | 0.84 | No ($p$=0.0314, $W$=0.9265) | Yes ($p$=0.0594, $F$(1,62)=3.6877) |
| Perspicuity with SSVC | 0.63 | 0.51 | No ($p$=0.0062, $W$=0.9001) | |
| Dependability with SVC | 1.75 | 1.34 | No ($p$=0.0042, $W$=0.8933) | Yes ($p$=0.6899, $F$(1,62)=0.1607) |
| Dependability with SSVC | -0.13 | 0.00 | Yes ($p$=0.6012, $W$=0.9735) | |

Table A.14: Tests for statistically significant differences of the pragmatic quality of the user experience between the uncoupled shared control designs.

| **Tested Modes** | **Significantly different** (Wilcoxon signed-rank test) |
|---|---|
| Efficiency with SVC & SSVC | Yes ($p$=0.0351, $r$=0.3725) |
| Perspicuity with SVC & SSVC | Yes ($p$=0.0242, $r$=0.3983) |
| Dependability with SVC & SSVC | Yes ($p$=5.7e-5, $r$=0.7117) |

## Preferred uncoupled shared control design

The agreement of the study participants to the question of which uncoupled shared control design is preferred is shown in Figure A.4.

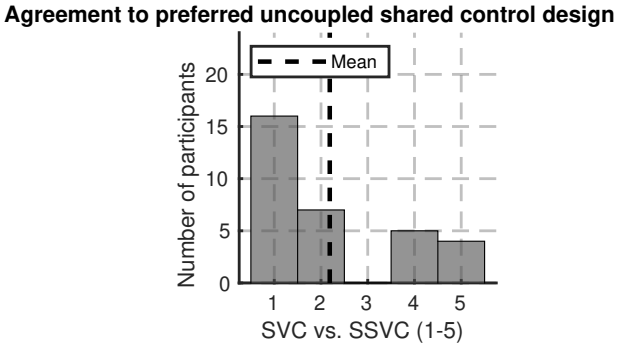


Figure A.4: Agreement to preferred uncoupled shared control design.